January 2005 • NREL/SR-500-36335

Subcontractor Report

Effect of Flap Deflection on Section Characteristics of S813 Airfoil

Period of Performance: 1993 – 1994

D.M. Somers
Airfoils, Inc.
State College, Pennsylvania

National Renewable Energy Laboratory
1617 Cole Boulevard, Golden, Colorado 80401-3393
303-275-3000 • www.nrel.gov

Operated for the U.S. Department of Energy
Office of Energy Efficiency and Renewable Energy
by Midwest Research Institute • Battelle

Contract No. DE-AC36-99-GO10337

January 2005 • NREL/SR-500-36335

Effect of Flap Deflection on Section Characteristics of S813 Airfoil

Period of Performance: 1993 – 1994

D.M. Somers
Airfoils, Inc.
State College, Pennsylvania

NREL Technical Monitor: Jim Tangler

Prepared under Subcontract No. AAM-7-16479-01

National Renewable Energy Laboratory
1617 Cole Boulevard, Golden, Colorado 80401-3393
303-275-3000 • www.nrel.gov

Operated for the U.S. Department of Energy
Office of Energy Efficiency and Renewable Energy
by Midwest Research Institute • Battelle

Contract No. DE-AC36-99-GO10337

Table of Contents

List of Tables

List of Figures

EFFECT OF FLAP DEFLECTION ON SECTION CHARACTERISTICS OF S813 AIRFOIL

Dan M. Somers

January 1994

ABSTRACT

The effect of small deflections of a 30-percent-chord, simple flap on the section characteristics of a tip airfoil, the S813, designed for 20- to 30-meter, stall-regulated, horizontal-axis wind turbines has been evaluated theoretically. The decrease in maximum lift coefficient due to leading-edge roughness increases in magnitude with increasing, positive flap deflection and with decreasing Reynolds number.

INTRODUCTION

Renewed interest in the use of simple flaps, called "ailerons" within the wind-energy community, to provide aerodynamic braking and to regulate peak power has led to the incorporation of such control surfaces in a number of recent horizontal-axis wind-turbine designs. In support of these activities, a theoretical evaluation of the effect of small deflections of a 30-percent-chord, simple flap on the section characteristics of a tip airfoil, the S813 (ref. 1), designed for 20- to 30-meter, stall-regulated, horizontal-axis wind turbines has been conducted. The specific tasks performed under this study are described in National Renewable Energy Laboratory (NREL) Subcontract Number AAO-3-13023-01-104879.

Because of the limitations of the theoretical methods (refs. 2 and 3) employed in this study, the range of flap deflections has been limited to $-10°$ to $10°$ and the results presented are in no way guaranteed to be accurate—either in an absolute or in a relative sense. This statement applies to the entire study.

SYMBOLS

C_p	pressure coefficient
c	airfoil chord, meters
c_d	section profile-drag coefficient

c_l	section lift coefficient
$c_{l,max}$	maximum section lift coefficient
c_m	section pitching-moment coefficient about quarter-chord point
$dc_{l,max}$	change in maximum section lift coefficient due to leading-edge roughness, $[(c_{l,max})_{free} - (c_{l,max})_{rough}]/(c_{l,max})_{free}$, percent
L.	lower surface
MU	boundary-layer transition mode (ref. 3)
R	Reynolds number based on free-stream conditions and airfoil chord
S.	boundary-layer separation location, $1 - s_{sep}/c$
s_{sep}	arc length along which boundary layer is separated, meters
s_{turb}	arc length along which boundary layer is turbulent including s_{sep}, meters
T.	boundary-layer transition location, $1 - s_{turb}/c$
U.	upper surface
x	airfoil abscissa, meters
y	airfoil ordinate, meters
α	angle of attack relative to chord line, degrees
δ_f	flap deflection, positive downward, degrees

Subscripts:

free	transition free, boundary-layer transition mode MU = 3 (ref. 3)
rough	rough, boundary-layer transition mode MU = 9 (ref. 3)

THEORETICAL PROCEDURE

A sealed, center-hinged, 30-percent-chord, simple flap was selected as representative of current designs. Thus, the location of the flap-hinge point is x/c = 0.700000, y/c = 0.019737. The airfoil shape with various flap deflections is shown in figure 1. The coordinates of the S813 airfoil with no flap deflection are contained in table I. The S813 airfoil thickness is 16-percent chord.

The Eppler Airfoil Design and Analysis Code (refs. 2 and 3) was used because of confidence gained during the design, analysis, and experimental verification of several other airfoils. (See refs. 4–6.) Because the panel method cannot evaluate sharp corners in the airfoil contour, an arc must be introduced between the flap and the forward portion of the airfoil. Positive flap deflections produce such an arc "automatically" in the upper surface of a real wind-turbine blade, but not in the lower surface where a corner is formed. In the real flow, a local separation "smooths" this concave corner and, therefore, it is reasonable to introduce an arc in the theoretical model. (See ref. 3.) The lengths of the arcs were varied linearly from 0 for both surfaces for a flap deflection of 0° to 12-percent chord for the upper surface and 8-percent chord for the lower surface for a flap deflection of −10° and to 8-percent chord for the upper surface and 12-percent chord for the lower surface for a flap deflection of 10°.

The section characteristics were predicted for Reynolds numbers of 1×10^6, 2×10^6 (the design Reynolds number of the S813 airfoil), and 3×10^6. The computations were performed with transition free, with transition fixed at 2-percent chord on the upper surface and 5-percent chord on the lower surface using transition mode MU = 1 (ref. 3), and 'rough' using transition mode MU = 9 (ref. 3), which simulates distributed roughness due to, for example, leading-edge contamination by insects or rain. Because the free-stream Mach number for all relevant, wind-turbine operating conditions remains below 0.2, all results presented are incompressible.

DISCUSSION OF RESULTS

Pressure Distributions

The inviscid (potential-flow) pressure distributions for various angles of attack with flap deflections of 0°, −5°, −10°, 5°, and 10° are shown in figure 2. The effect of negative flap deflection on the inviscid pressure distribution at $\alpha = 4°$ is summarized in figure 3(a) and the effect of positive flap deflection at $\alpha = 0°$, in figure 3(b).

Transition and Separation Locations

The variation of boundary-layer transition location with lift coefficient for a flap deflection of 0° is shown in figure 4. It should be remembered that the method of references 2 and 3 'defines'

the transition location as the end of the laminar boundary layer whether due to natural transition or laminar separation. Thus, for conditions which result in relatively long laminar separation bubbles (low lift coefficients for the upper surface and high lift coefficients for the lower surface and/or low Reynolds numbers), poor agreement between the predicted 'transition' locations and the locations measured experimentally can be expected. This poor agreement is worsened by the fact that transition is normally confirmed in the wind tunnel only by the detection of attached turbulent flow. For conditions which result in shorter laminar separation bubbles (high lift coefficients for the upper surface and low lift coefficients for the lower surface and/or high Reynolds numbers), the agreement between theory and experiment should be quite good. (See ref. 7.)

The variation of turbulent boundary-layer separation location with lift coefficient for a flap deflection of 0° is also shown in figure 4. A small separation is predicted on the upper surface at higher lift coefficients. This separation, which is caused by the 'separation ramp' (ref. 8), the steep adverse pressure gradient aft of about 90-percent chord (fig. 2(a)), increases in length with transition fixed near the leading edge.

The variations of transition and turbulent-separation locations with lift coefficient for negative (upward) flap deflections are shown in figures 5–14. A small separation is predicted on the upper surface at higher lift coefficients. This separation increases in length with transition fixed near the leading edge. Separation is predicted on the lower surface at lower lift coefficients for flap deflections more negative than –4°. The separation is particularly large for a Reynolds number of 1×10^6. Such separation usually has little effect on the section characteristics, however. This separation decreases in length with transition fixed near the leading edge.

The variations of transition and turbulent-separation locations with lift coefficient for positive (downward) flap deflections are shown in figures 15–24. A small separation is predicted on the upper surface at higher lift coefficients. This separation increases in length with transition fixed near the leading edge and with increasing flap deflection. Separation is predicted on the lower surface at lower lift coefficients for flap deflections greater than 8°. The separation is particularly large for a Reynolds number of 1×10^6. This separation is not considered important, however, because it occurs at lift coefficients which are not typical of normal wind-turbine operations. Such separation usually has little effect on the section characteristics. (See ref. 7.)

Section Characteristics

Effect of flap deflection.- The section characteristics with a flap deflection of 0° are shown in figure 4. It should be noted that the maximum lift coefficient predicted by the method of references 2 and 3 is not always realistic. Accordingly, an empirical criterion should be applied to the computed results. This criterion assumes that the maximum lift coefficient has been reached if the drag coefficient of the upper surface is greater than 0.0240 or if the length of turbulent separation along the upper surface is greater than 0.10. Thus, the maximum lift coefficient for the design Reynolds number of the S813 airfoil, 2×10^6, is predicted to be 1.12. Low profile-drag

coefficients are predicted over the range of lift coefficients from about 0 to about 1.0. The zero-lift pitching-moment coefficient is predicted to be –0.0770. However, the method of references 2 and 3 generally overpredicts the pitching-moment coefficient by about 10 percent. Thus, the actual zero-lift pitching-moment coefficient should be about –0.07. An additional analysis (not shown) indicates that significant (drag-producing) laminar separation bubbles should not occur on either surface for any relevant operating condition.

The section characteristics with negative flap deflections are shown in figures 5–14. The angle of attack for zero lift coefficient and the pitching-moment coefficients increase with increasing, negative flap deflection. The maximum lift coefficient and the upper limit of the low-drag range of lift coefficients decrease with increasing, negative flap deflection. In addition, negative flap deflection alters the pressure distribution in the vicinity of the flap hinge (fig. 3(a)), nullifying the transition ramp incorporated into the lower surface (ref. 1). As a result, significant laminar separation bubbles are predicted for flap deflections more negative than –2°. Thus, although the minimum drag coefficient generally decreases with increasing, negative flap deflection, the predicted drag coefficients are probably too low because of the bubbles.

The section characteristics with positive flap deflections are shown in figures 15–24. The angle of attack for zero lift coefficient and the pitching-moment coefficients decrease with increasing, positive flap deflection. The maximum lift coefficient and the upper limit of the low-drag range of lift coefficients generally increase with increasing, positive flap deflection. For the larger, positive flap deflections, the maximum lift coefficient coincides with the upper limit of the low-drag range. This coincidence occurs for flap deflections greater than 0° for a Reynolds number of 1×10^6, for flap deflections greater than 5° for a Reynolds number of 2×10^6, and for flap deflections greater than 8° for a Reynolds number of 3×10^6. Positive flap deflection alters the pressure distribution in the vicinity of the flap hinge (fig.3(b)), nullifying the transition ramps incorporated into both the upper and lower surfaces (ref. 1). As a result, significant laminar separation bubbles are predicted for all positive flap deflections. The bubbles are particularly severe for flap deflections greater than 6°.

The effect of flap deflection on maximum lift coefficient is summarized in figure 25.

Effect of roughness.- The effect of roughness on the section characteristics with a flap deflection of 0° is shown in figure 4. The maximum lift coefficient is unaffected by fixing transition because transition on the upper surface is predicted to occur forward of 2-percent chord at the maximum lift coefficient. For the rough condition, the maximum lift coefficient for the design Reynolds number of the S813 airfoil, 2×10^6, is predicted to be 1.10, a reduction of less than two percent from that for the transition-free condition. The drag coefficients are, of course, adversely affected by the roughness.

The effect of roughness on the section characteristics with negative flap deflections are shown in figures 5–14. The maximum lift coefficient is relatively unaffected by leading-edge roughness.

The effect of roughness on the section characteristics with positive flap deflections are shown in figures 15–24. For flap deflections where the maximum lift coefficient coincides with the upper limit of the low-drag range, the maximum lift coefficient is affected by fixing transition because transition on the upper surface is predicted to occur aft of 2-percent chord at the maximum lift coefficient. The decrease in maximum lift coefficient due to leading-edge roughness increases in magnitude with increasing flap deflection and with decreasing Reynolds number.

The effect of flap deflection on the percent change in maximum lift coefficient due to leading-edge roughness is summarized in figure 26.

CONCLUDING REMARKS

The effect of small deflections of a 30-percent-chord, simple flap on the section characteristics of a tip airfoil, the S813, designed for 20- to 30-meter, stall-regulated, horizontal-axis wind turbines has been evaluated theoretically. The decrease in maximum lift coefficient due to leading-edge roughness increases in magnitude with positive flap deflection and with decreasing Reynolds number.

REFERENCES

1. Somers, Dan M.: The S809 through S813 Airfoils. Airfoils, Inc., 1988.

2. Eppler, Richard: Airfoil Design and Data. Springer-Verlag (Berlin), 1990.

3. Eppler, R.: Airfoil Program System. User's Guide. R. Eppler, c.1991.

4. Somers, Dan M.: Design and Experimental Results for the S809 Airfoil. Airfoils, Inc., 1989.

5. Somers, Dan M.: Design and Experimental Results for the S805 Airfoil. Airfoils, Inc., 1988.

6. Somers, Dan M.: Subsonic Natural-Laminar-Flow Airfoils. Natural Laminar Flow and Laminar Flow Control, R. W. Barnwell and M. Y. Hussaini, eds., Springer-Verlag New York, Inc., 1992, pp. 143–176.

7. Somers, Dan M.: Design and Experimental Results for a Natural-Laminar-Flow Airfoil for General Aviation Applications. NASA TP-1861, 1981.

8. Maughmer, Mark D.; and Somers, Dan M.: Design and Experimental Results for a High-Altitude, Long-Endurance Airfoil. J. Aircr., vol. 26, no. 2, Feb. 1989, pp. 148–153.

TABLE I.- S813 AIRFOIL COORDINATES

Upper Surface		Lower Surface	
x/c	y/c	x/c	y/c
0.00261	0.00713	0.00002	−0.00057
.01017	.01587	.00355	−.00747
.02259	.02504	.01332	−.01450
.03971	.03441	.02821	−.02162
.06130	.04377	.04797	−.02848
.08714	.05294	.07237	−.03492
.11693	.06173	.10117	−.04077
.15034	.07001	.13406	−.04595
.18702	.07761	.17071	−.05036
.22656	.08441	.21075	−.05394
.26852	.09026	.25375	−.05664
.31245	.09505	.29926	−.05843
.35786	.09864	.34677	−.05927
.40425	.10092	.39578	−.05914
.45109	.10174	.44572	−.05801
.49785	.10089	.49604	−.05580
.54414	.09799	.54617	−.05237
.58991	.09277	.59573	−.04745
.63530	.08526	.64476	−.04084
.68048	.07589	.69355	−.03305
.72532	.06549	.74176	−.02508
.76921	.05491	.78848	−.01771
.81126	.04473	.83277	−.01138
.85064	.03527	.87364	−.00638
.88649	.02669	.91013	−.00283
.91823	.01890	.94134	−.00066
.94559	.01202	.96649	.00032
.96820	.00644	.98493	.00047
.98539	.00259	.99620	.00019
.99626	.00057	1.00000	.00000
1.00000	.00000		

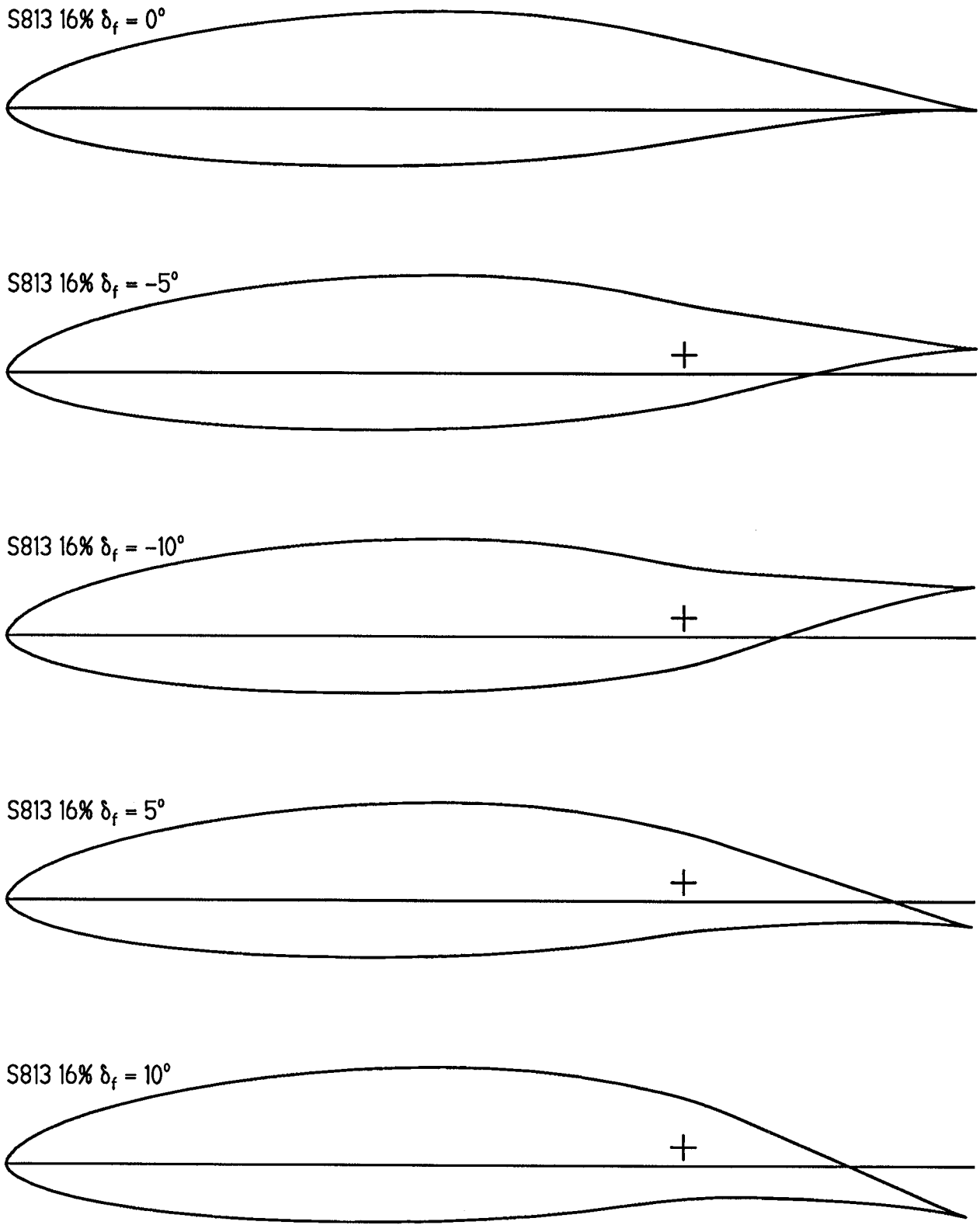

Figure 1.- S813 airfoil shape with $\delta_f = 0°, -5°, -10°, 5°$, and 10°.

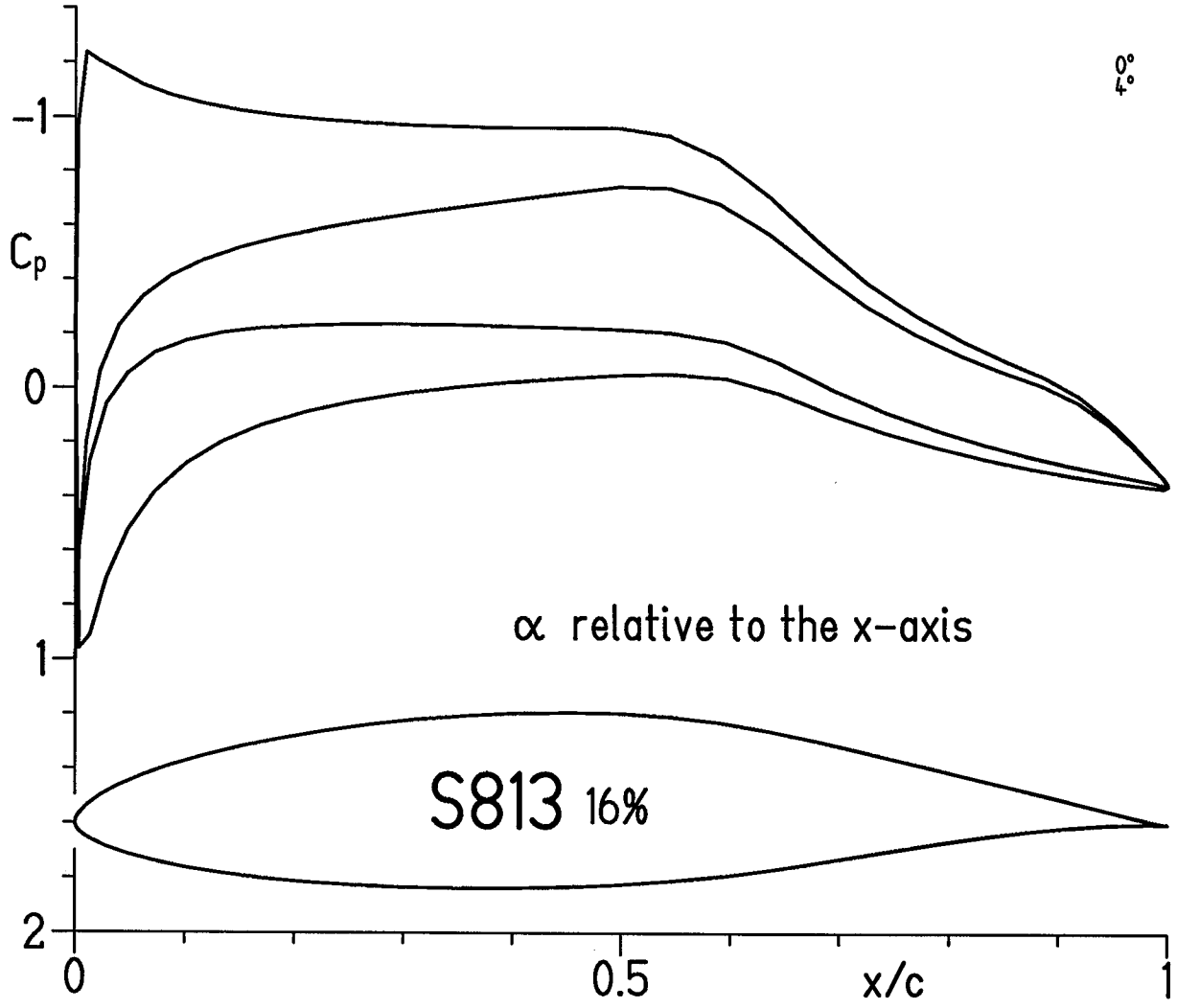

(a) $\delta_f = 0°$; $\alpha = 0°$ and 4°.

Figure 2.- Inviscid pressure distributions.

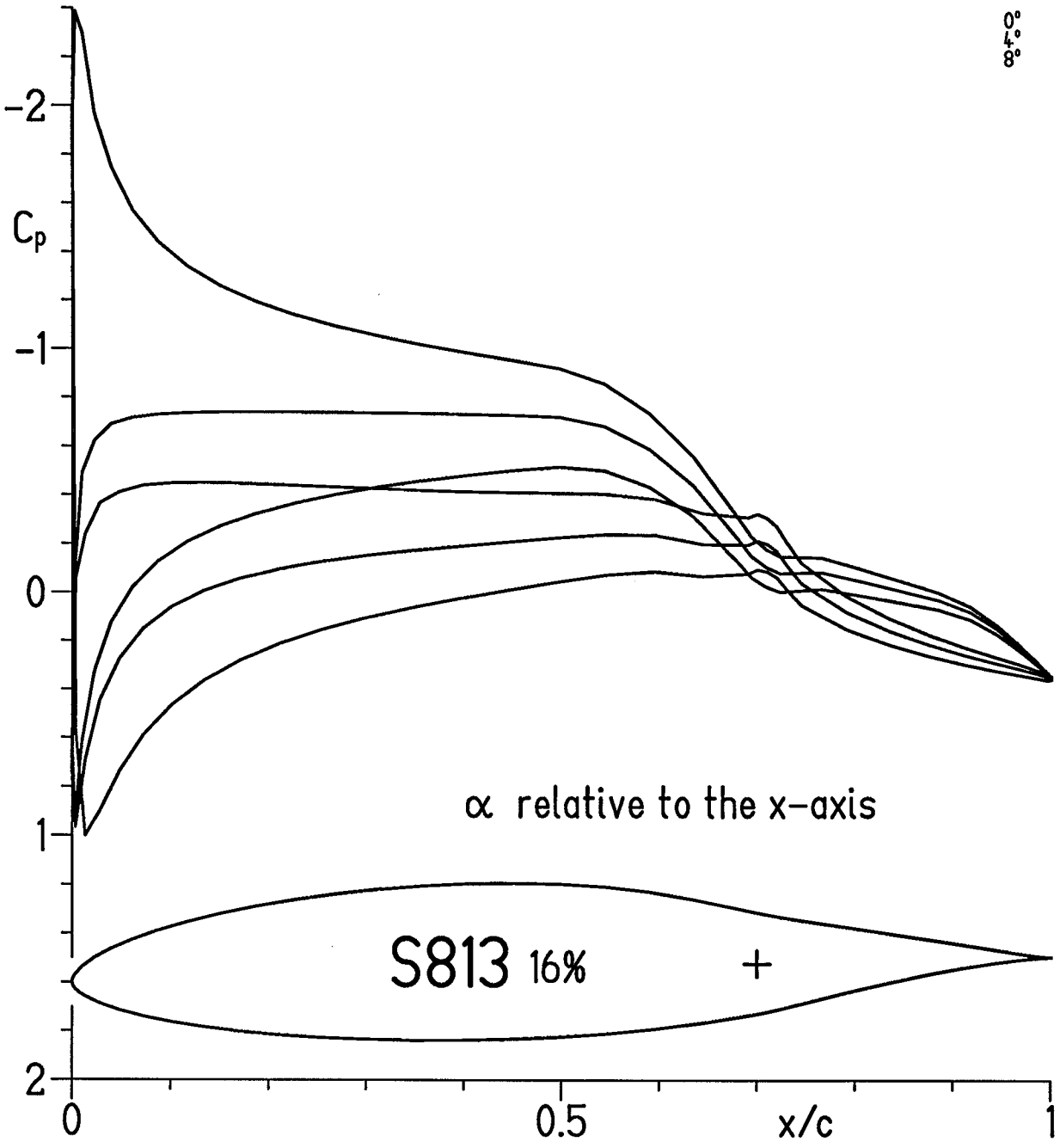

(b) $\delta_f = -5°$; $\alpha = 0°$, 4°, and 8°.

Figure 2.- Continued.

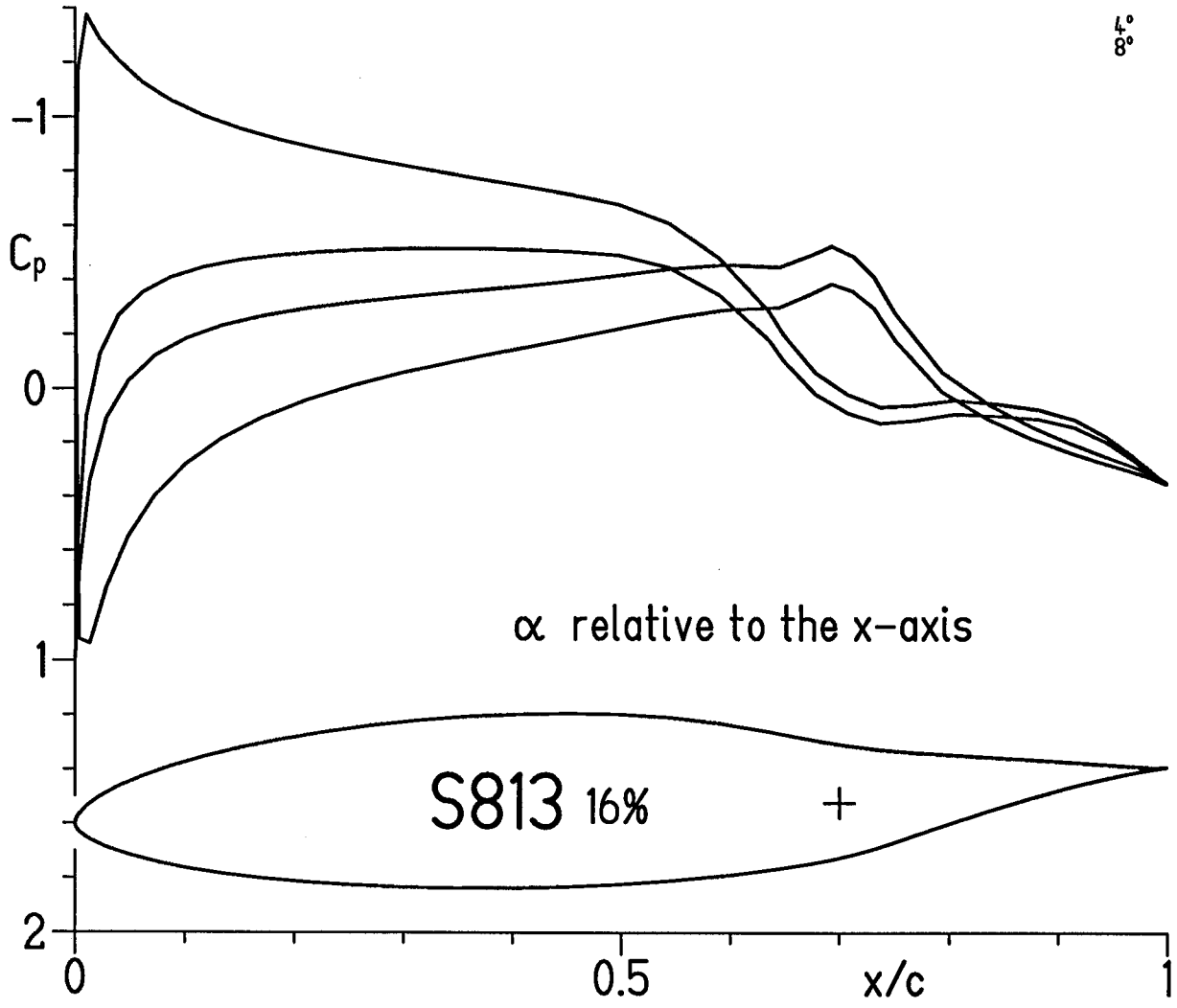

(c) $\delta_f = -10°$; $\alpha = 4°$ and 8°.

Figure 2.- Continued.

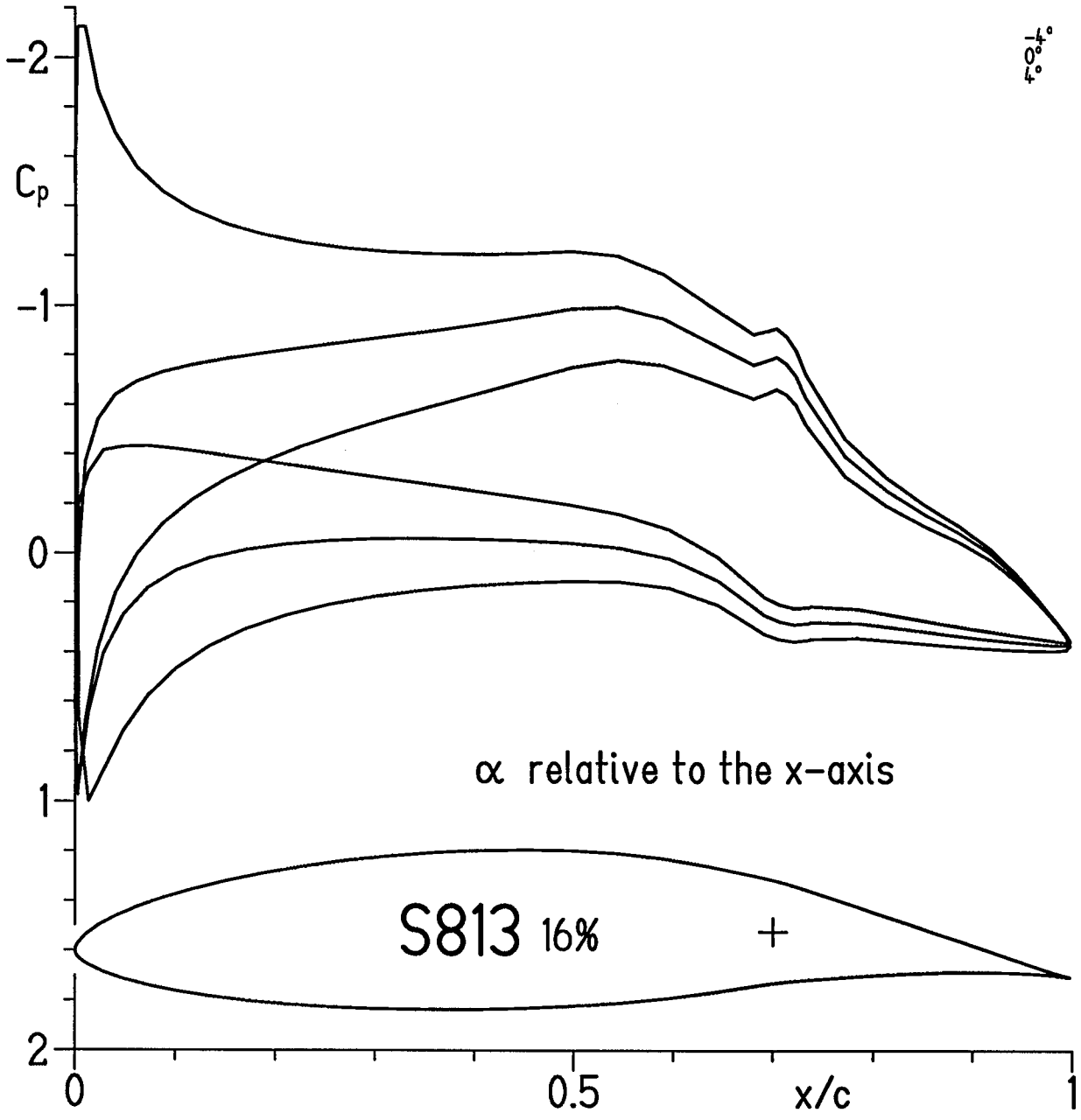

(d) $\delta_f = 5°$; $\alpha = -4°$, 0°, and 4°.

Figure 2.- Continued.

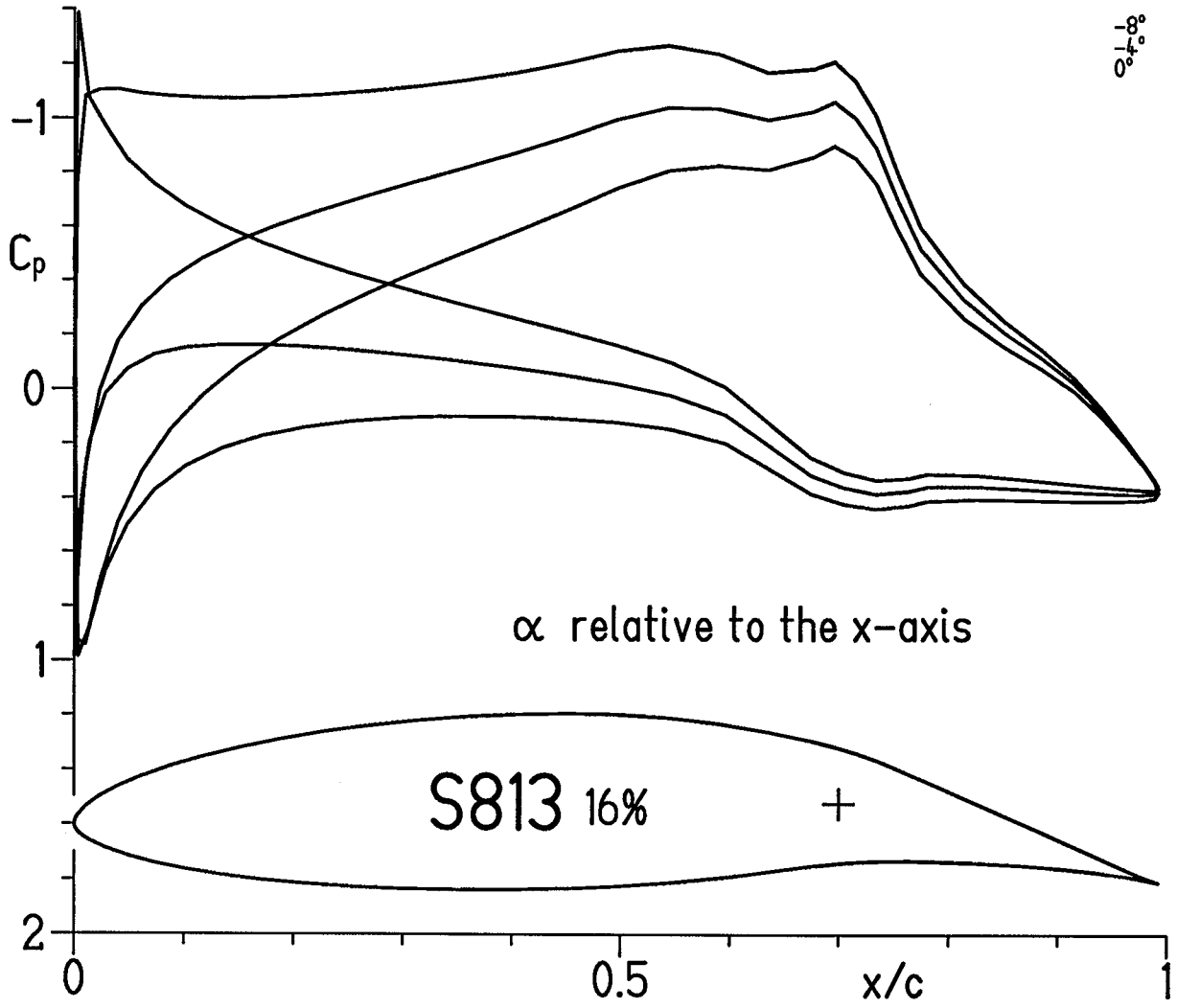

(e) $\delta_f = 10°$; $\alpha = -8°, -4°$, and $0°$.

Figure 2.- Concluded.

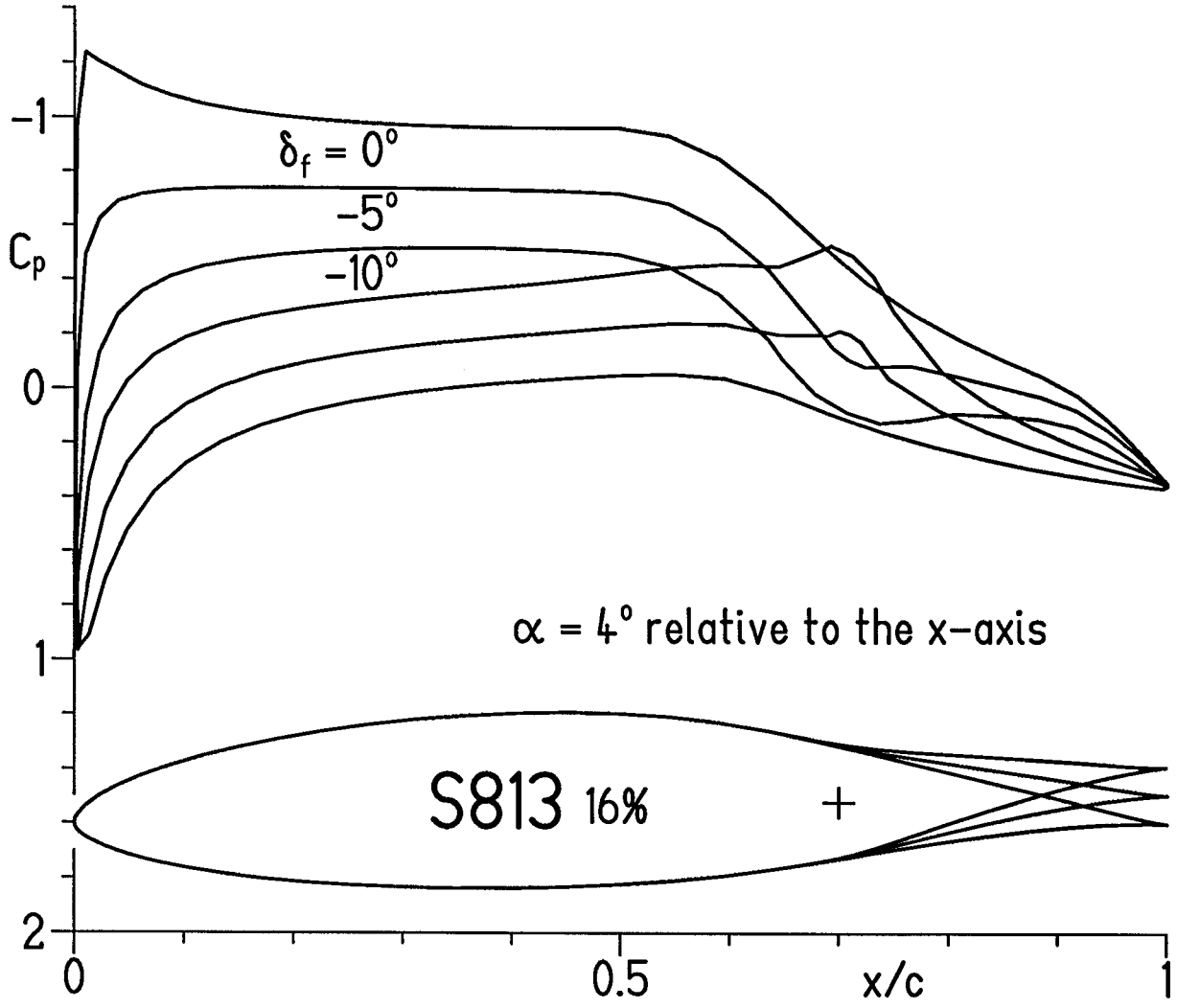

(a) $\delta_f = 0°, -5°$, and $-10°$; $\alpha = 4°$.

Figure 3.- Effect of flap deflection on inviscid pressure distribution.

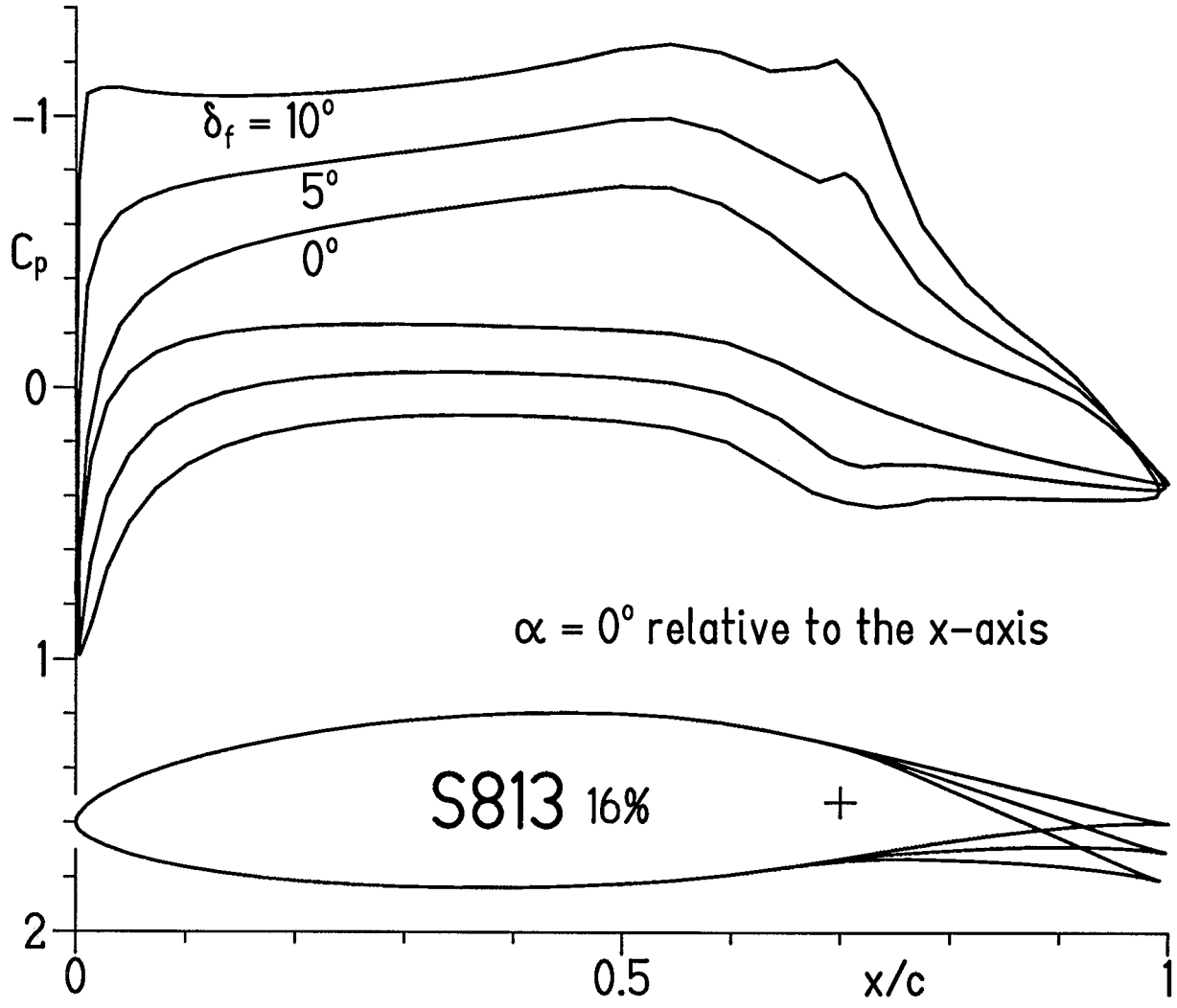

(b) $\delta_f = 0°$, 5°, and 10°; $\alpha = 0°$.

Figure 3.- Concluded.

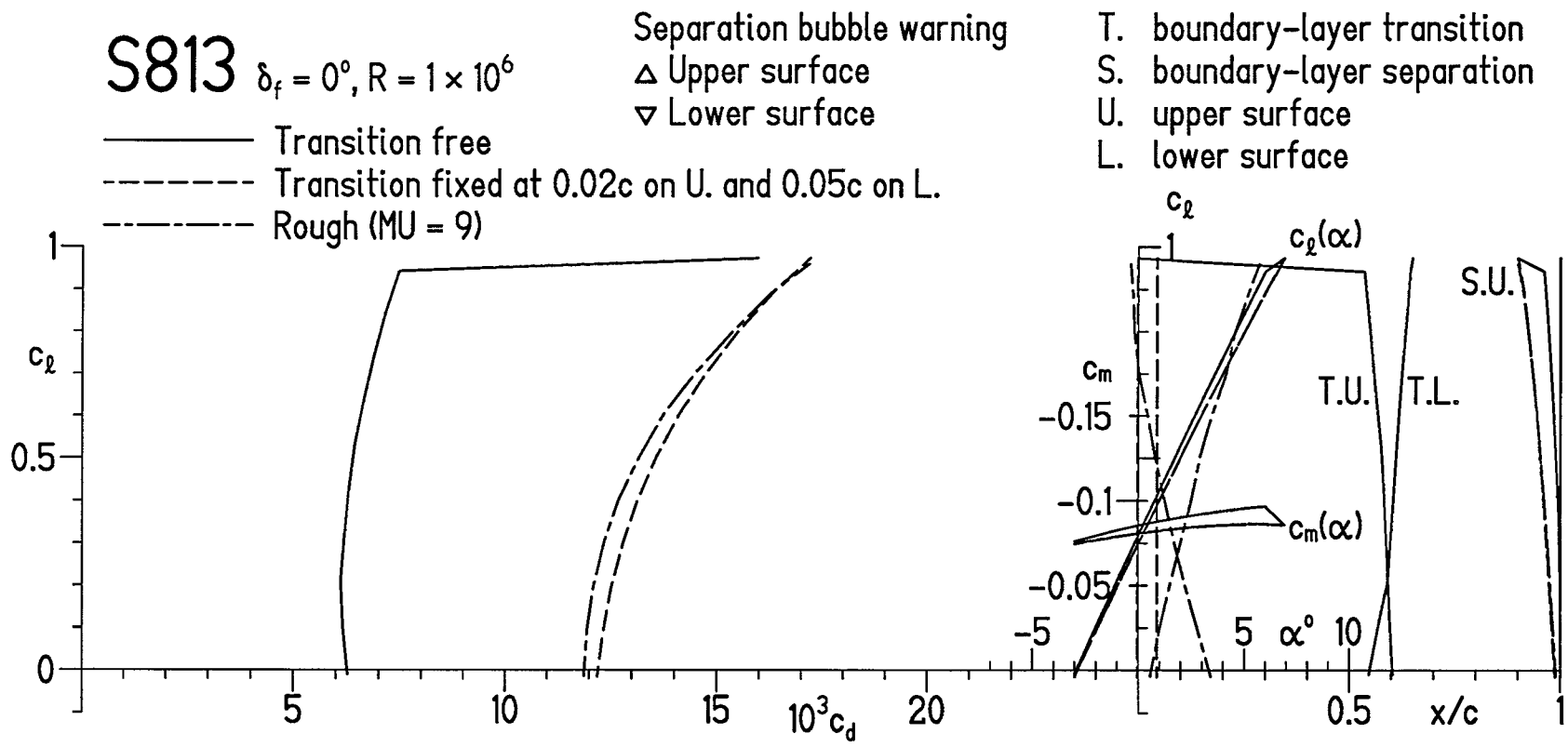

(a) $R = 1 \times 10^6$.

Figure 4.- Section characteristics with $\delta_f = 0°$ and transition free, transition fixed, and rough.

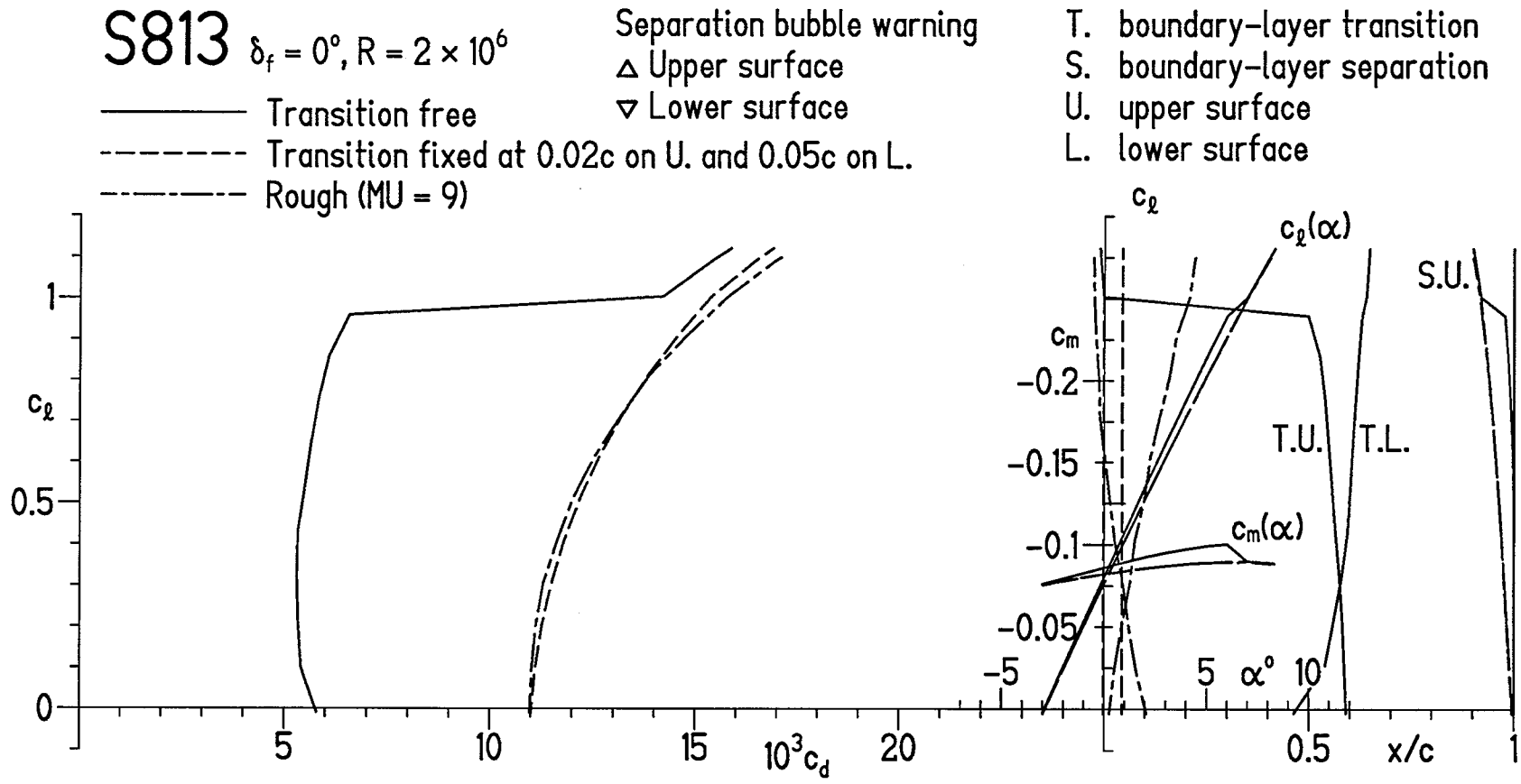

(b) $R = 2 \times 10^6$.

Figure 4.- Continued.

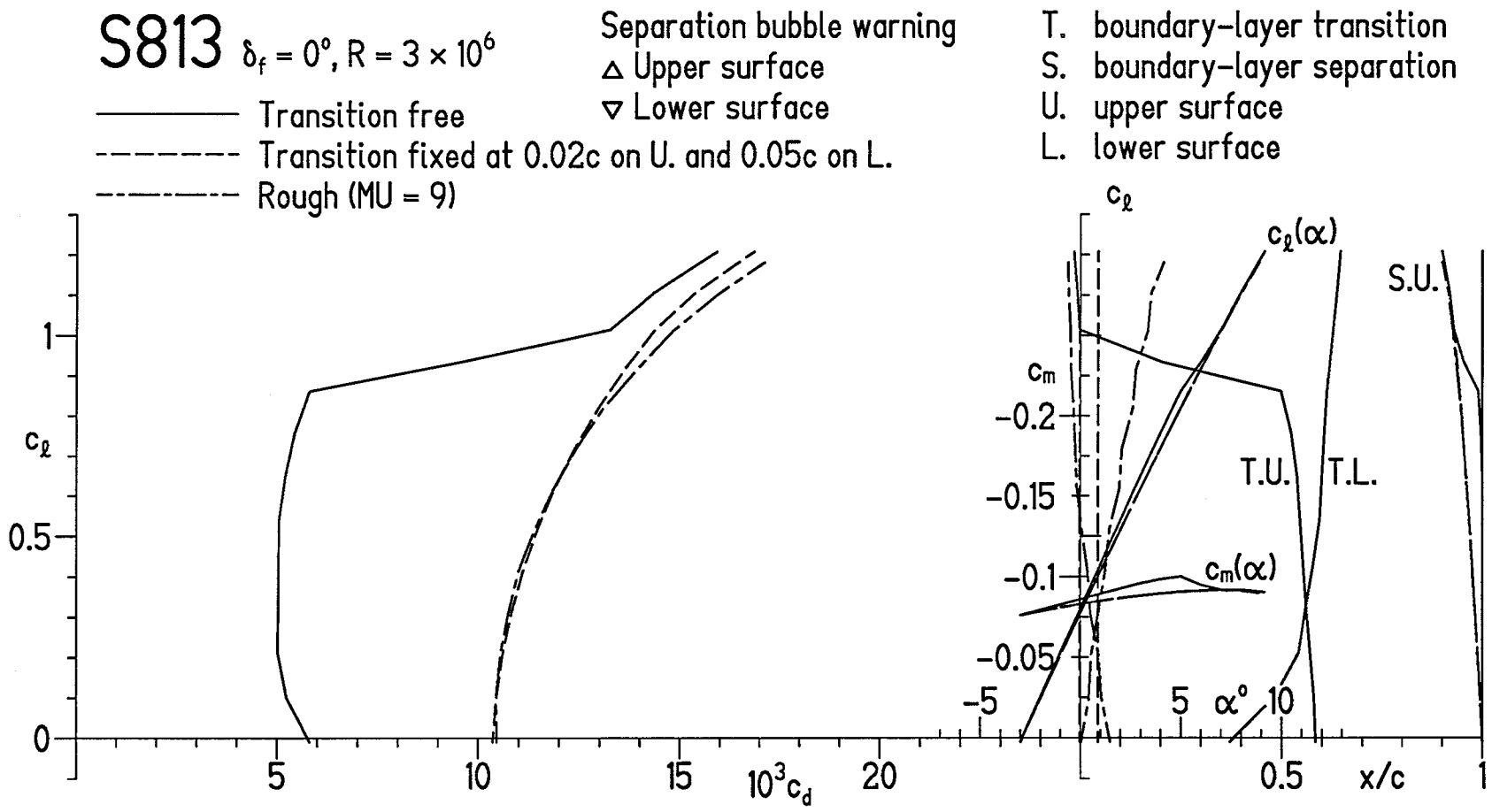

(c) R = 3×10^6.

Figure 4.- Concluded.

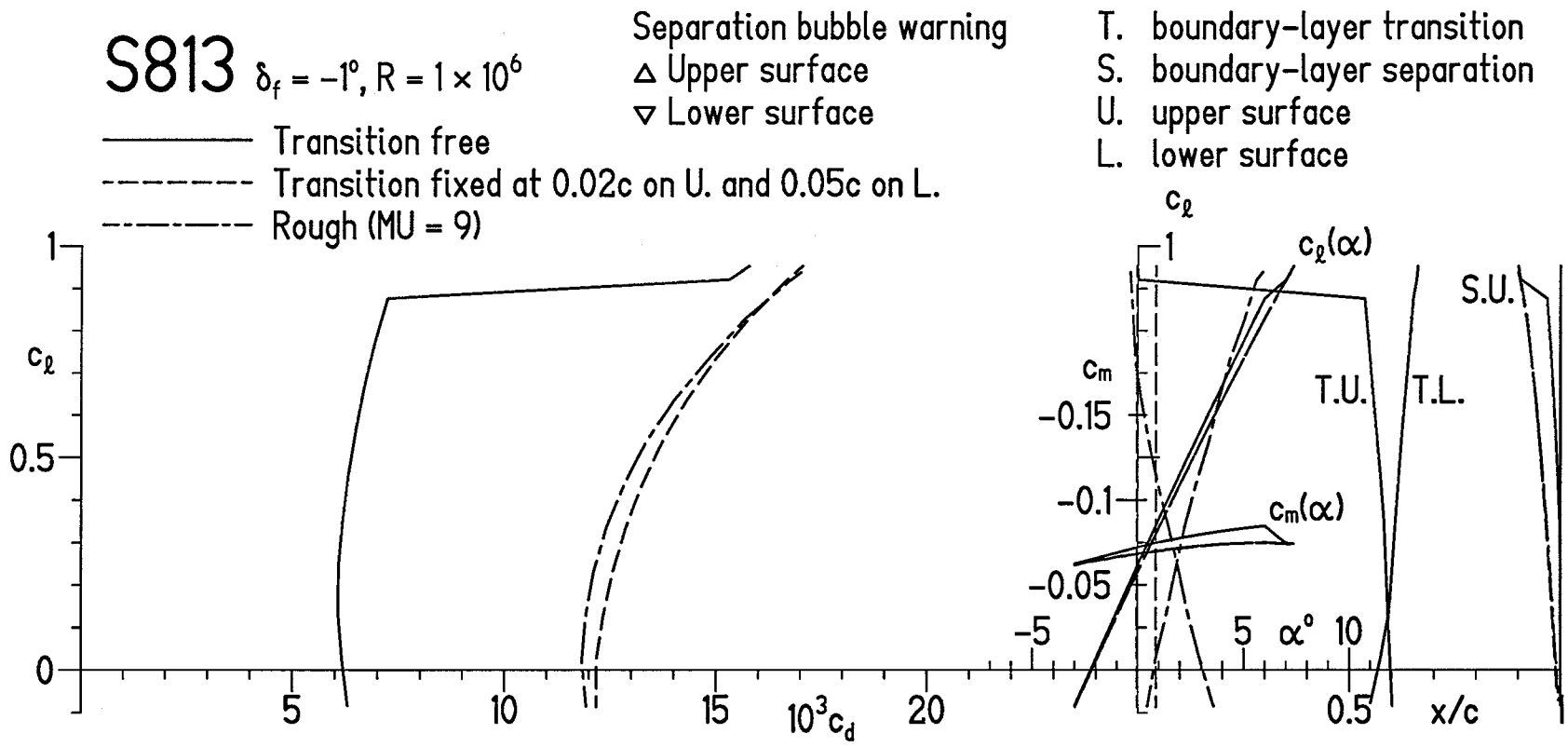

(a) $R = 1 \times 10^6$.

Figure 5.- Section characteristics with $\delta_f = -1°$ and transition free, transition fixed, and rough.

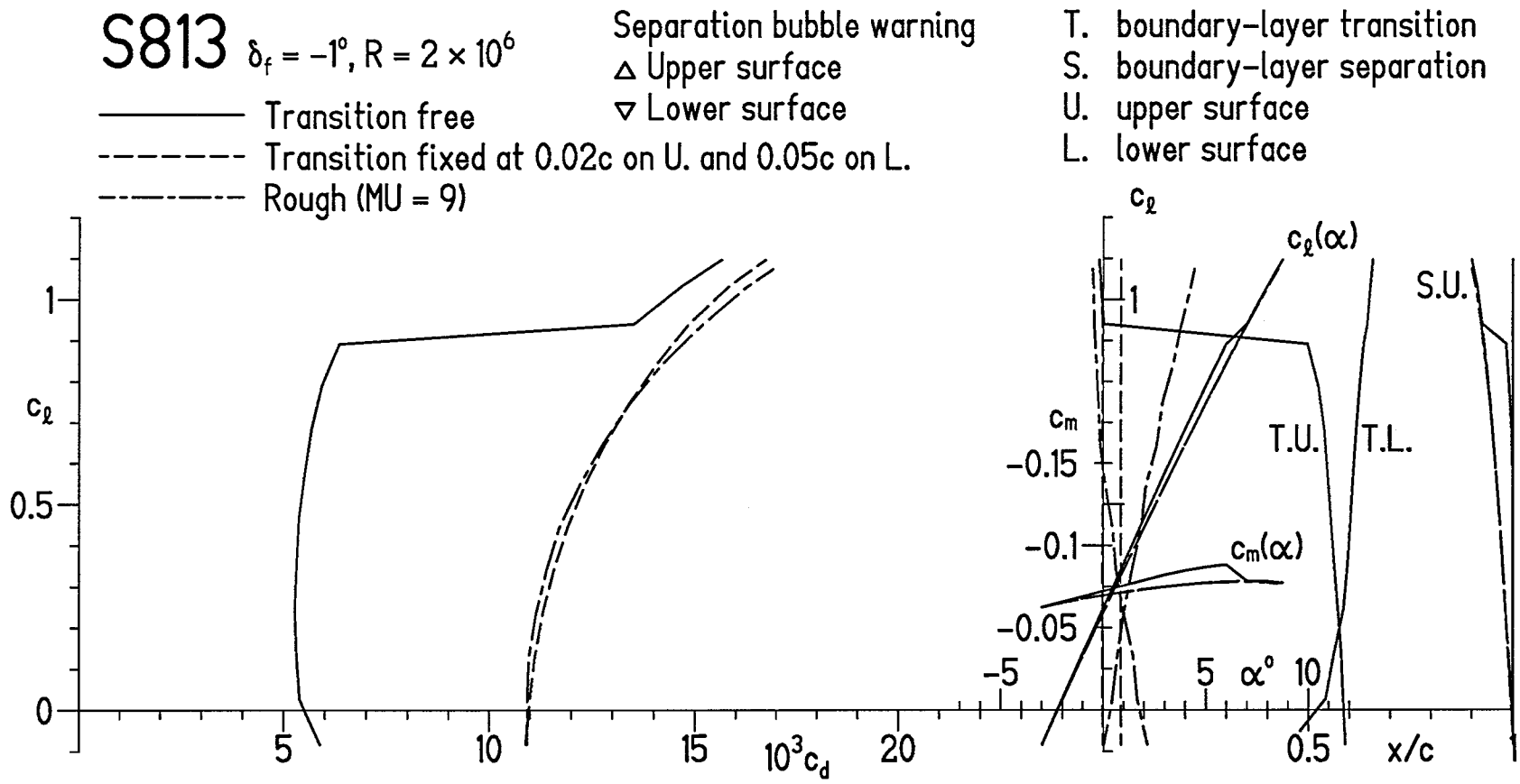

(b) $R = 2 \times 10^6$.

Figure 5.- Continued.

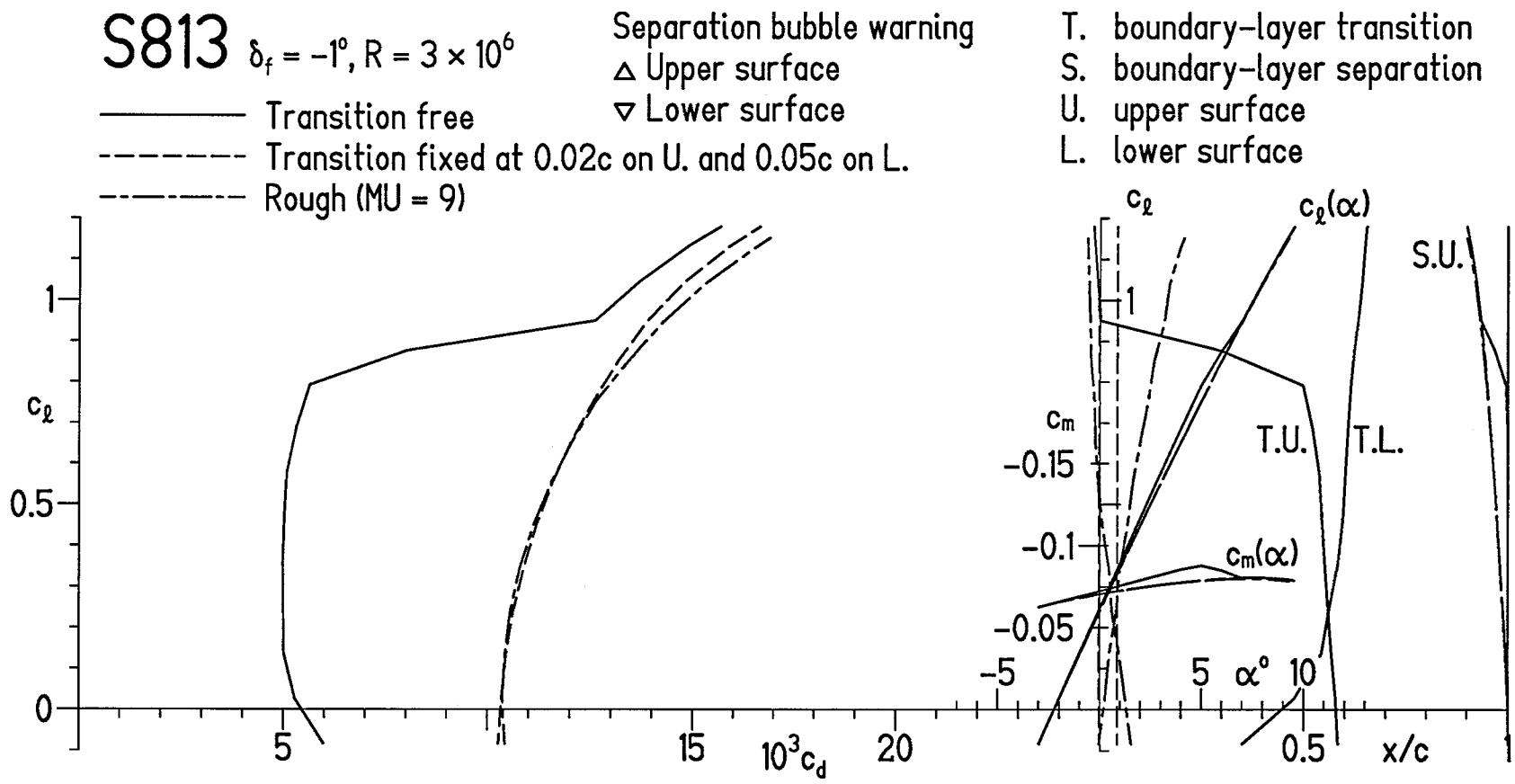

(c) $R = 3 \times 10^6$.

Figure 5.- Concluded.

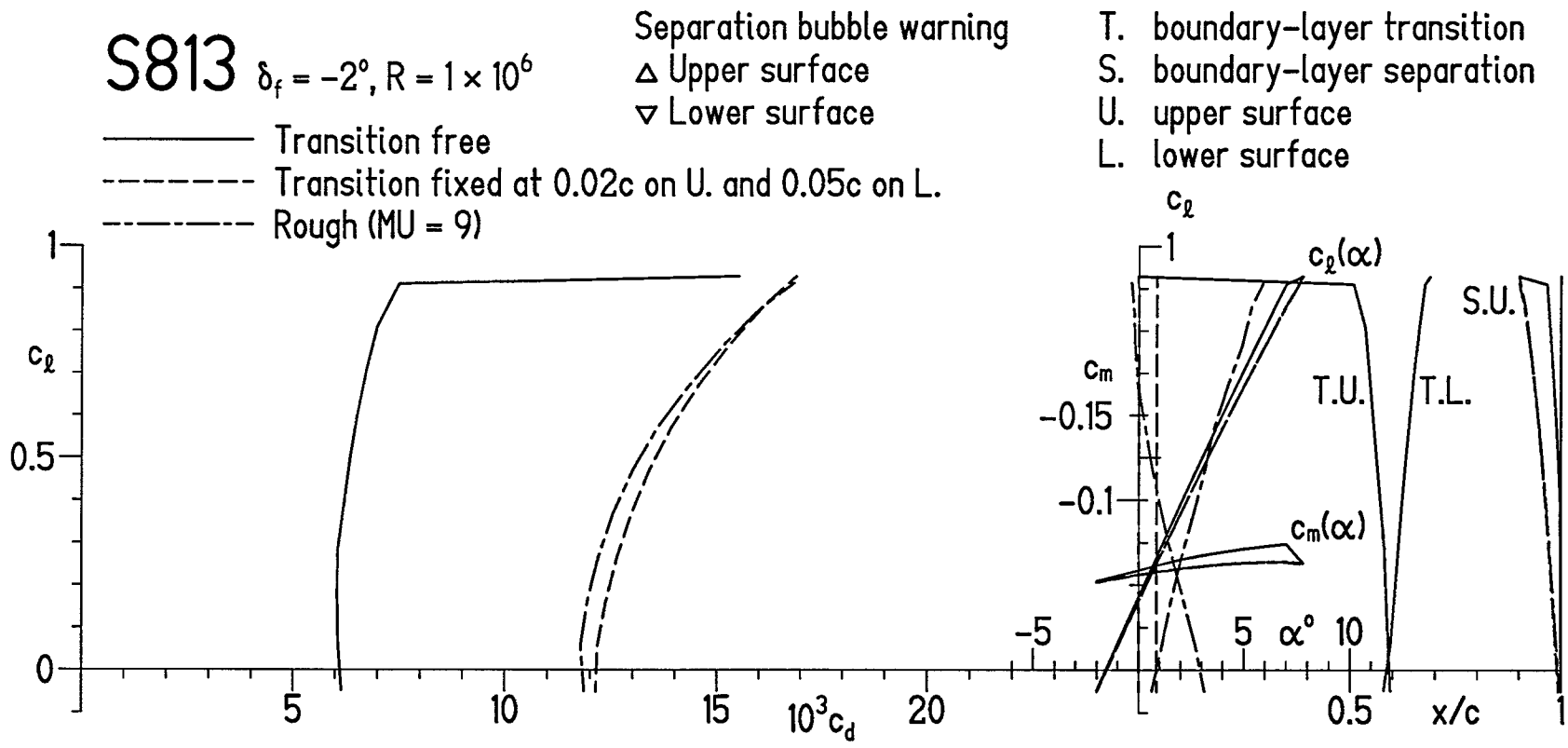

(a) $R = 1 \times 10^6$.

Figure 6.- Section characteristics with $\delta_f = -2°$ and transition free, transition fixed, and rough.

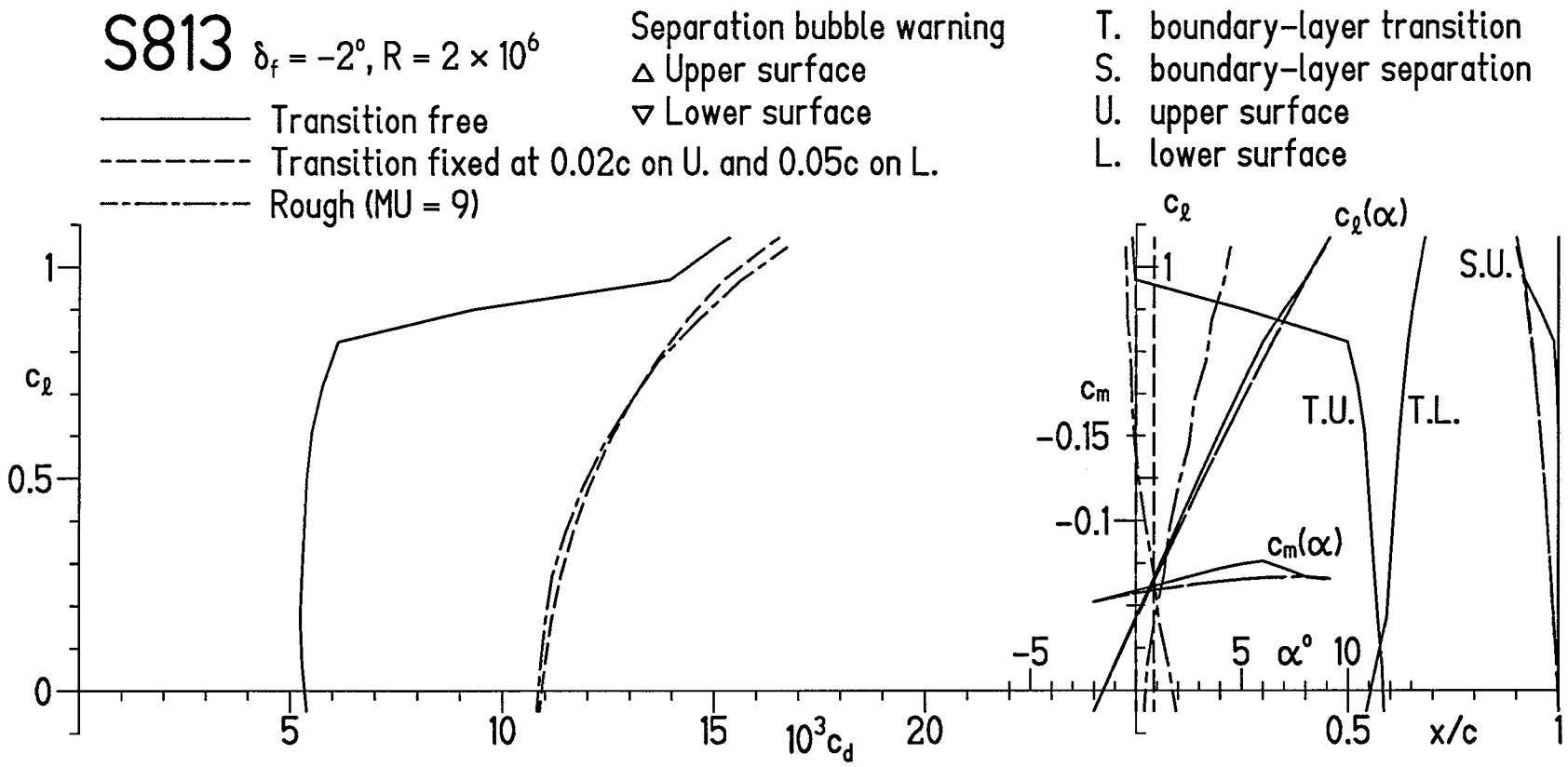

(b) R = 2×10^6.

Figure 6.- Continued.

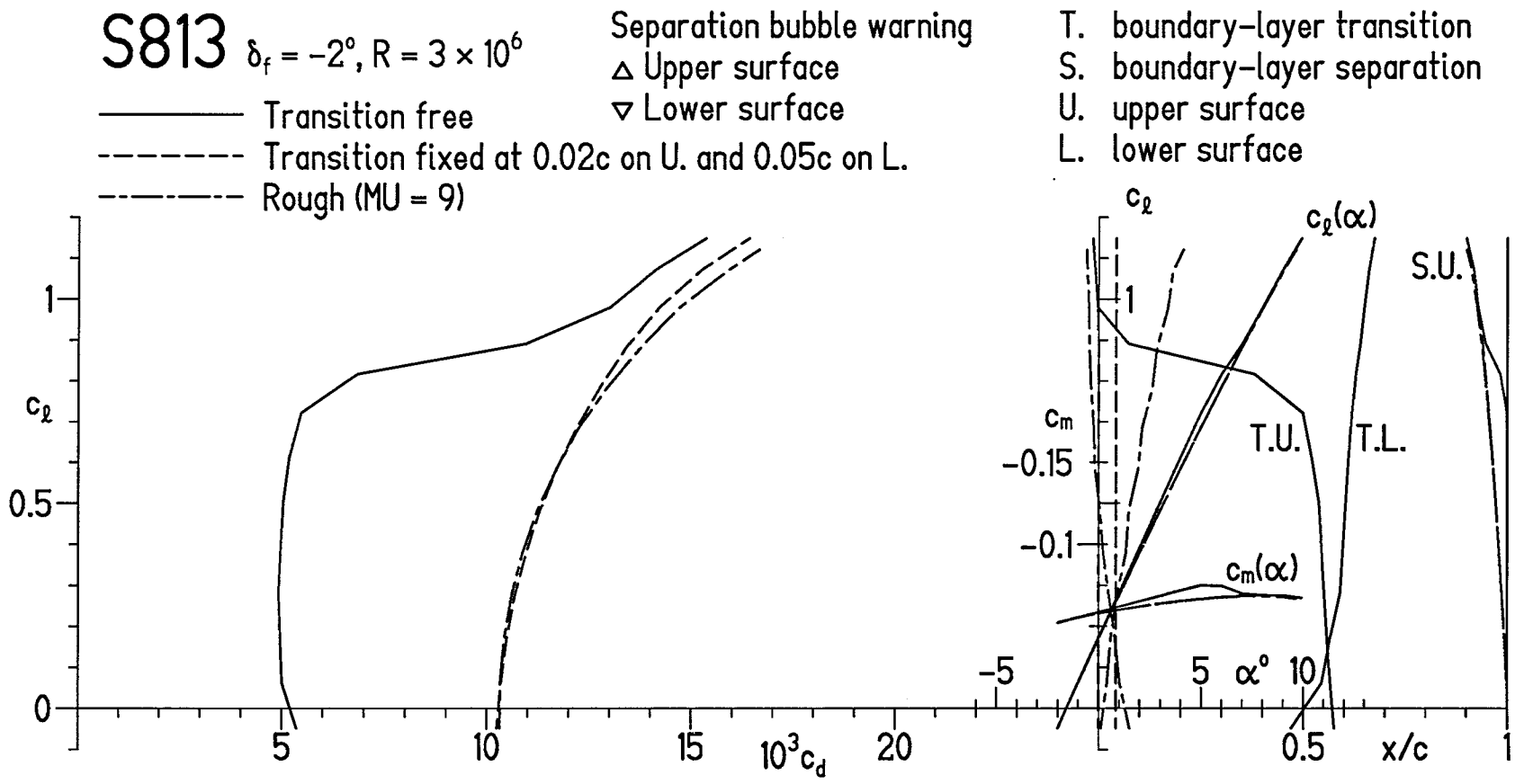

(c) R = 3×10^6.

Figure 6.- Concluded.

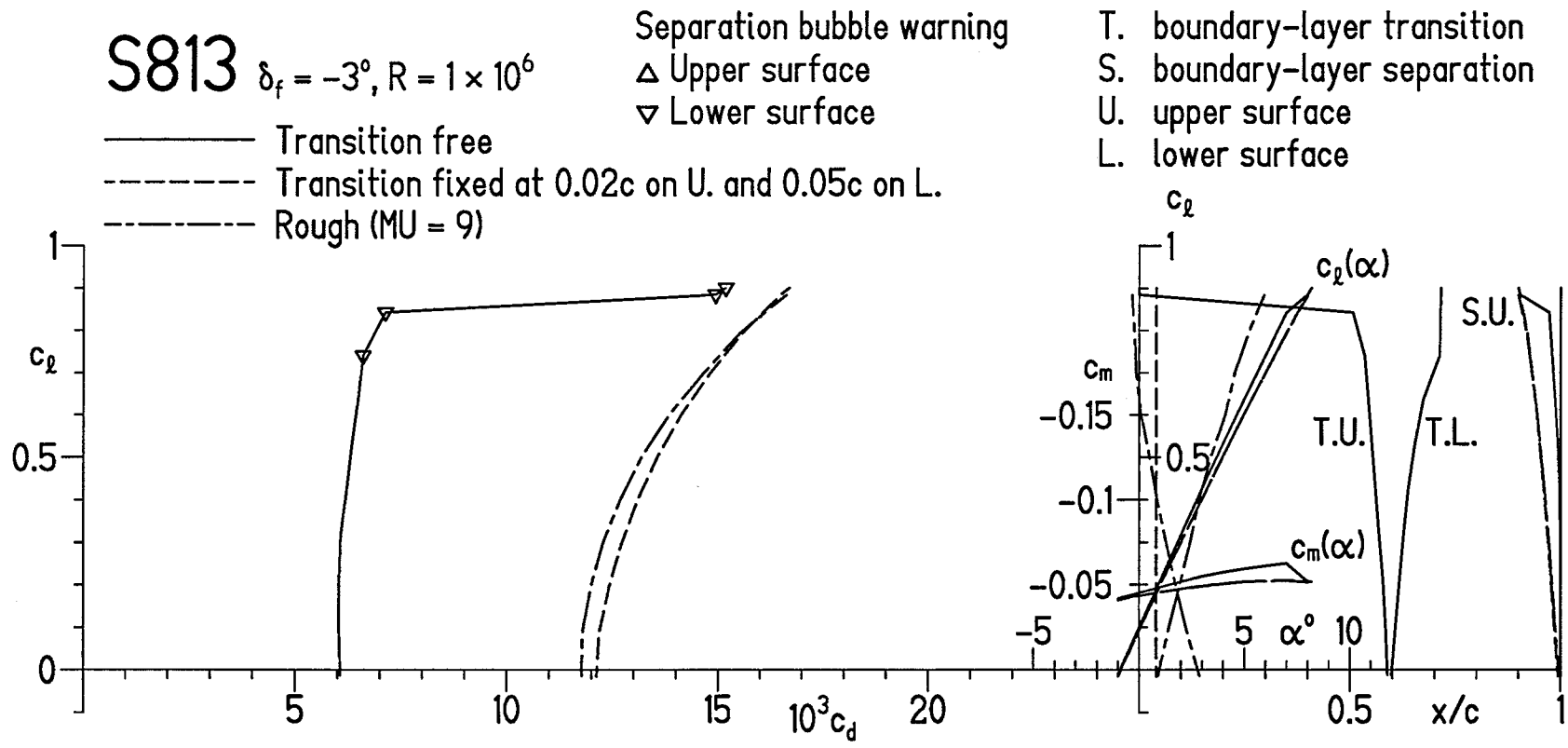

(a) $R = 1 \times 10^6$.

Figure 7.- Section characteristics with $\delta_f = -3°$ and transition free, transition fixed, and rough.

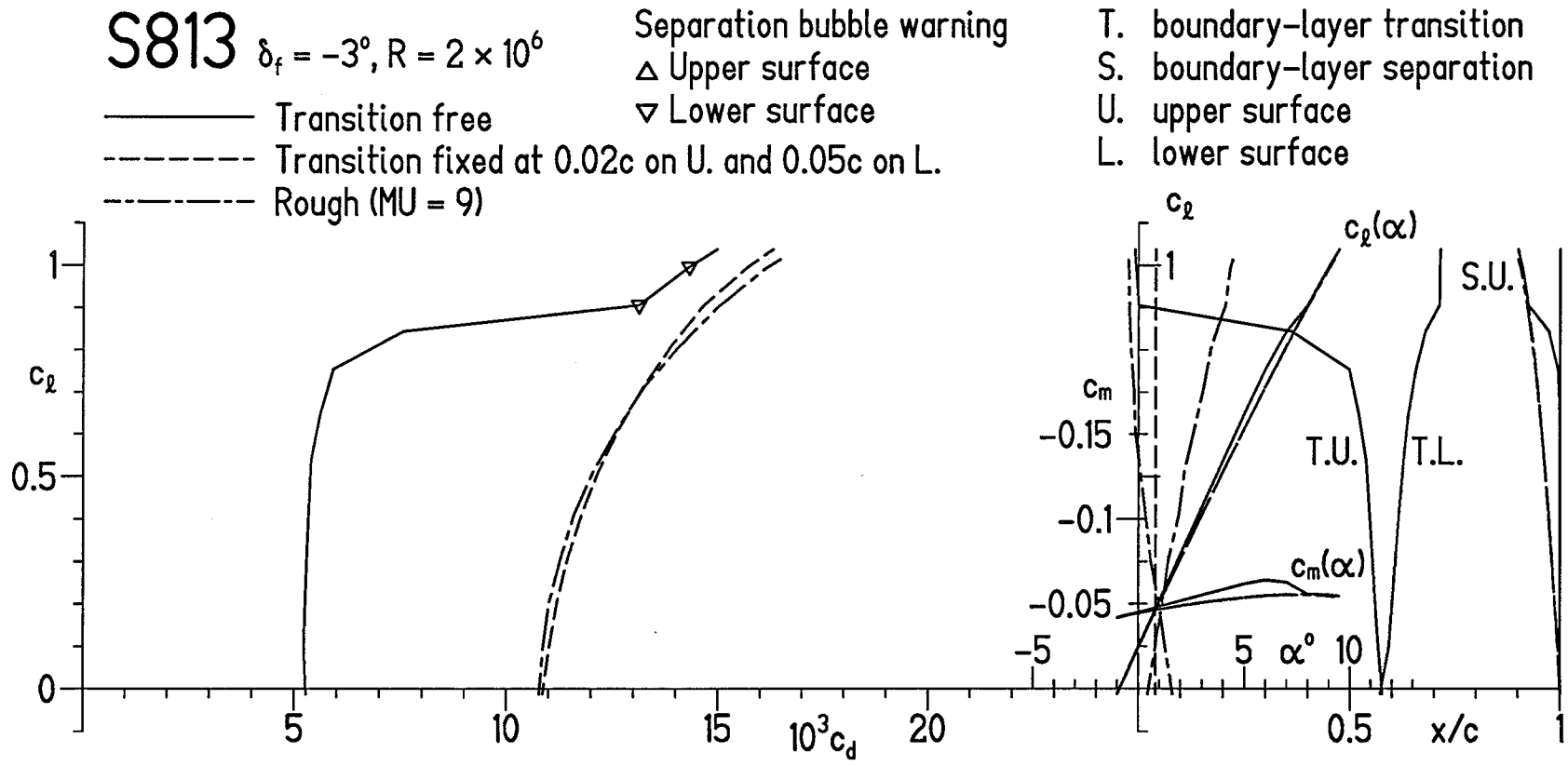

(b) R = 2×10^6.

Figure 7.- Continued.

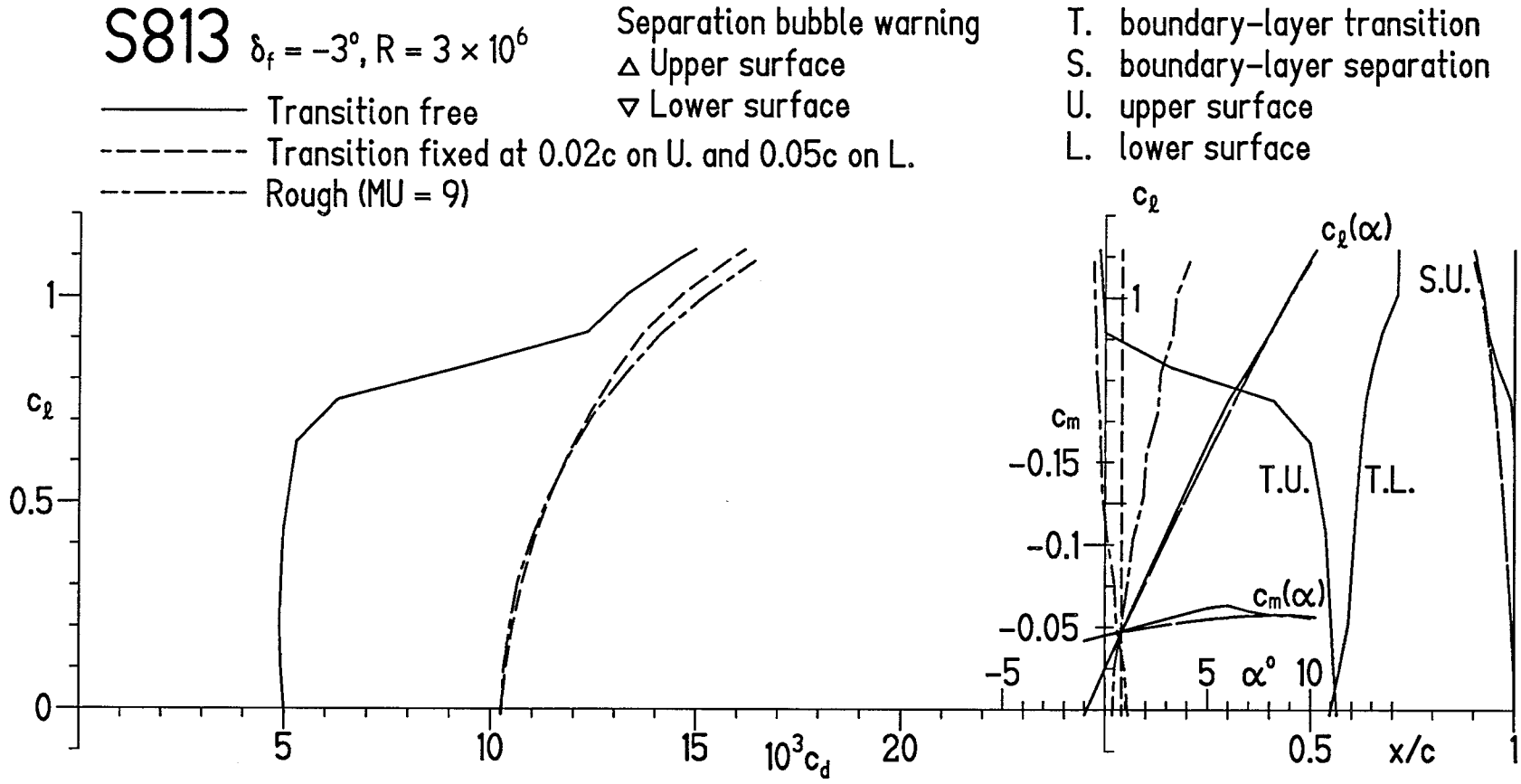

(c) $R = 3 \times 10^6$.

Figure 7.- Concluded.

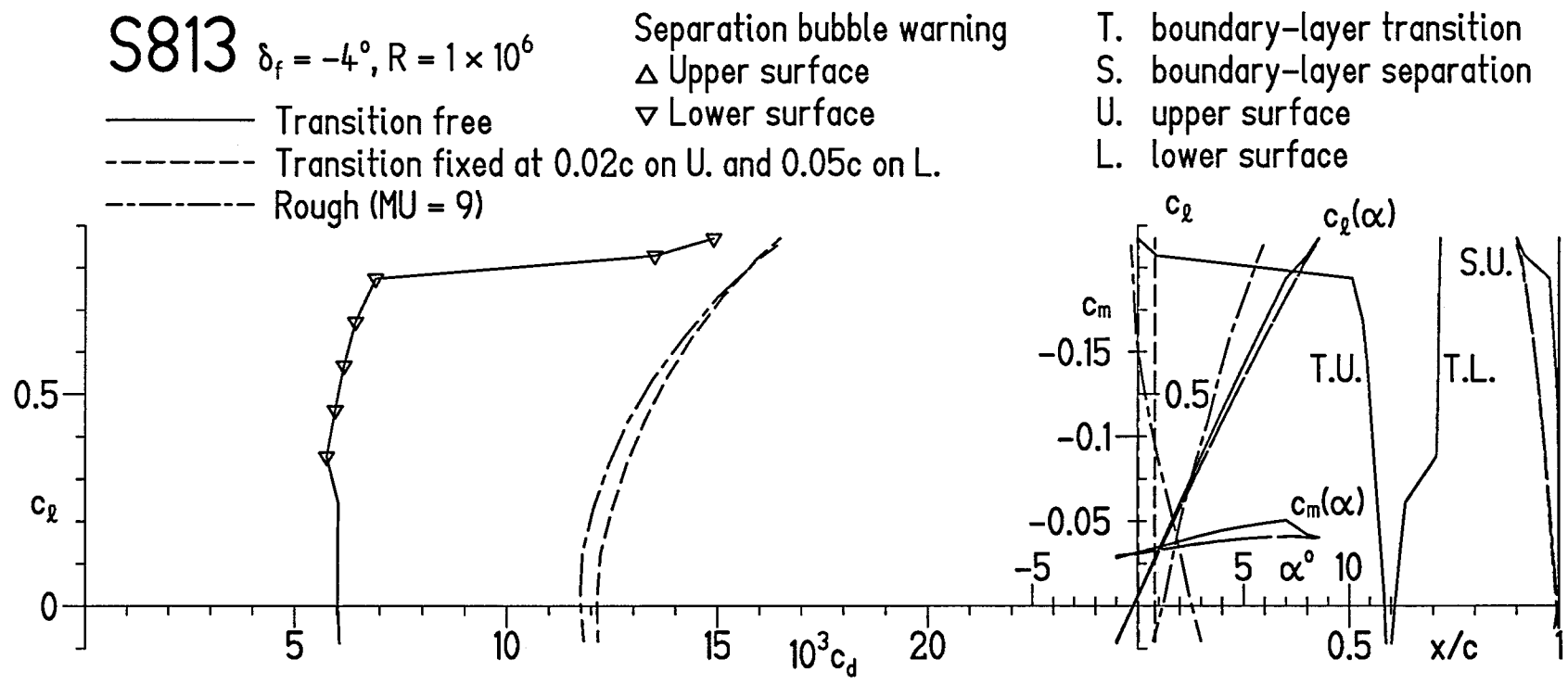

(a) $R = 1 \times 10^6$.

Figure 8.- Section characteristics with $\delta_f = -4°$ and transition free, transition fixed, and rough.

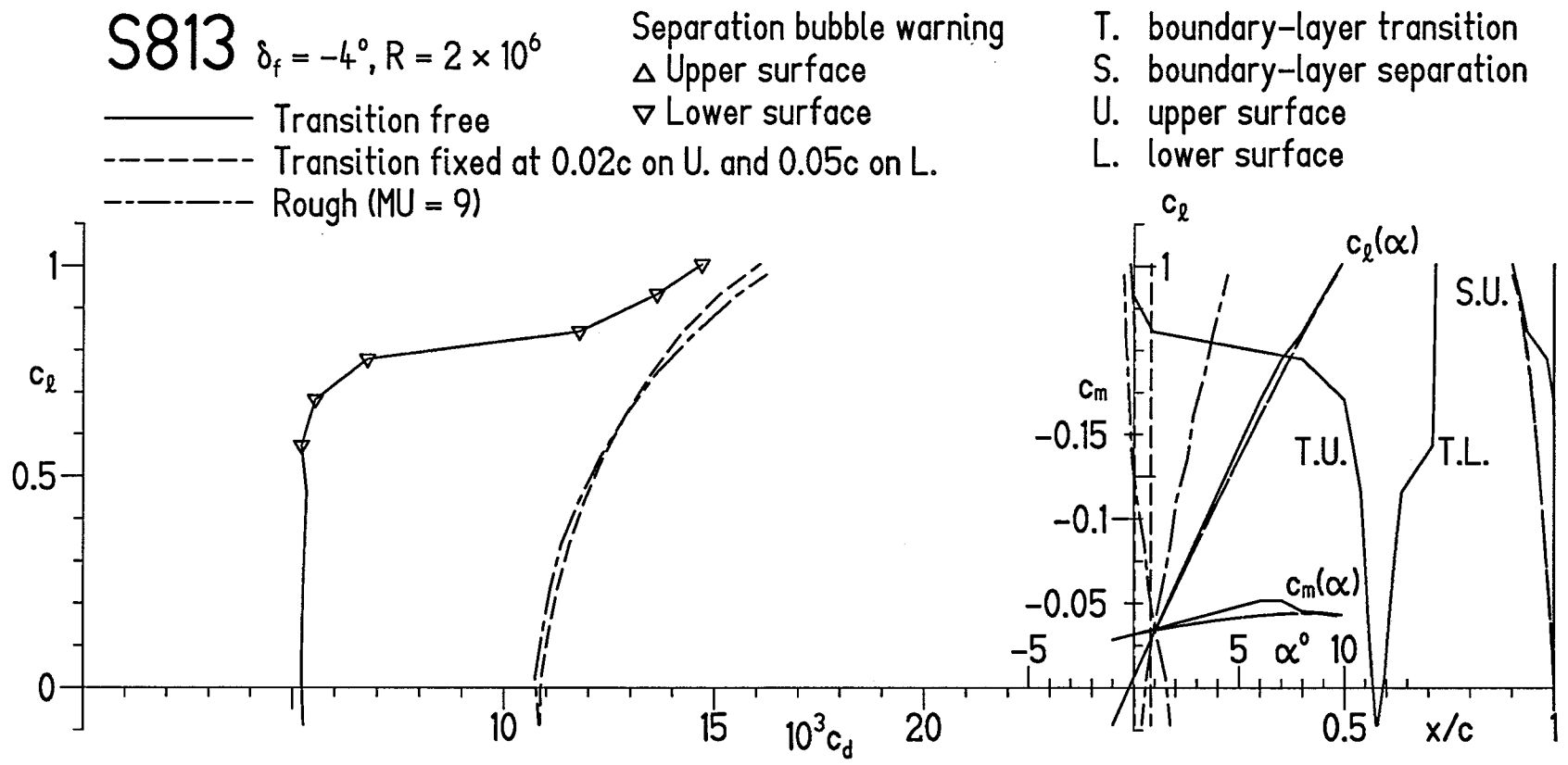

(b) $R = 2 \times 10^6$.

Figure 8.- Continued.

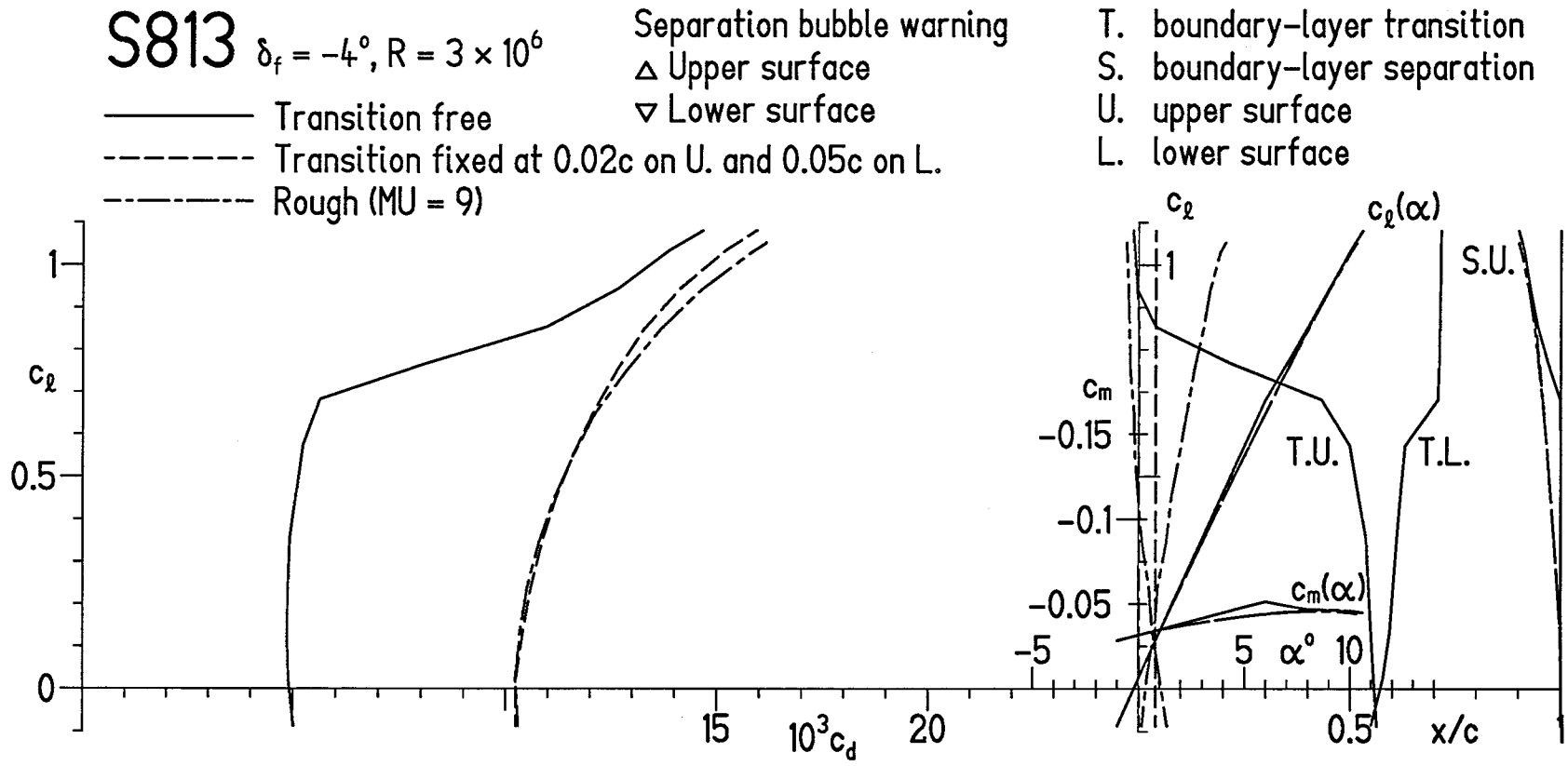

(c) R = 3 × 10^6.

Figure 8.- Concluded.

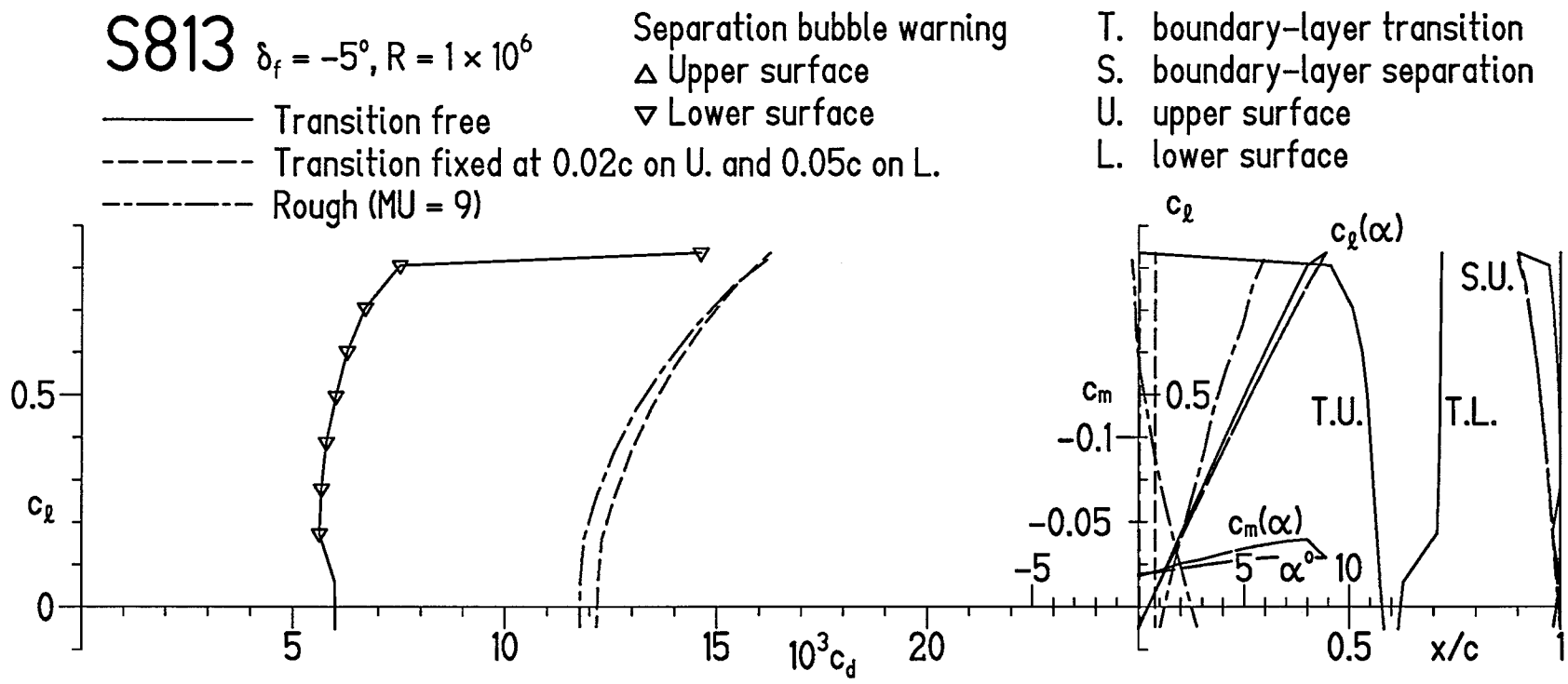

(a) R = 1 × 10^6.

Figure 9.- Section characteristics with $\delta_f = -5°$ and transition free, transition fixed, and rough.

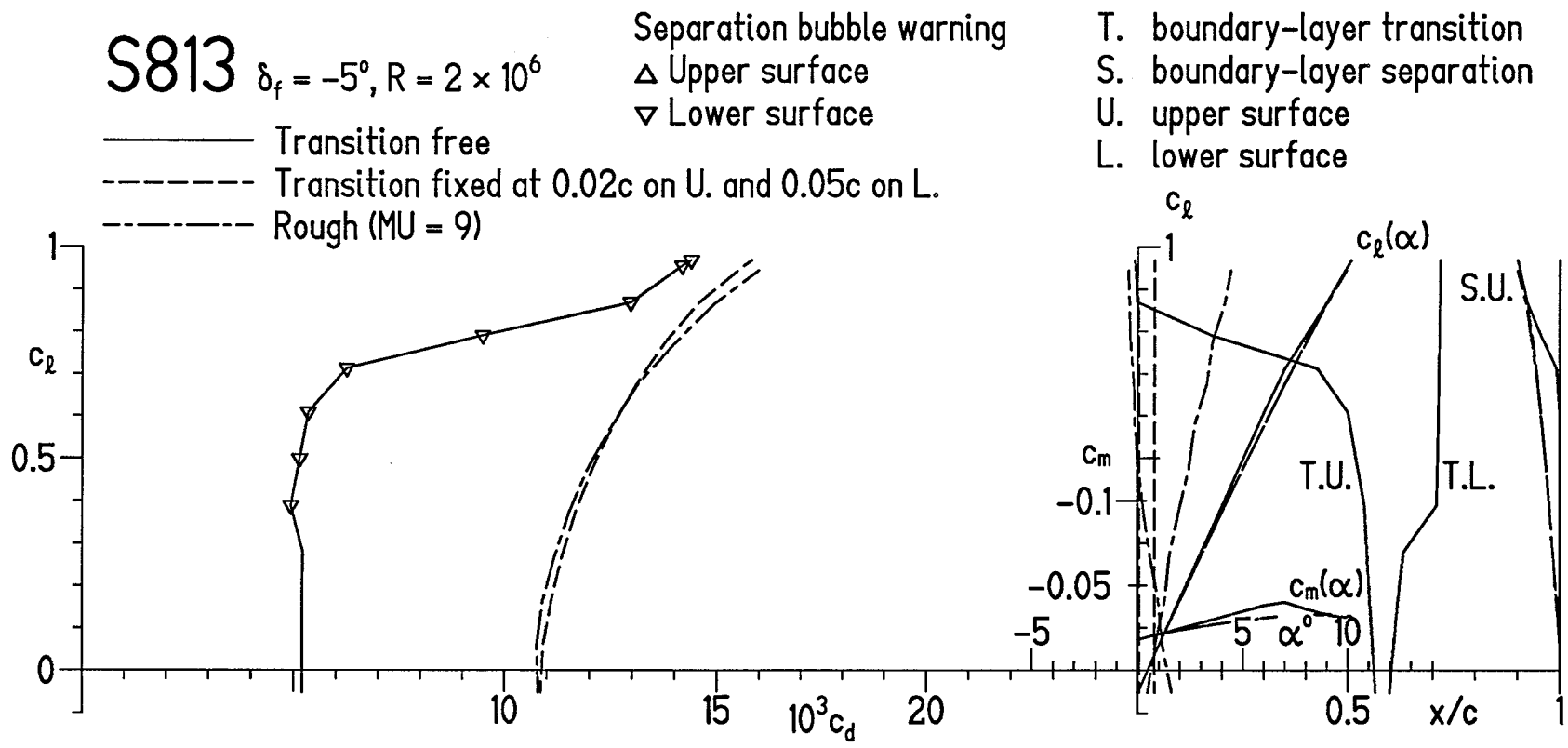

(b) R = 2×10^6.

Figure 9.- Continued.

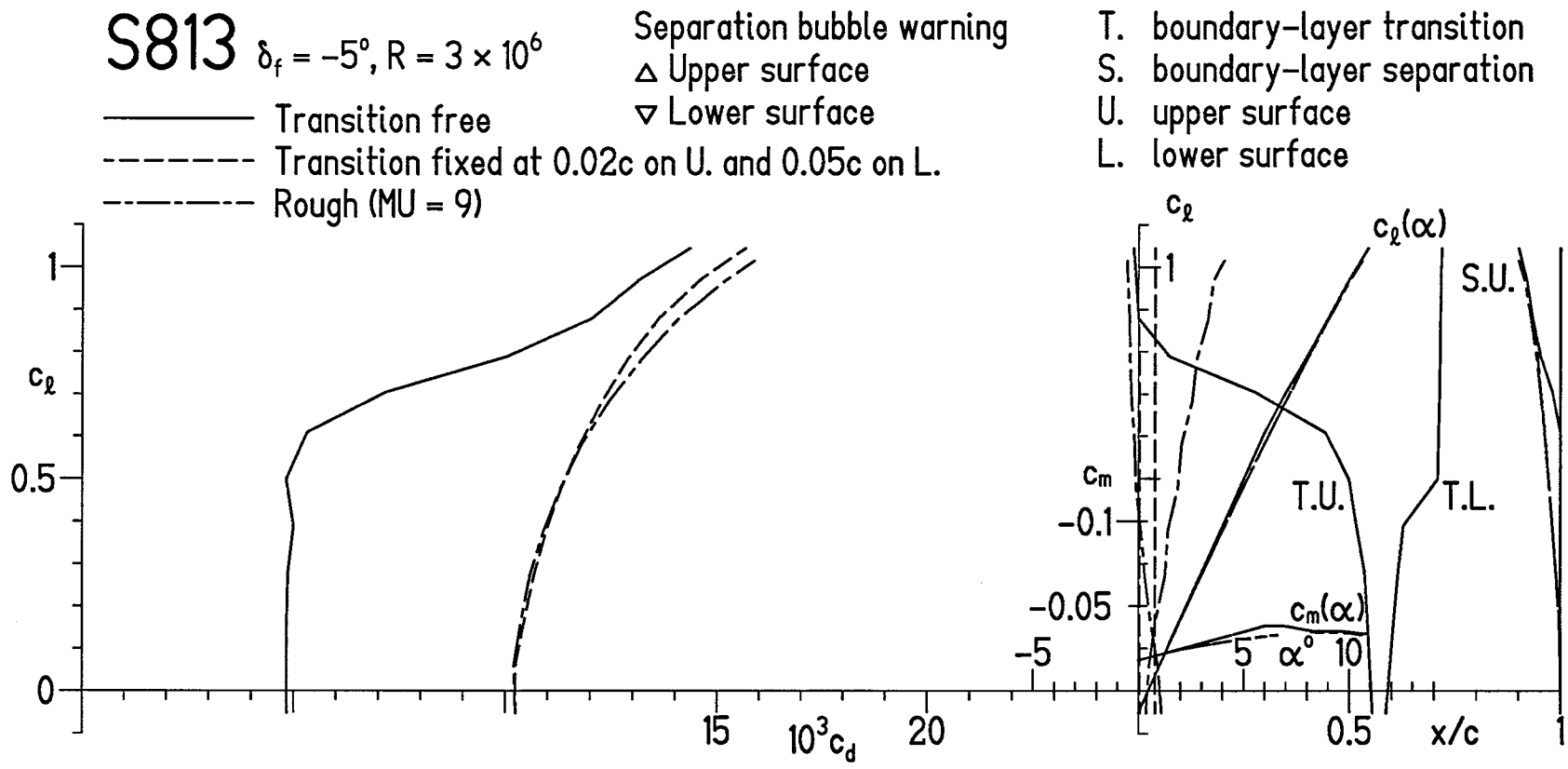

(c) R = 3×10^6.

Figure 9.- Concluded.

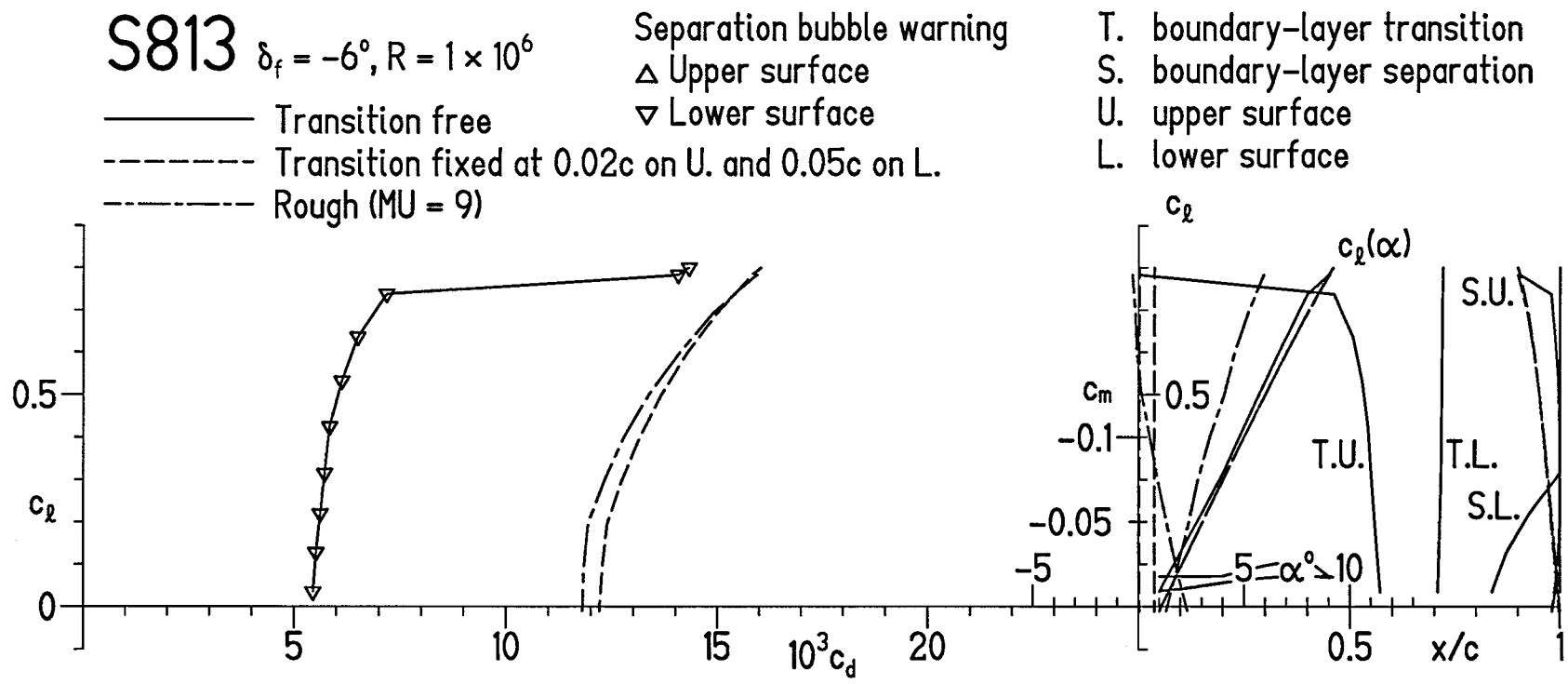

(a) R = 1 × 10^6.

Figure 10.- Section characteristics with $\delta_f = -6°$ and transition free, transition fixed, and rough.

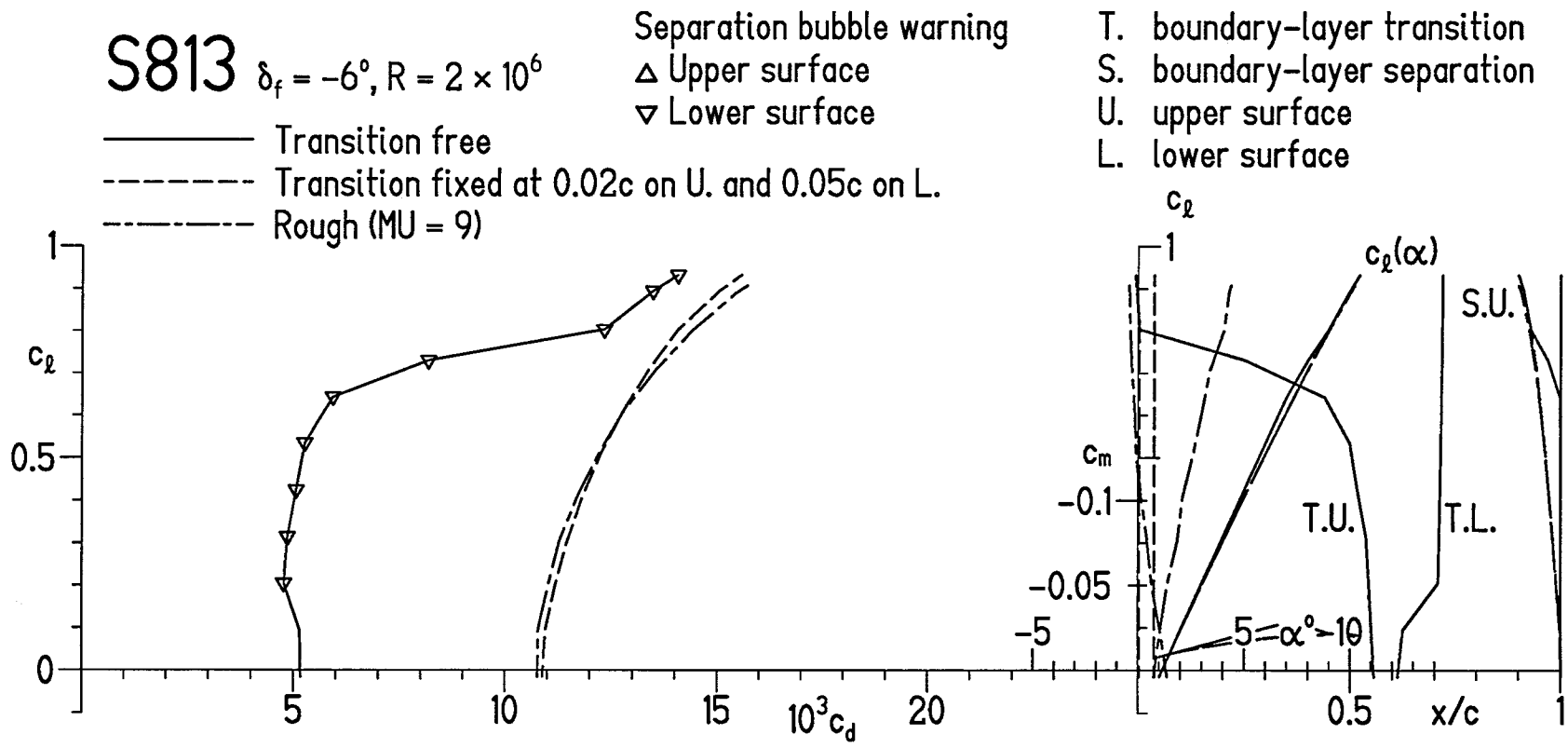

(b) $R = 2 \times 10^6$.

Figure 10.- Continued.

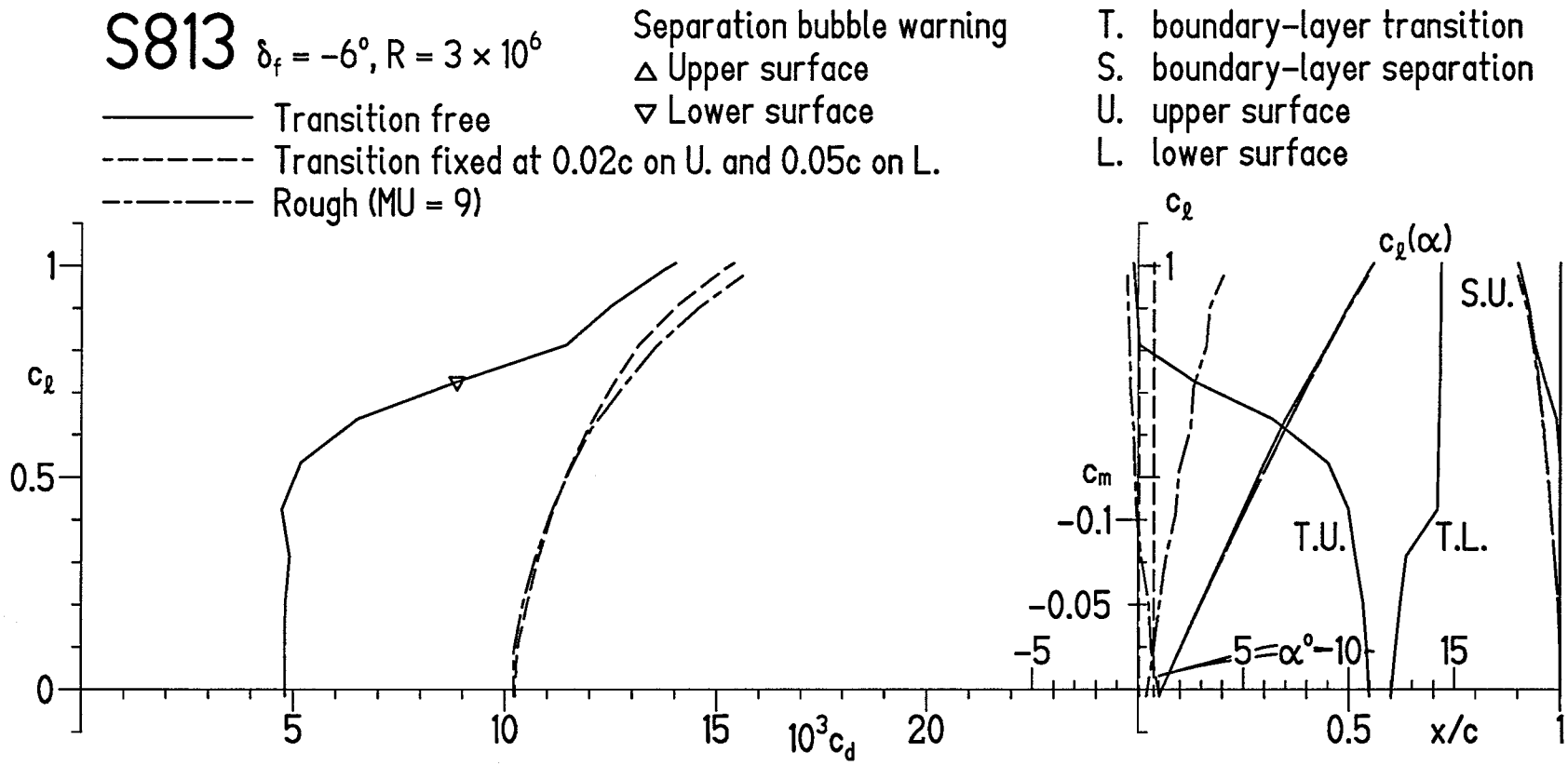

(c) R = 3×10^6.

Figure 10.- Concluded.

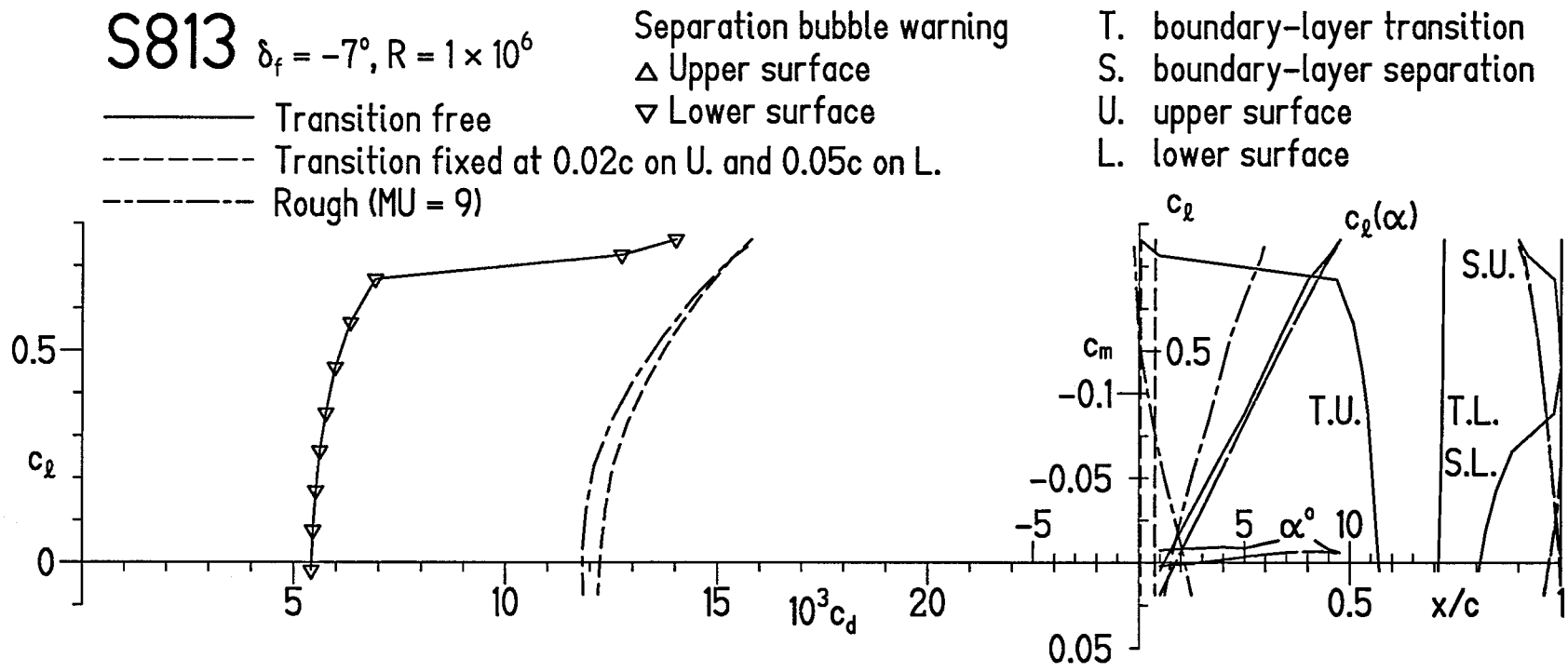

(a) R = 1 × 10^6.

Figure 11.- Section characteristics with $\delta_f = -7°$ and transition free, transition fixed, and rough.

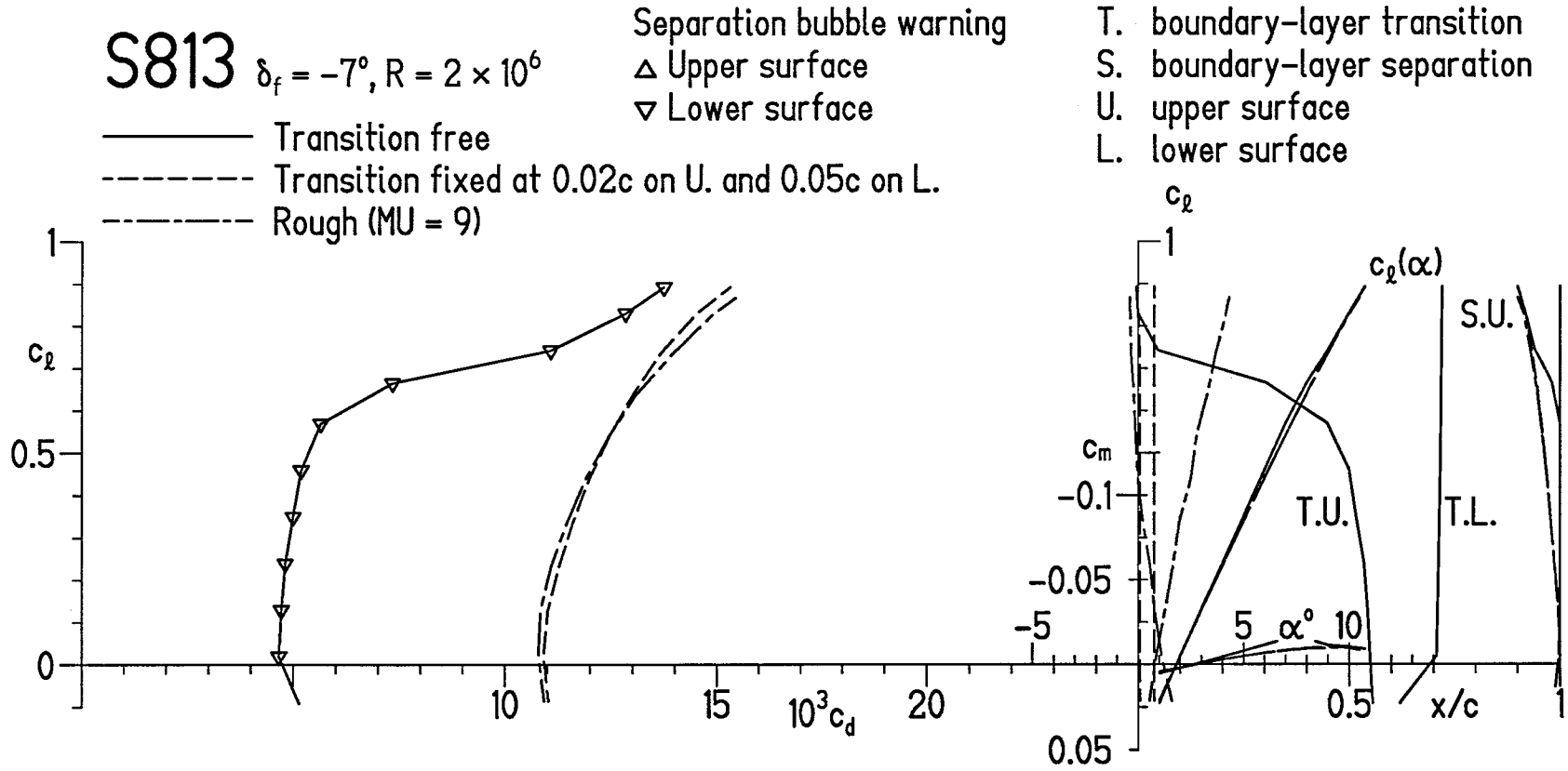

(b) R = 2×10^6.

Figure 11.- Continued.

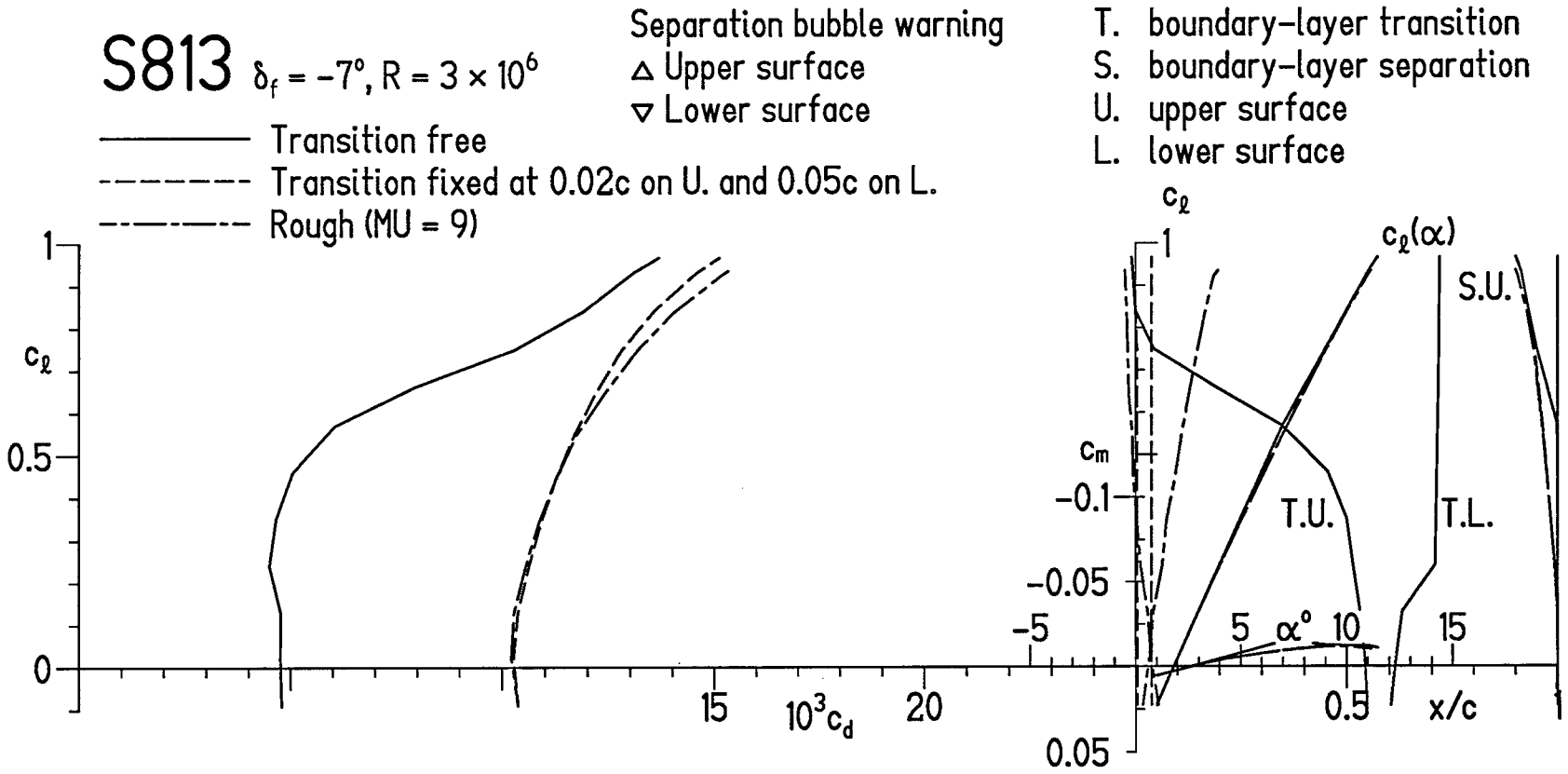

(c) R = 3×10^6.

Figure 11.- Concluded.

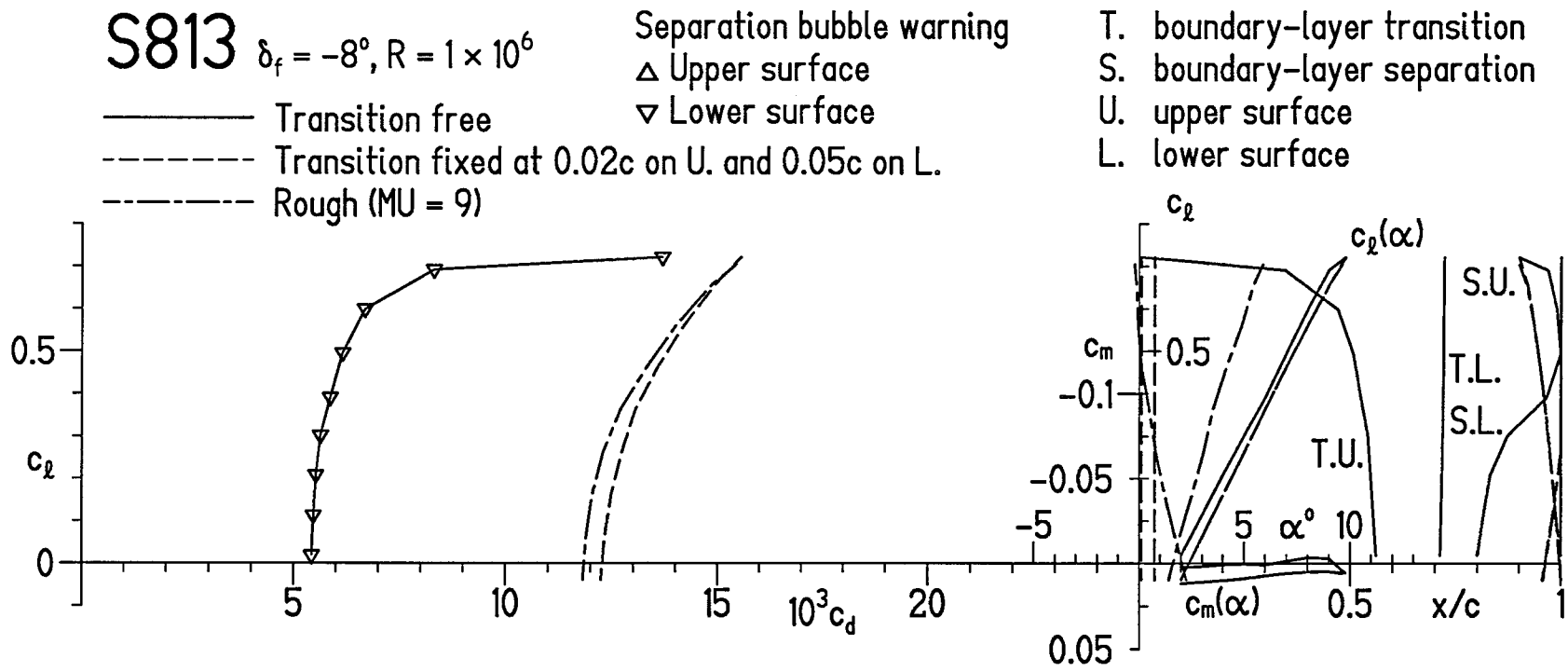

(a) $R = 1 \times 10^6$.

Figure 12.- Section characteristics with $\delta_f = -8°$ and transition free, transition fixed, and rough.

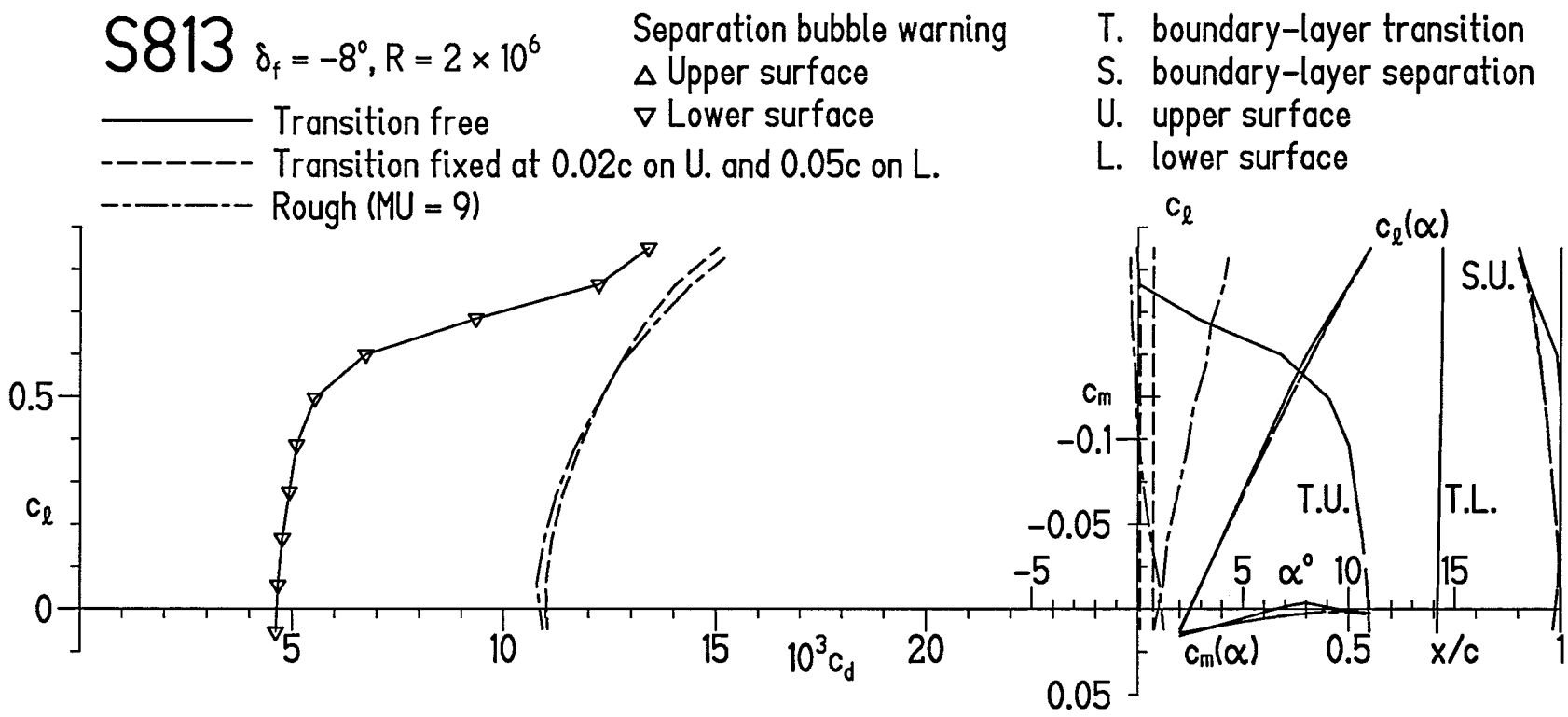

(b) $R = 2 \times 10^6$.

Figure 12.- Continued.

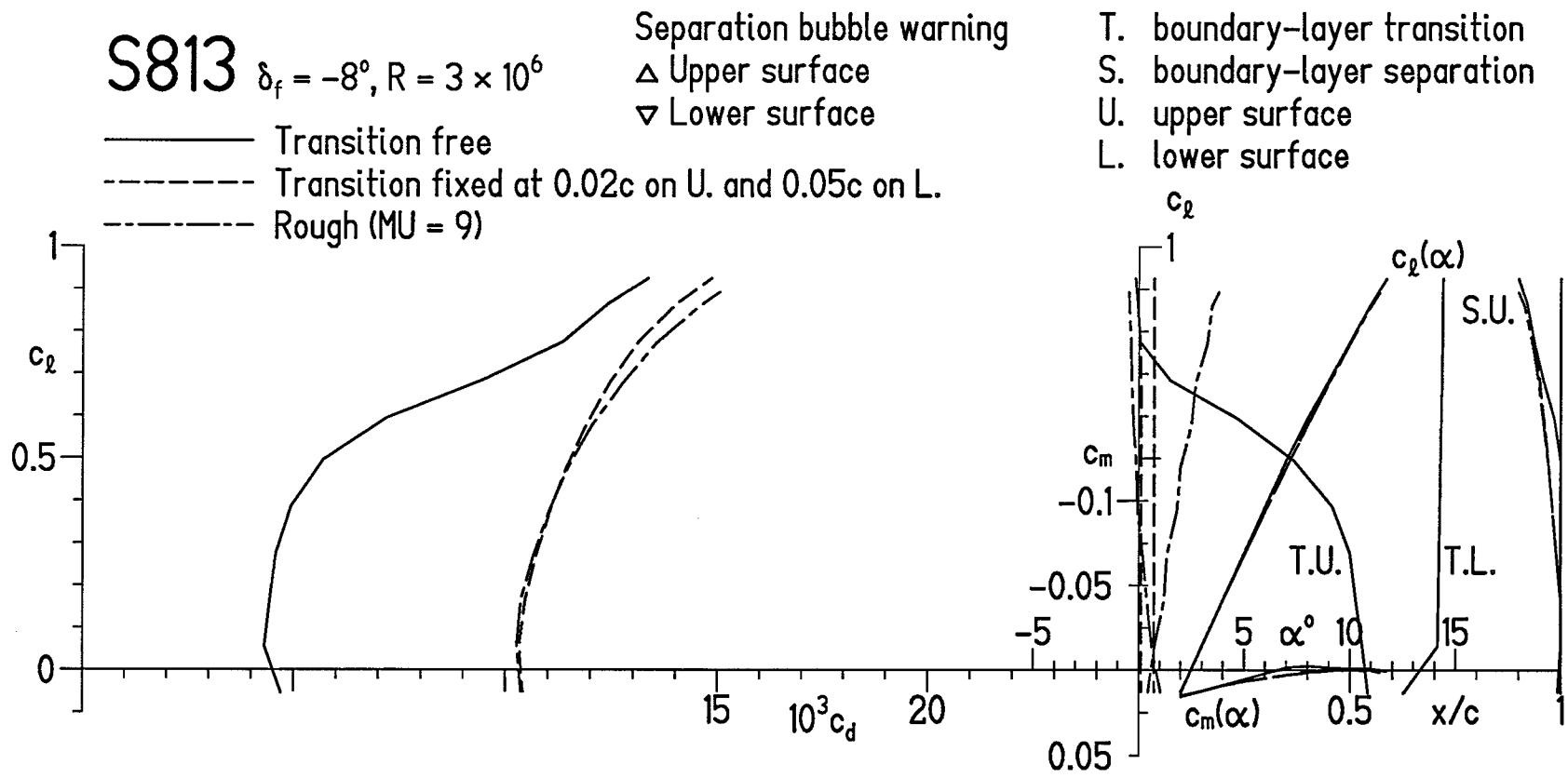

(c) R = 3×10^6.

Figure 12.- Concluded.

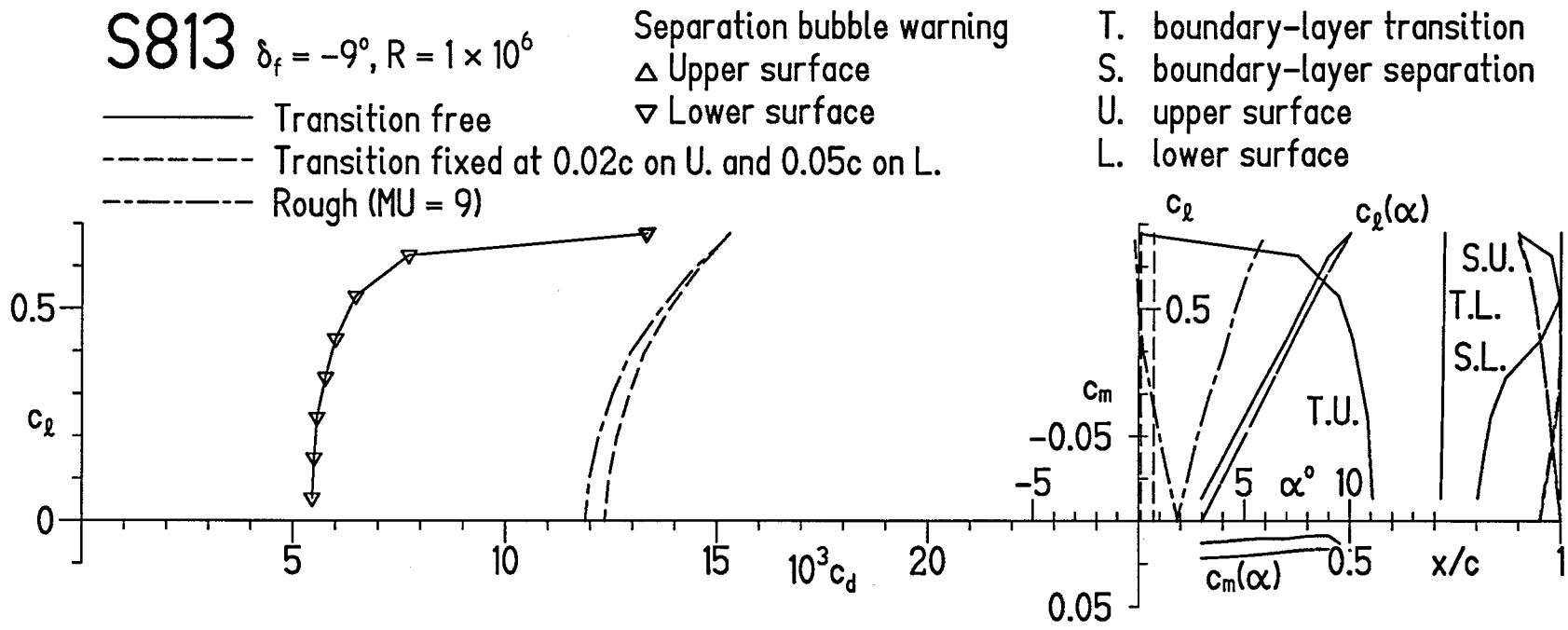

(a) R = 1 × 10^6.

Figure 13.- Section characteristics with $\delta_f = -9°$ and transition free, transition fixed, and rough.

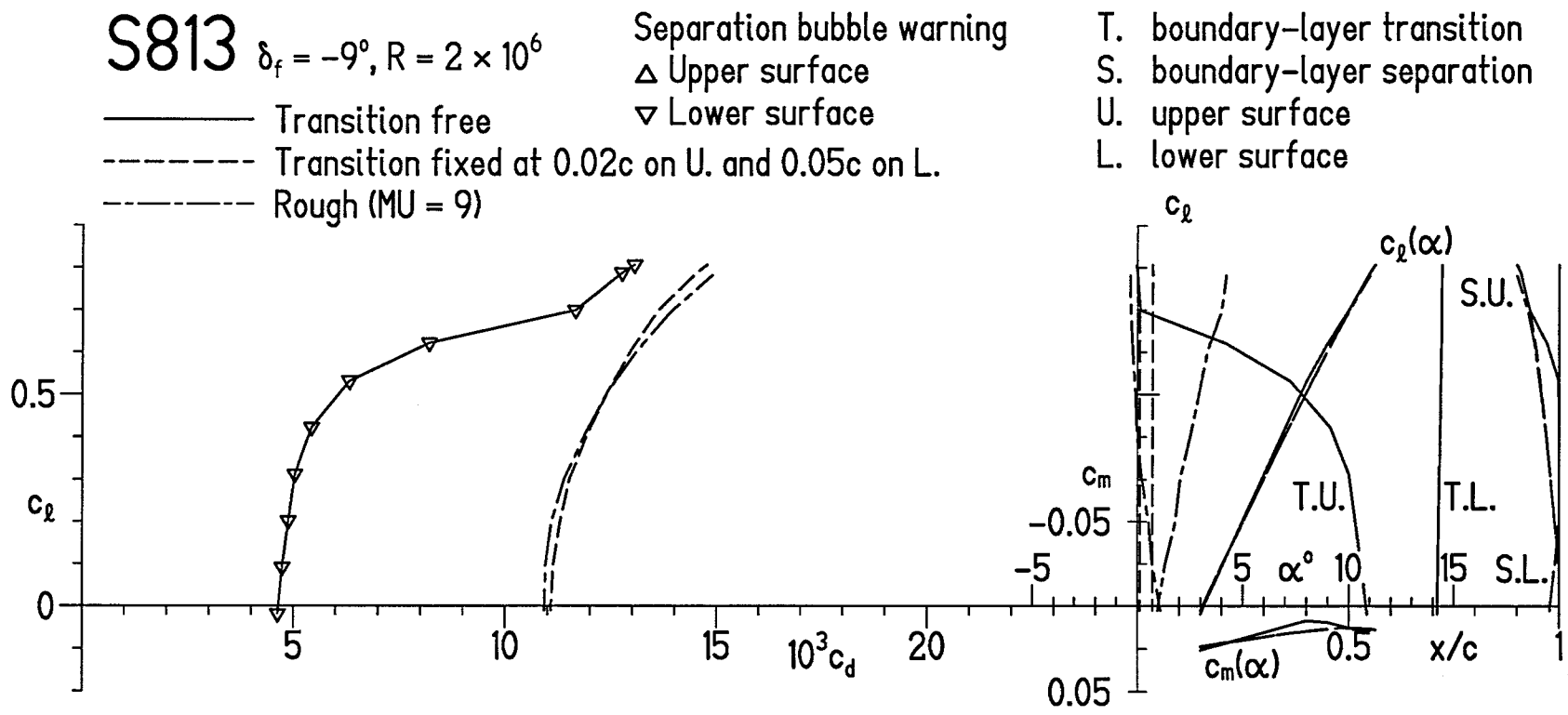

(b) R = 2×10^6.

Figure 13.- Continued.

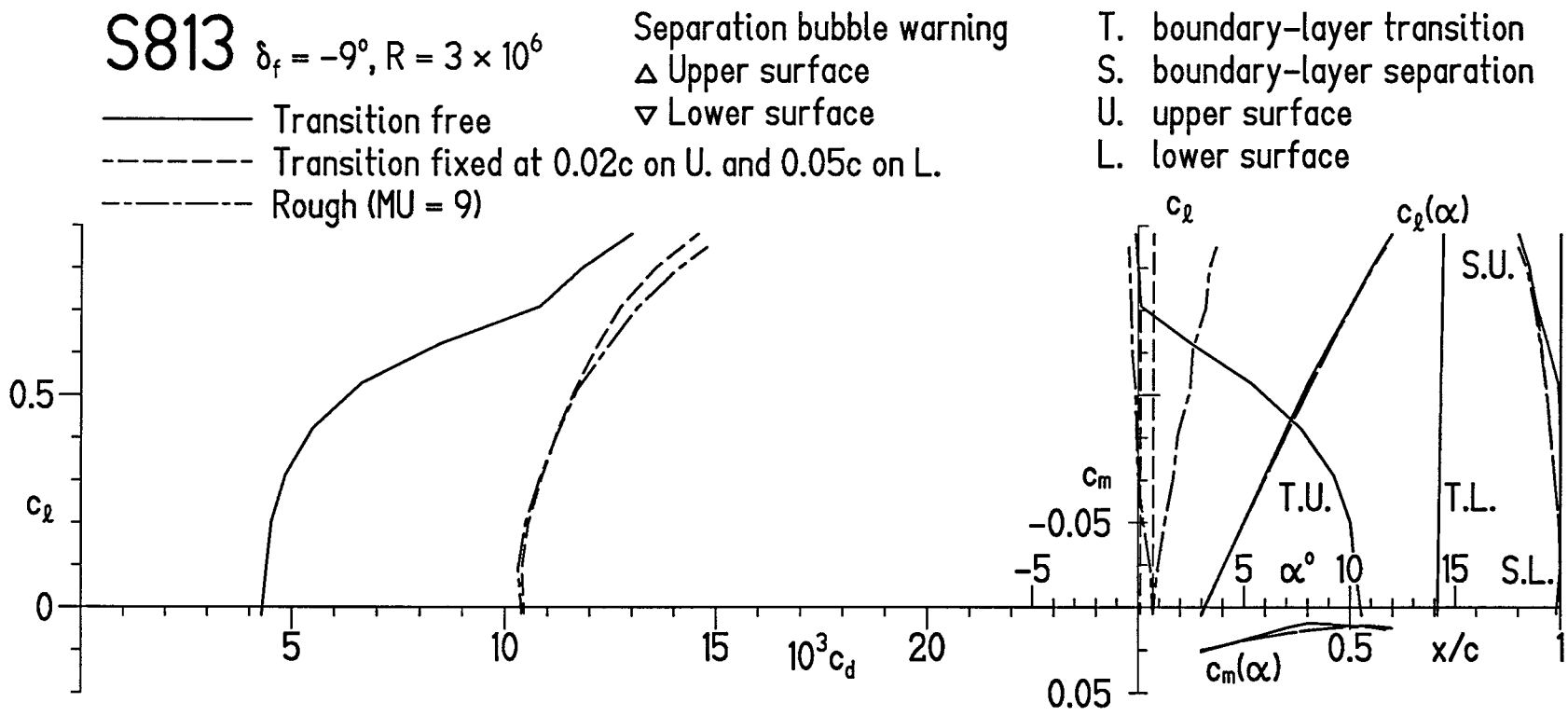

(c) R = 3×10^6.

Figure 13.- Concluded.

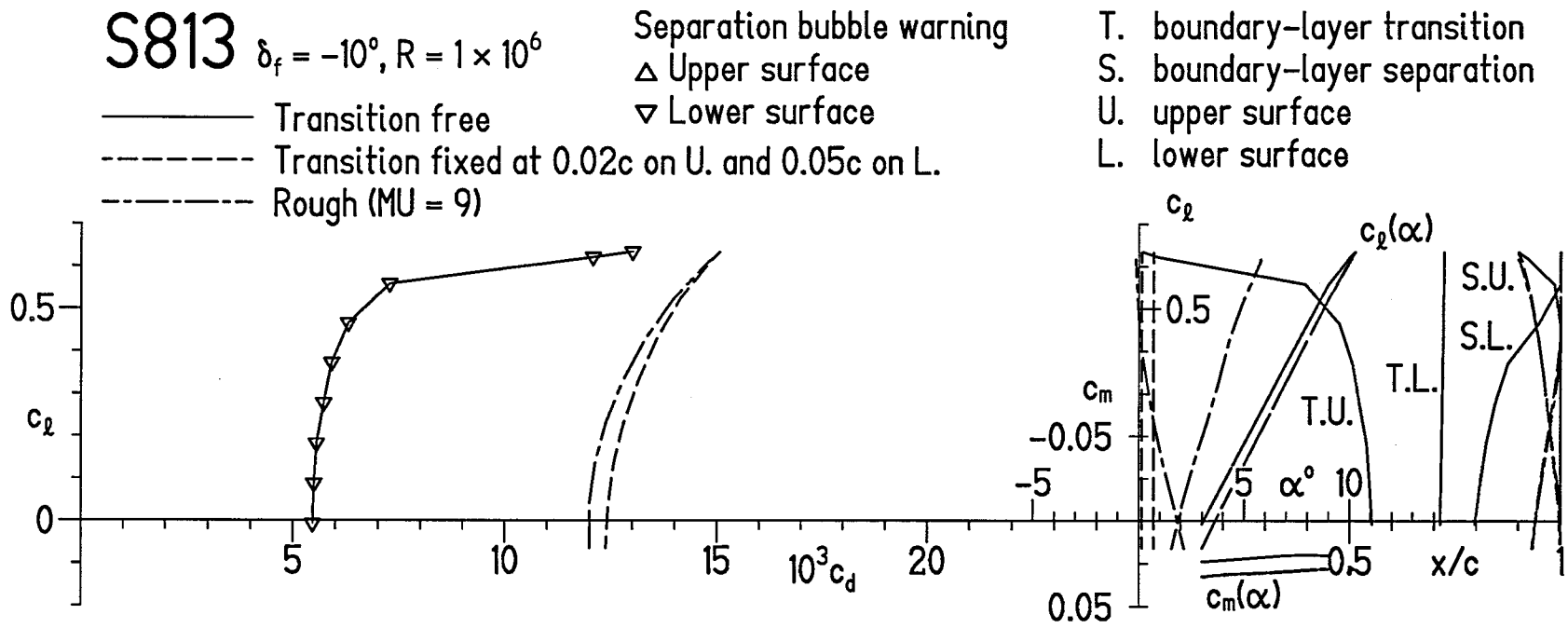

(a) $R = 1 \times 10^6$.

Figure 14.- Section characteristics with $\delta_f = -10°$ and transition free, transition fixed, and rough.

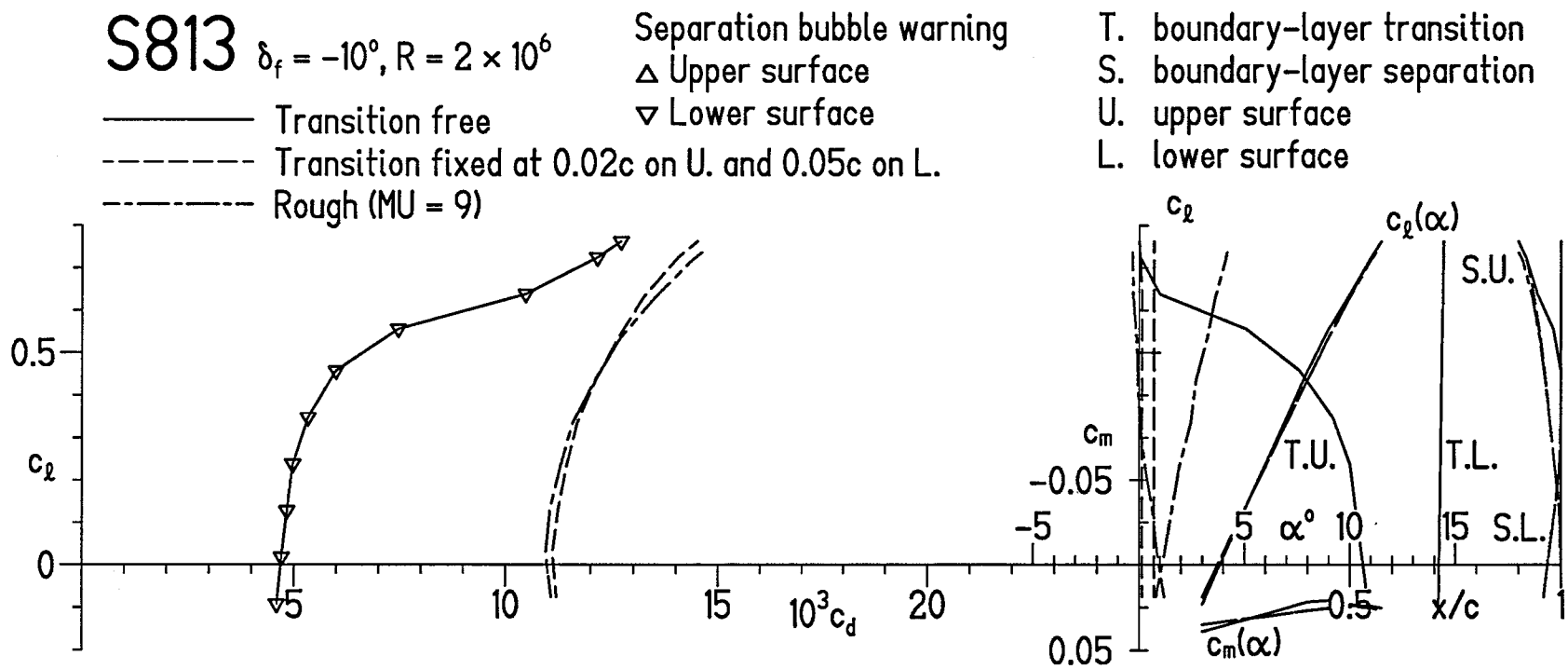

(b) R = 2×10^6.

Figure 14.- Continued.

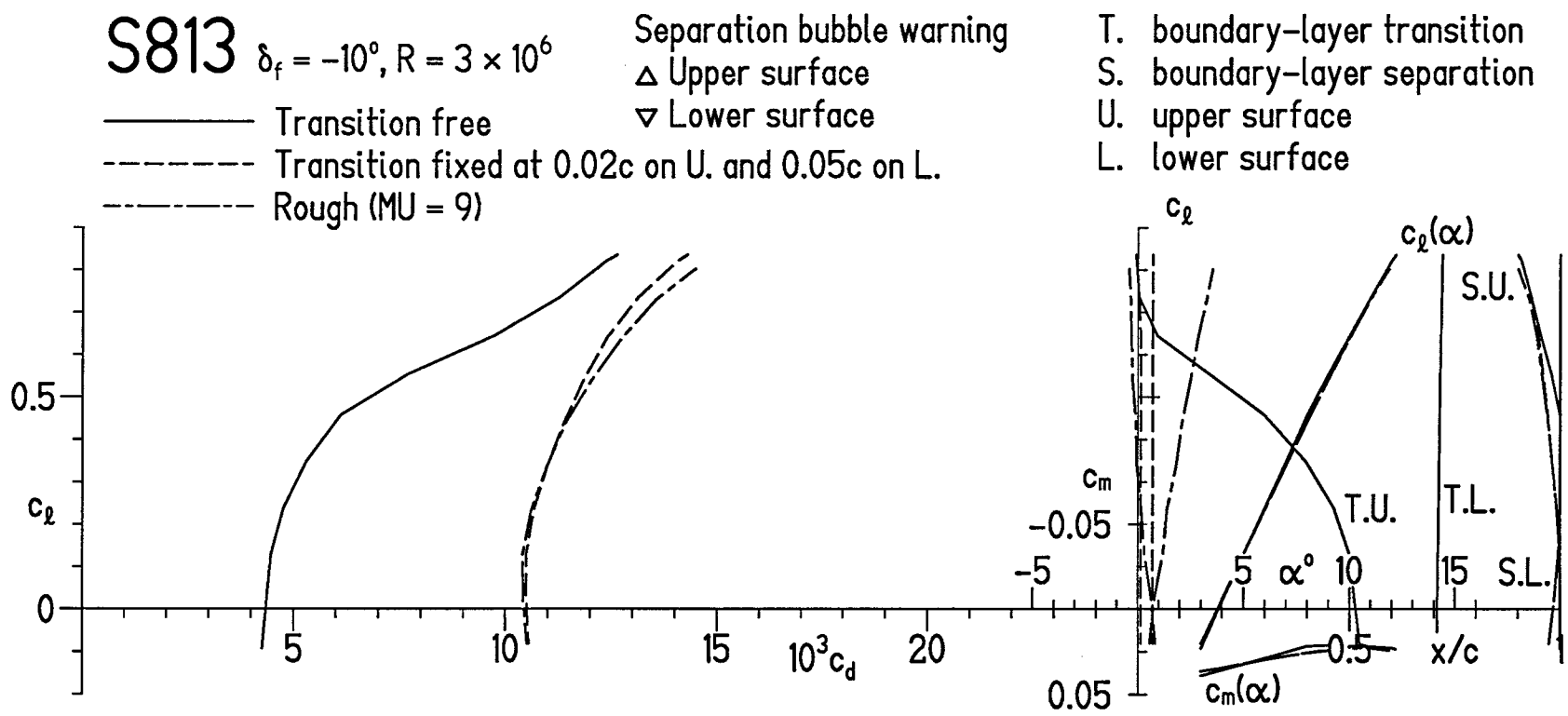

(c) $R = 3 \times 10^6$.

Figure 14.- Concluded.

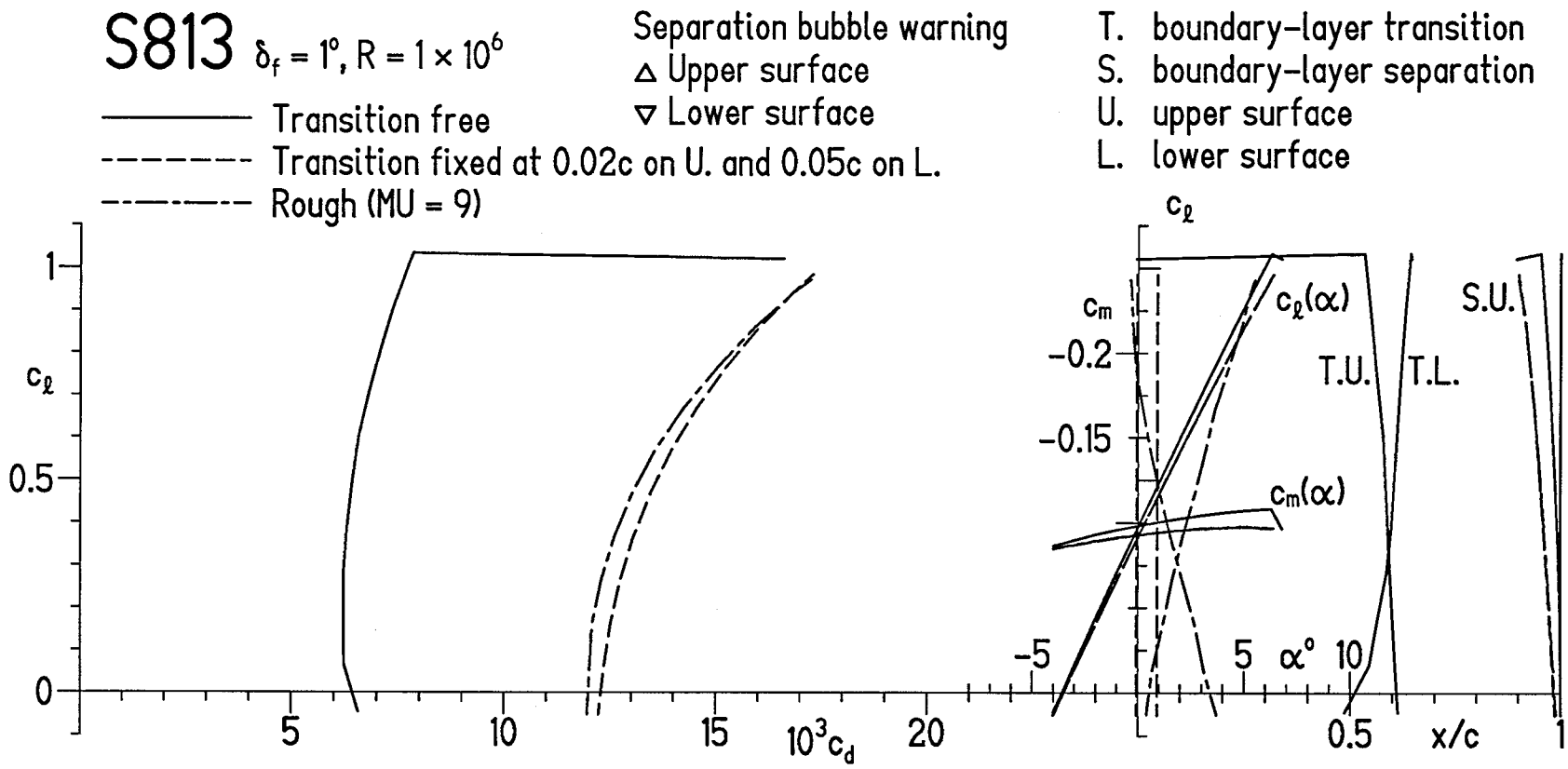

(a) $R = 1 \times 10^6$.

Figure 15.- Section characteristics with $\delta_f = 1°$ and transition free, transition fixed, and rough.

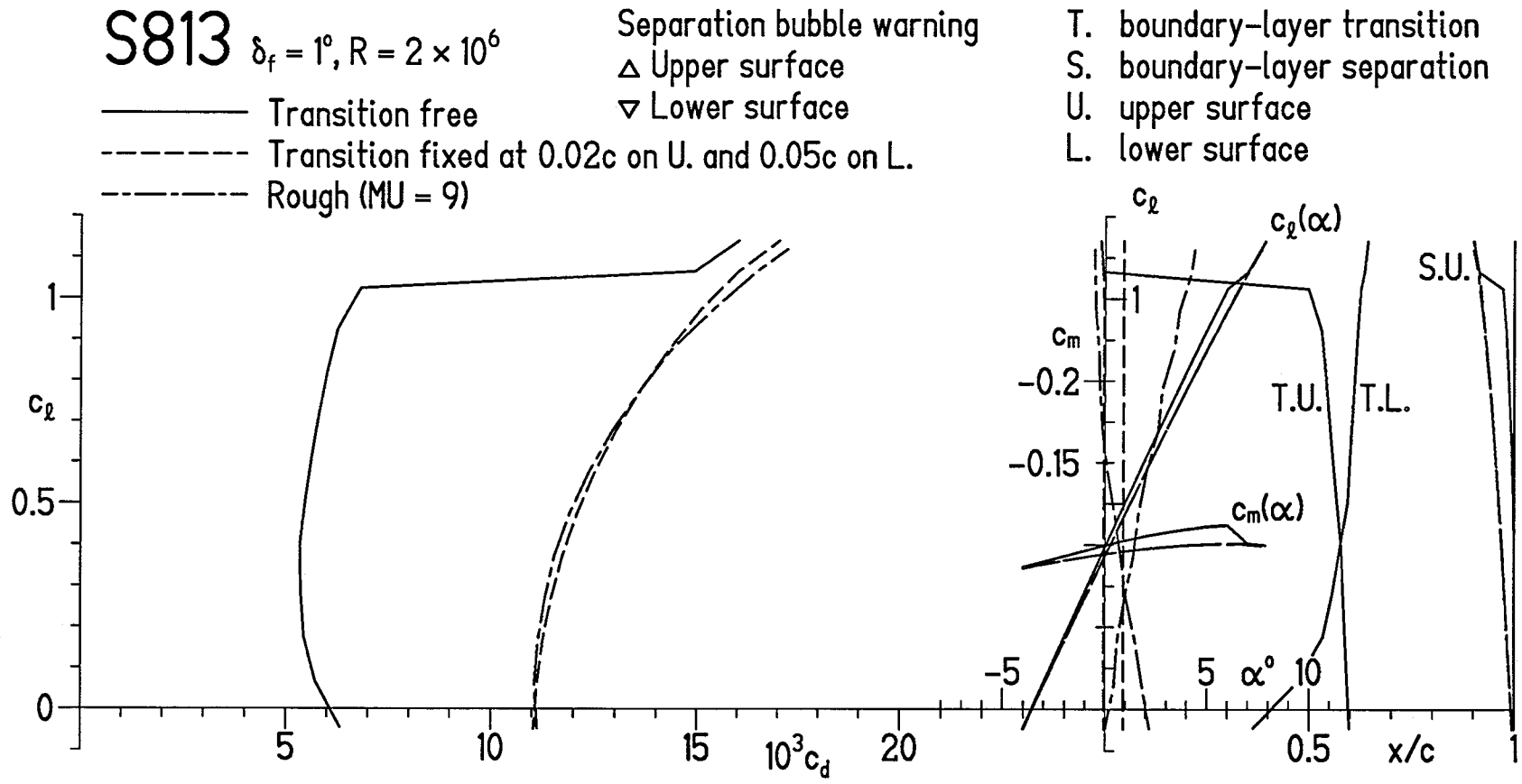

(b) R = 2 × 10^6.

Figure 15.- Continued.

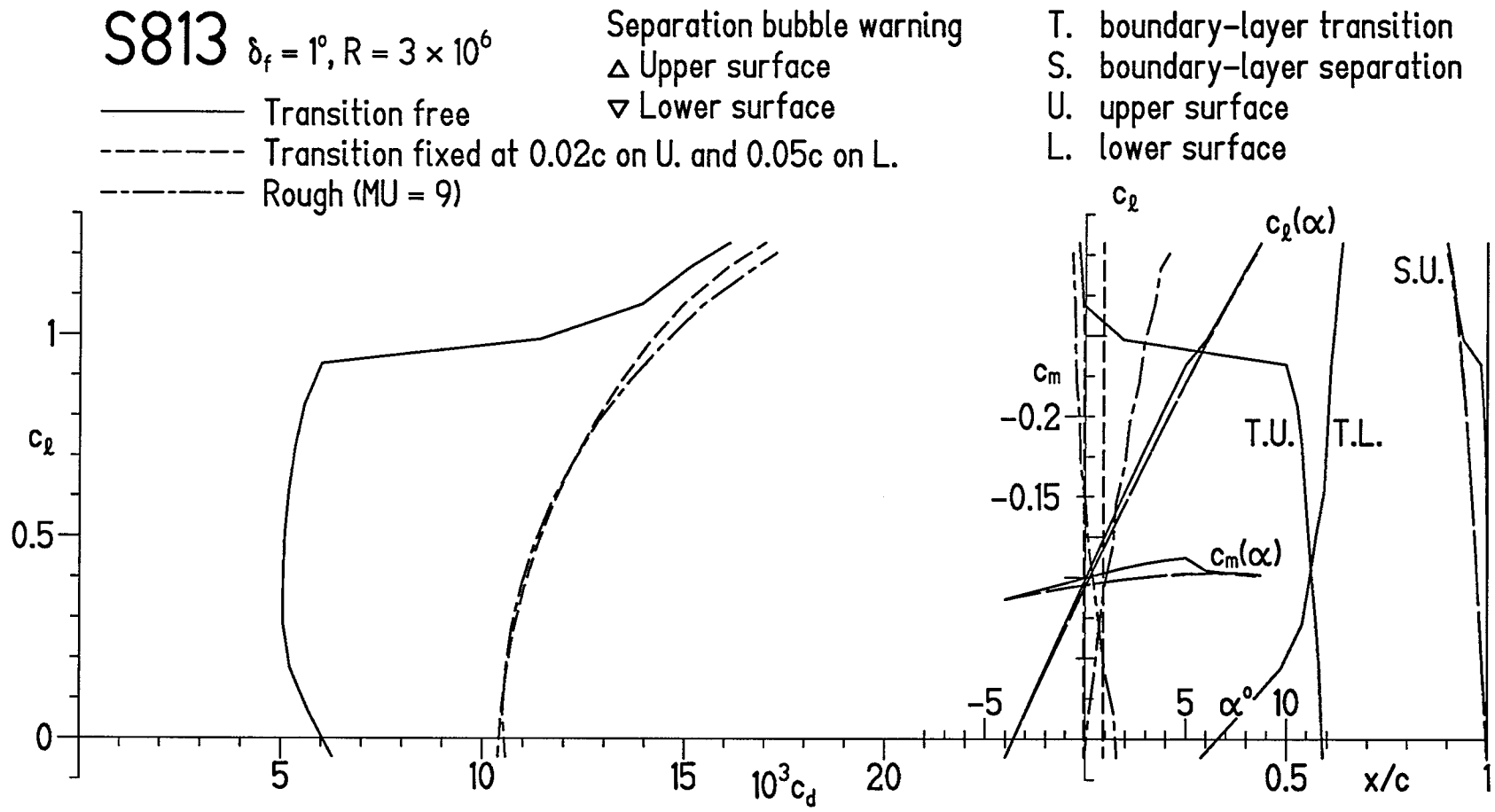

(c) $R = 3 \times 10^6$.

Figure 15.- Concluded.

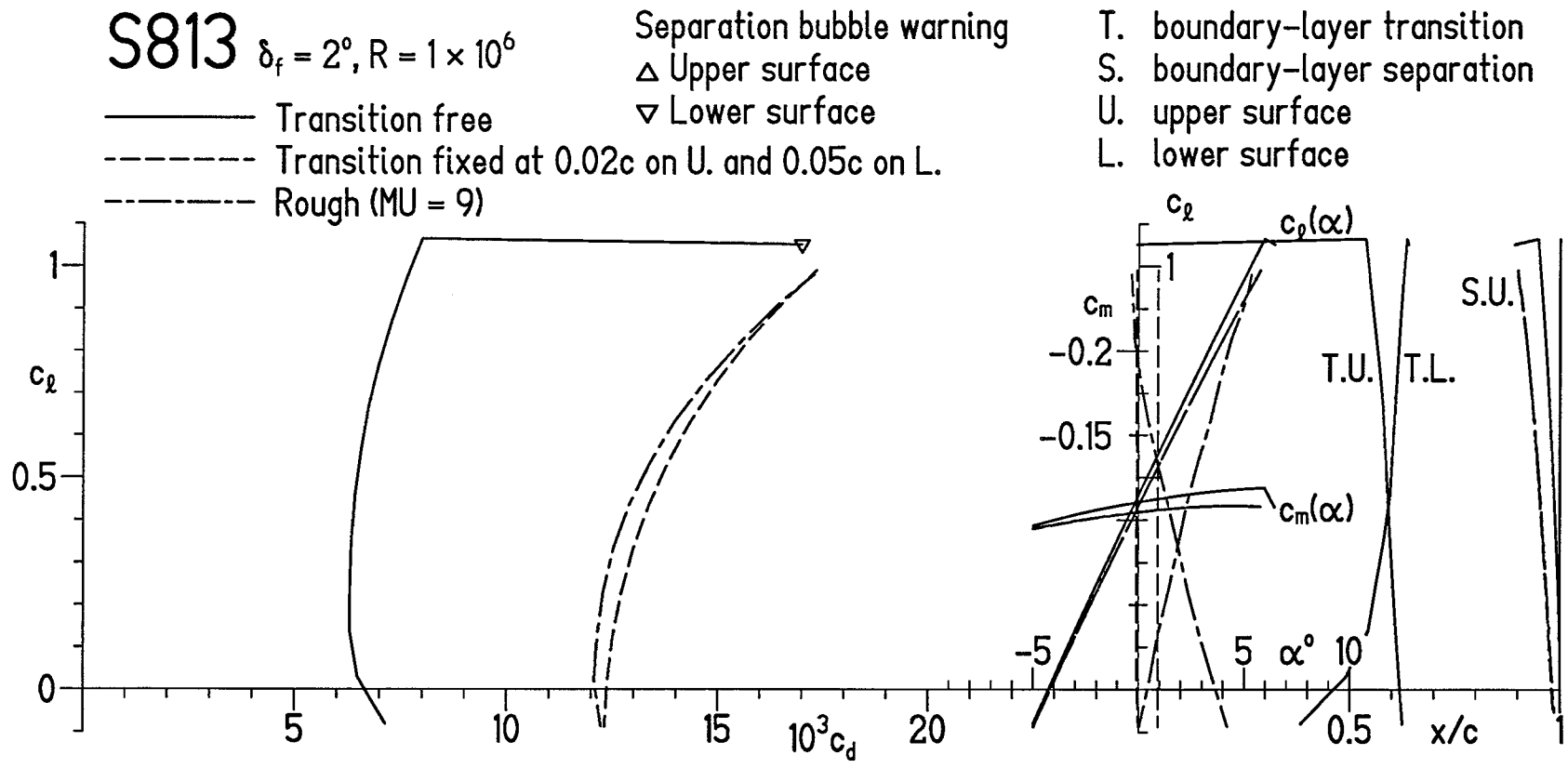

(a) $R = 1 \times 10^6$.

Figure 16.- Section characteristics with $\delta_f = 2°$ and transition free, transition fixed, and rough.

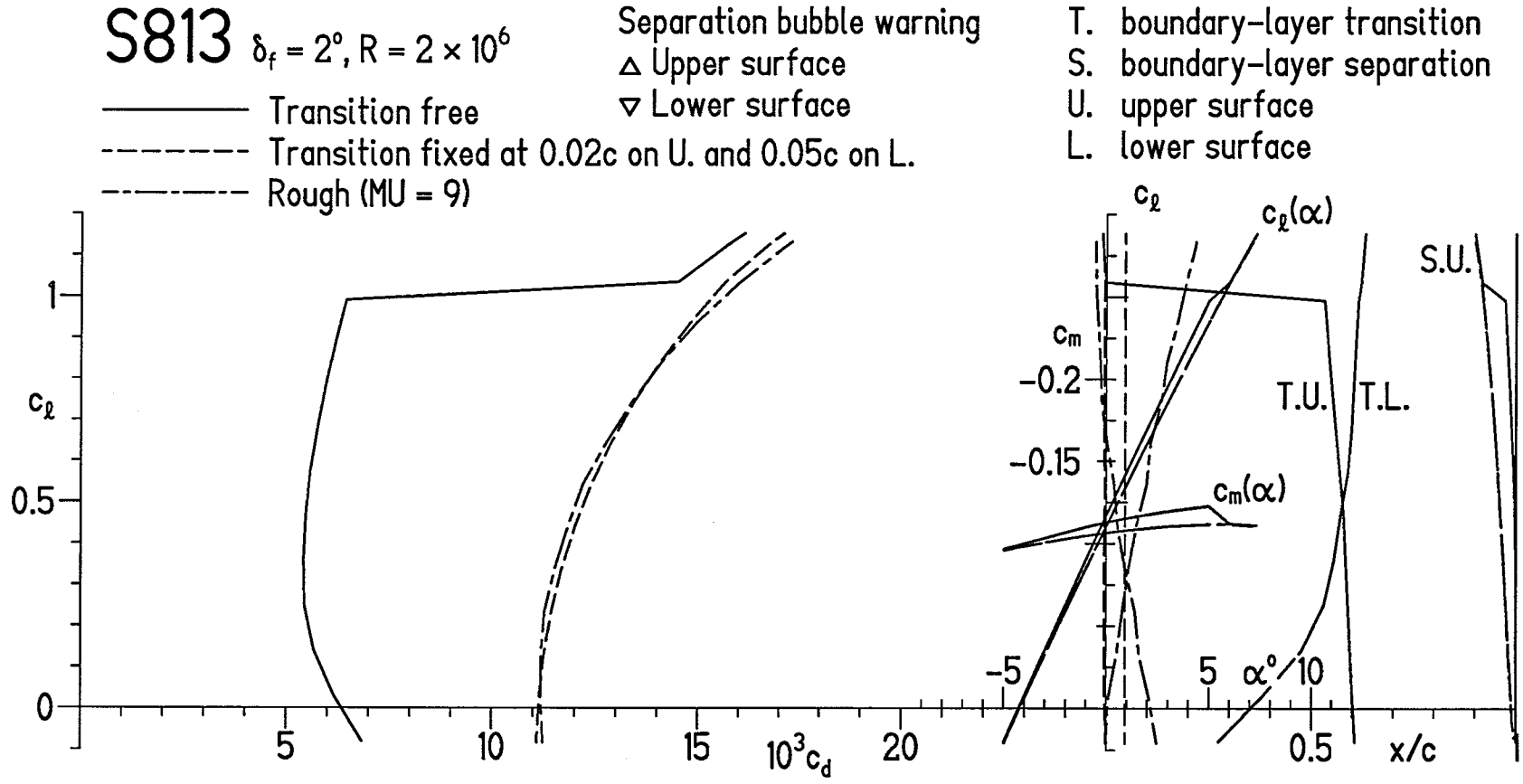

(b) $R = 2 \times 10^6$.

Figure 16.- Continued.

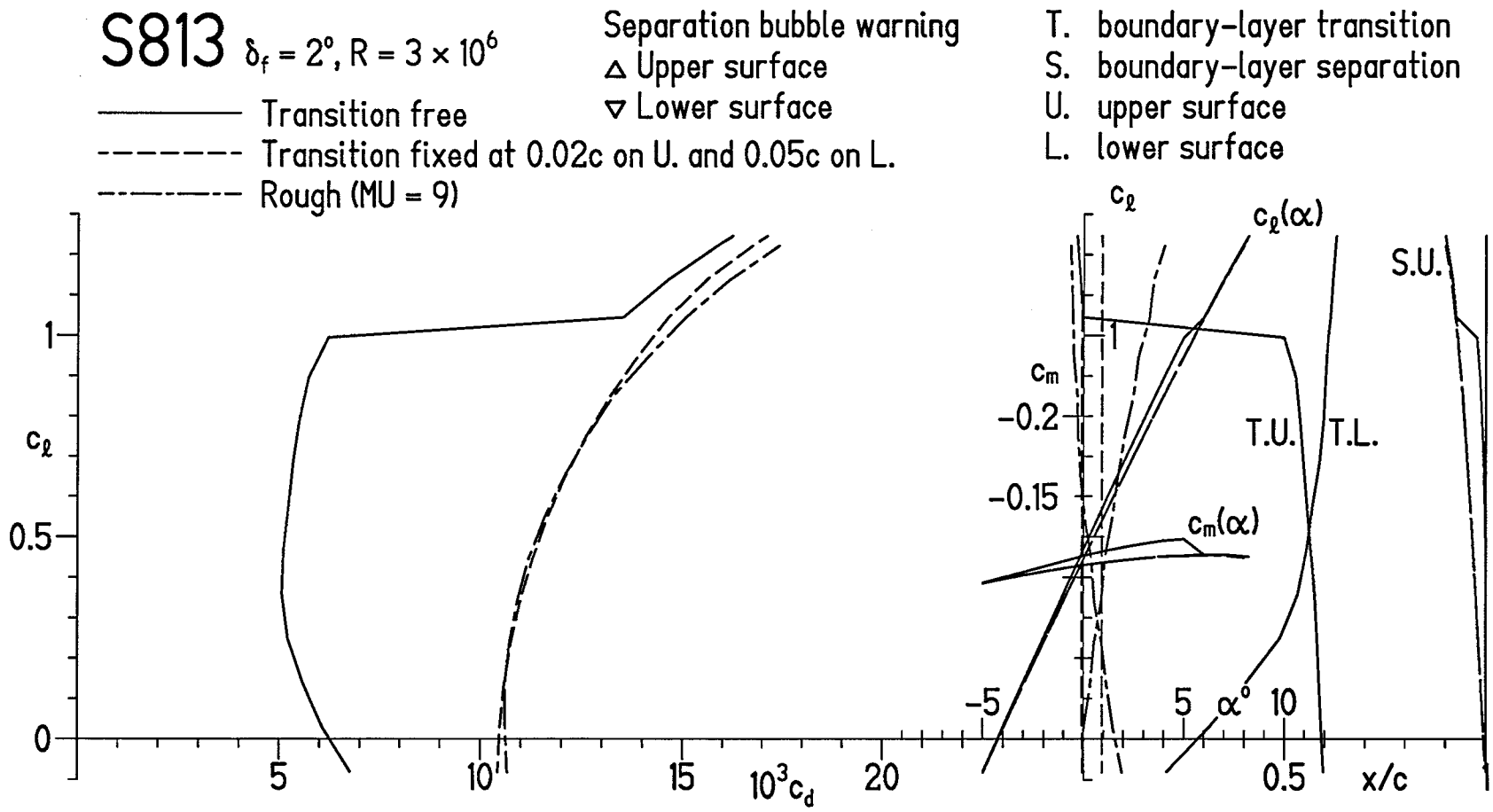

(c) R = 3×10^6.

Figure 16.- Concluded.

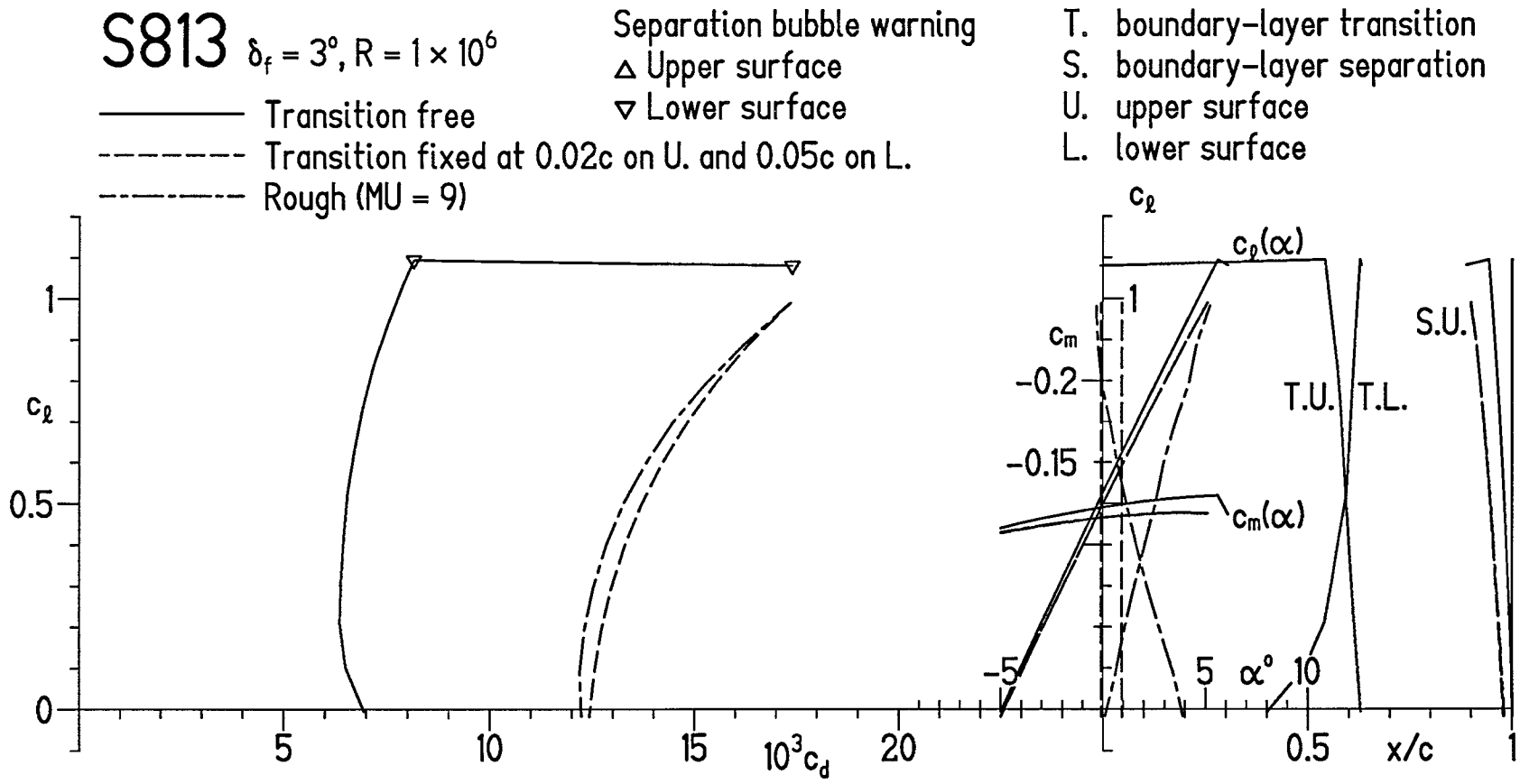

(a) $R = 1 \times 10^6$.

Figure 17.- Section characteristics with $\delta_f = 3°$ and transition free, transition fixed, and rough.

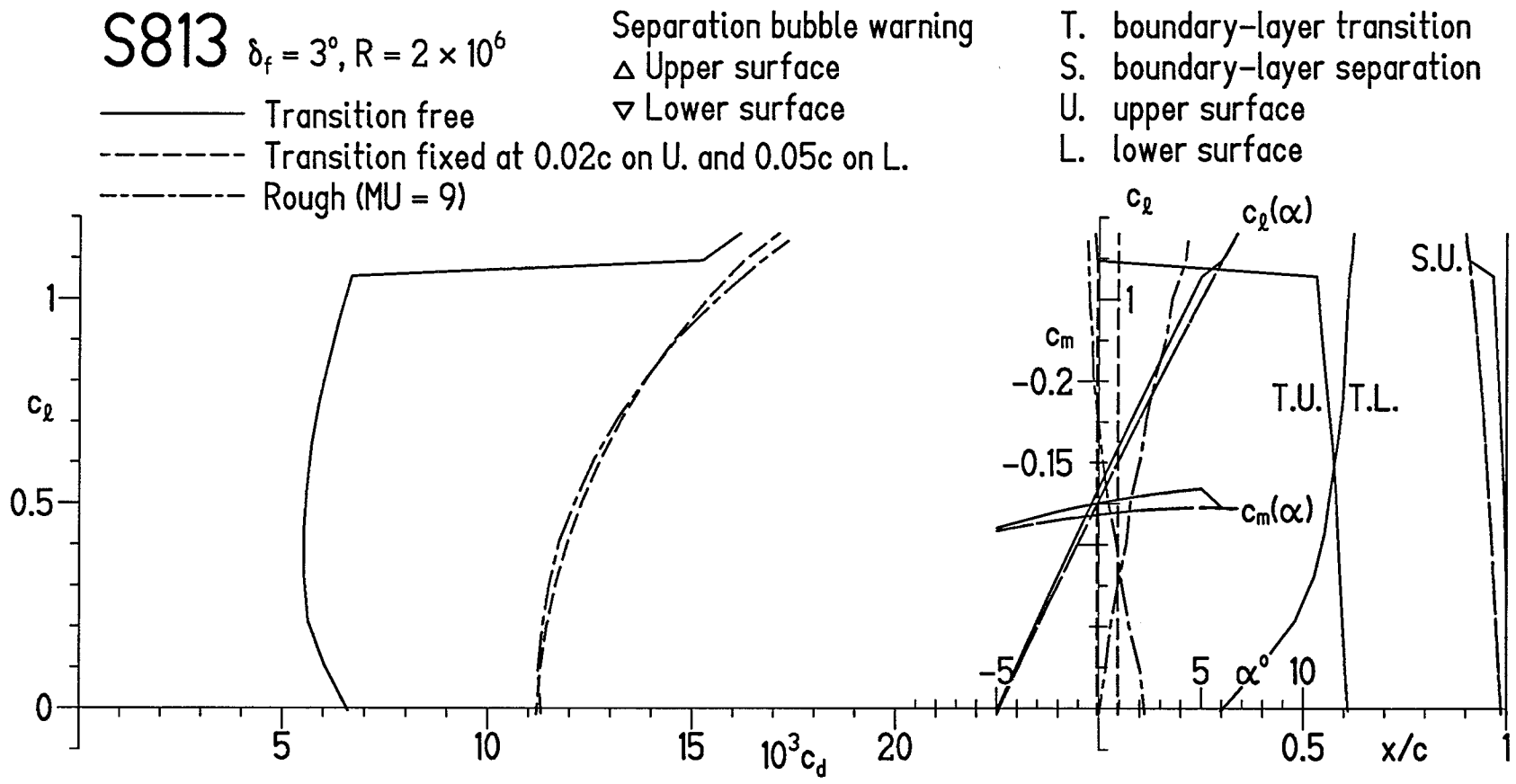

(b) $R = 2 \times 10^6$.

Figure 17.- Continued.

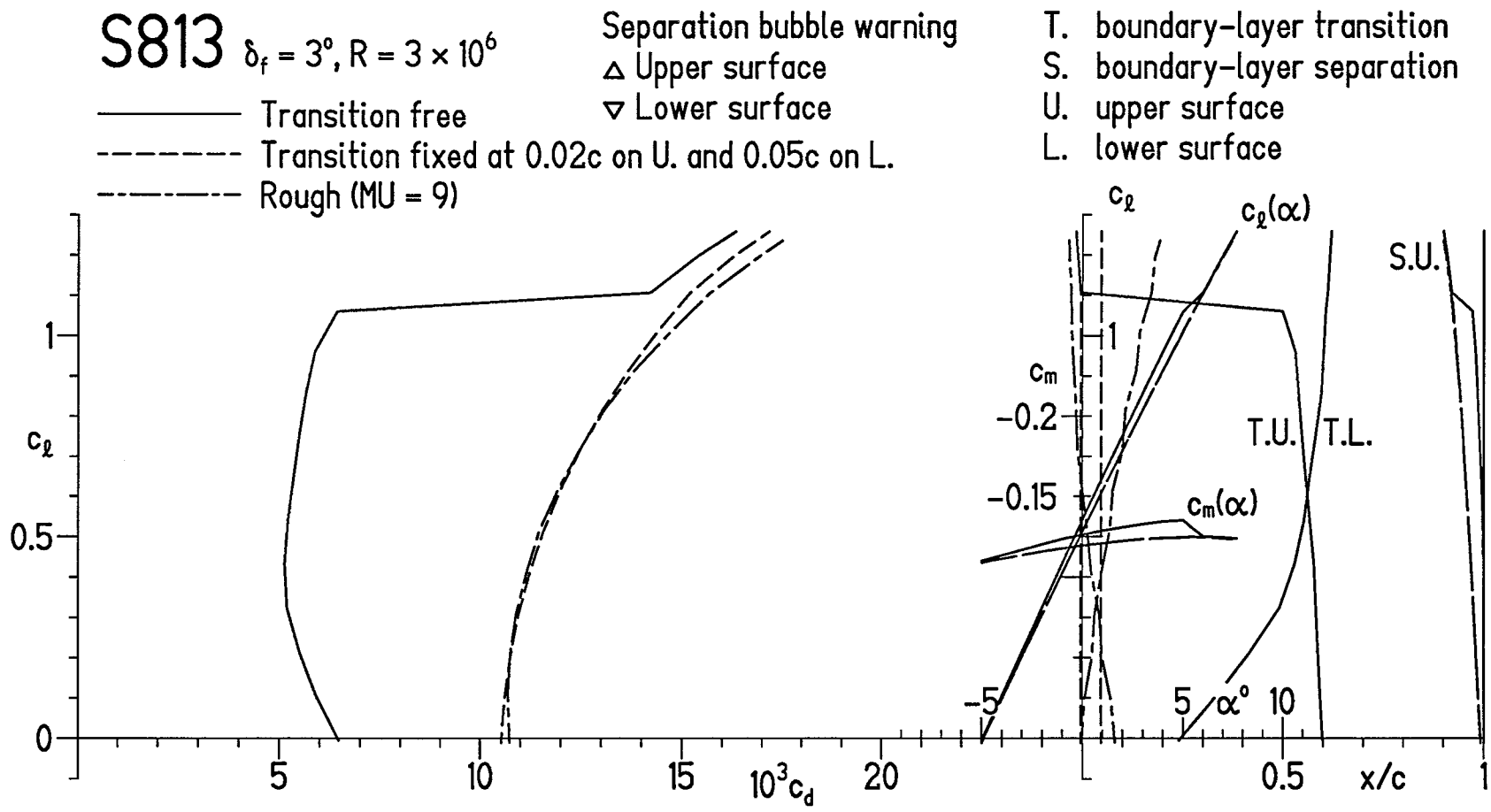

(c) $R = 3 \times 10^6$.

Figure 17.- Concluded.

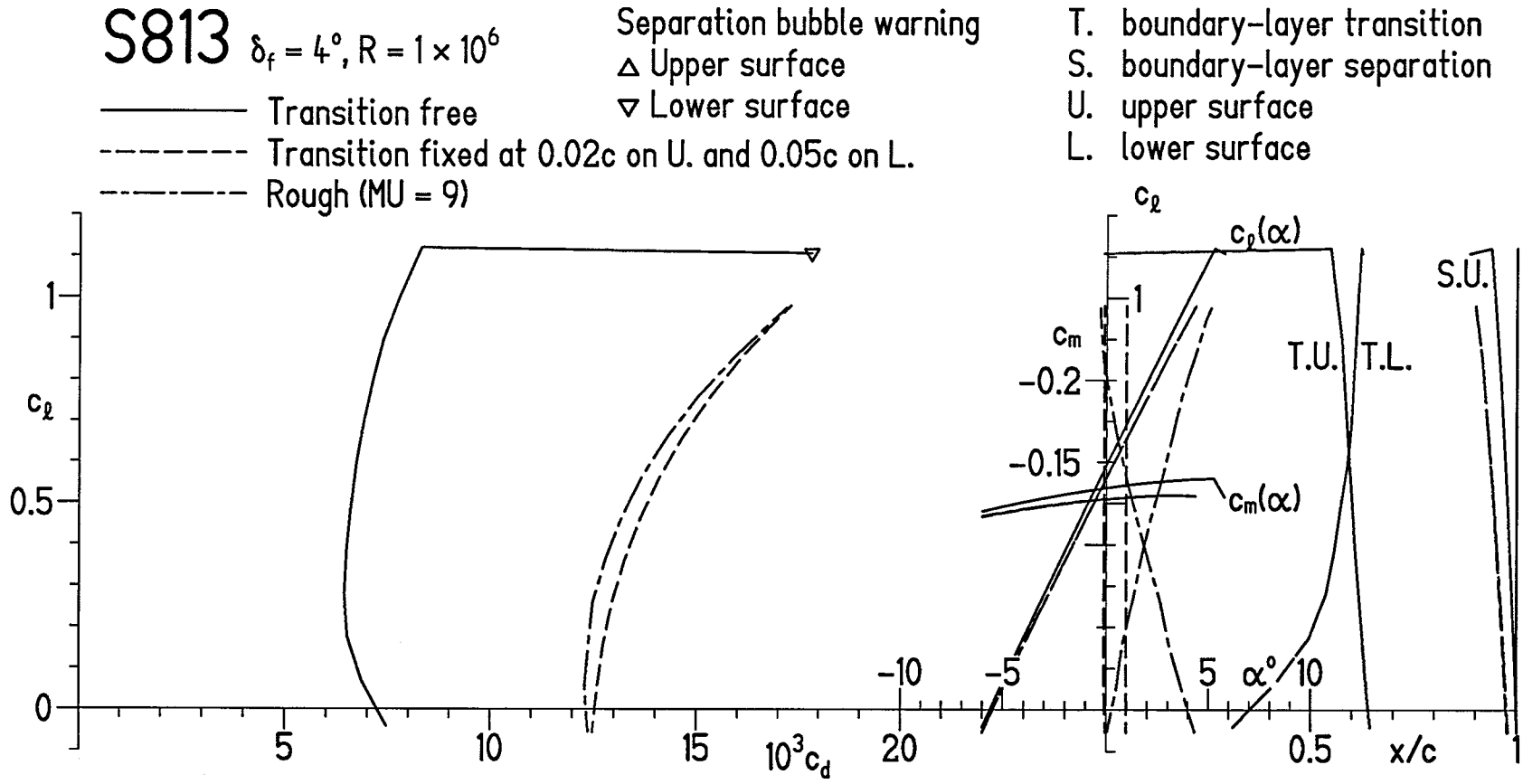

(a) $R = 1 \times 10^6$.

Figure 18.- Section characteristics with $\delta_f = 4°$ and transition free, transition fixed, and rough.

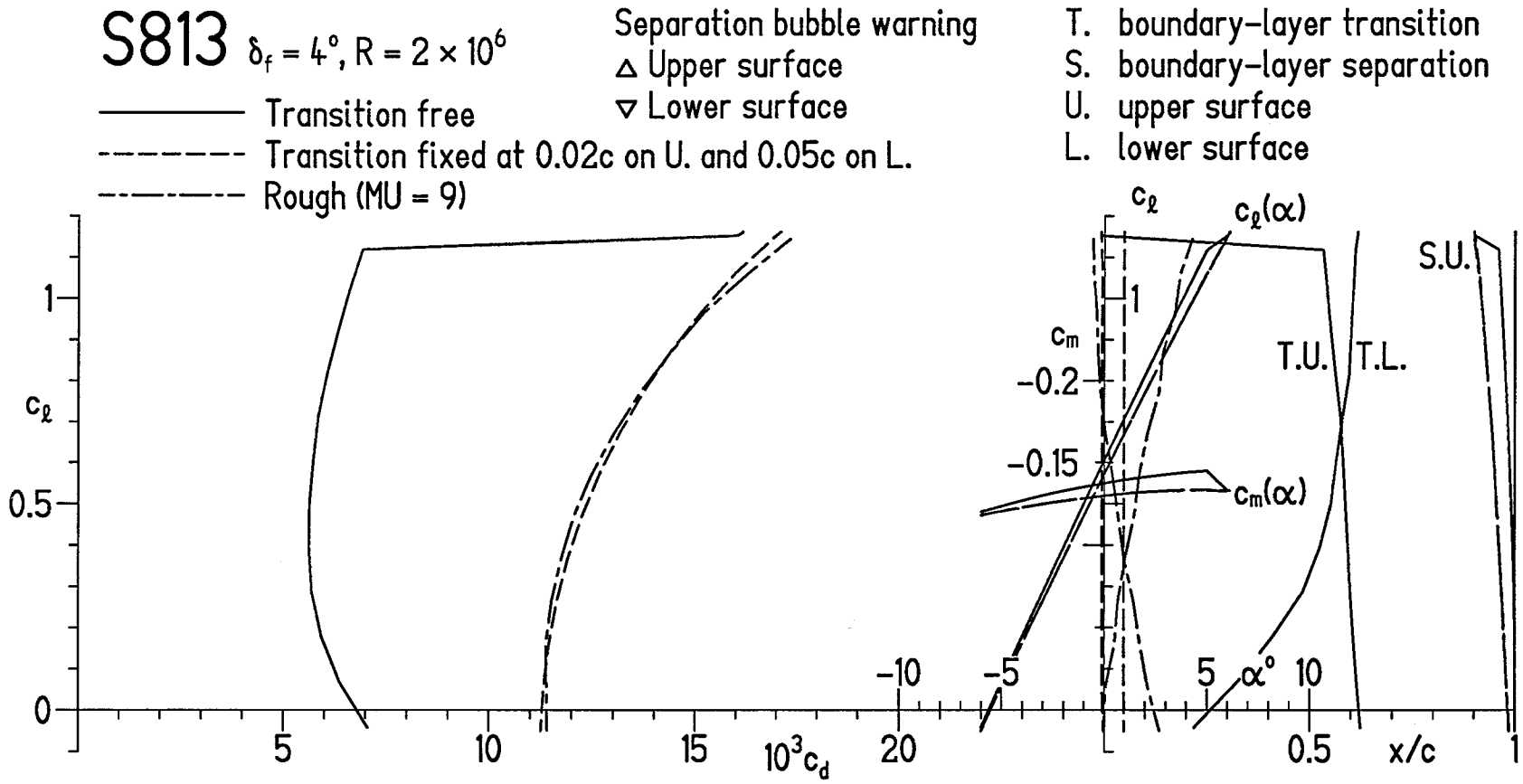

(b) R = 2×10^6.

Figure 18.- Continued.

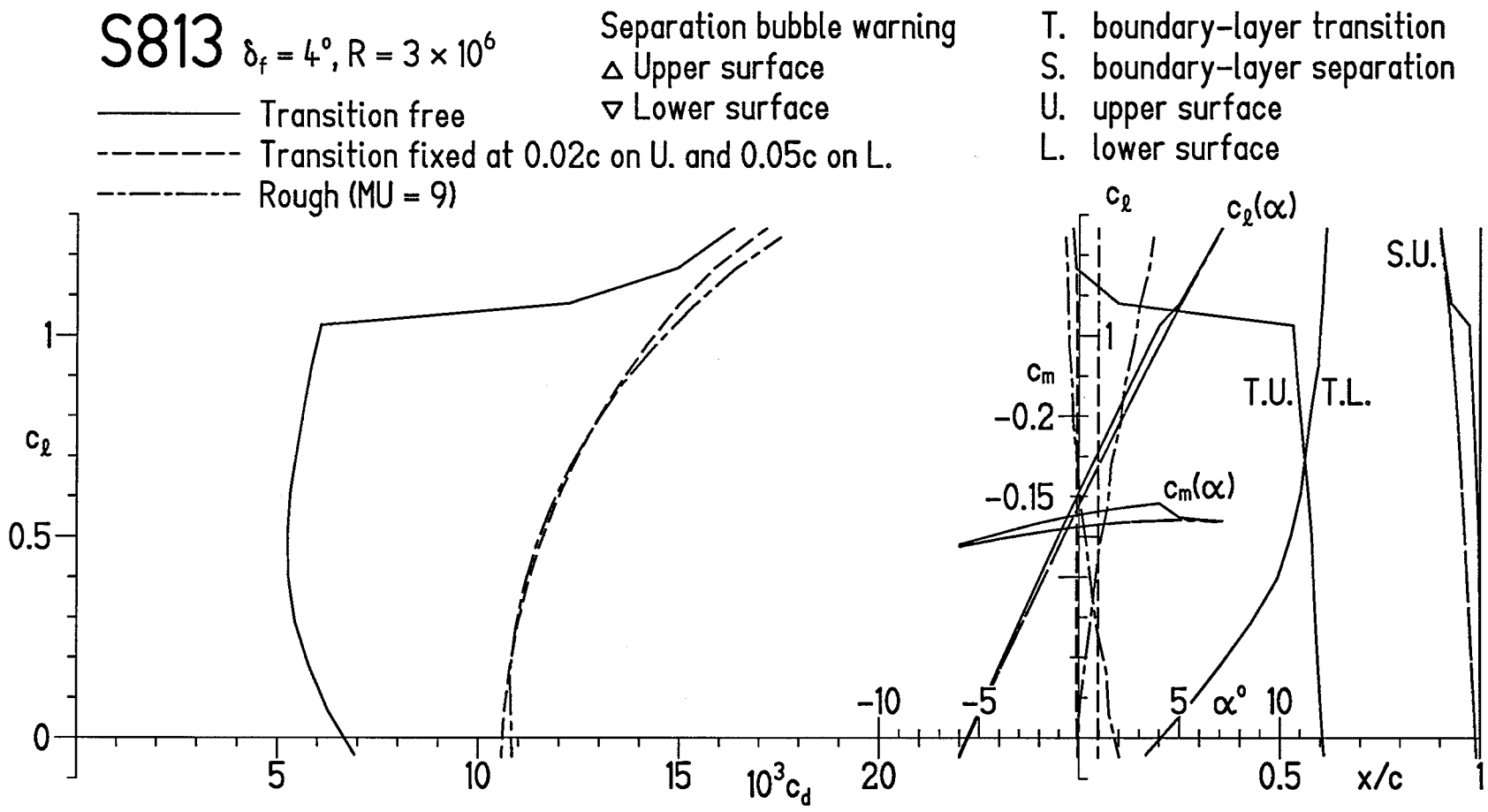

(c) R = 3 × 10^6.

Figure 18.- Concluded.

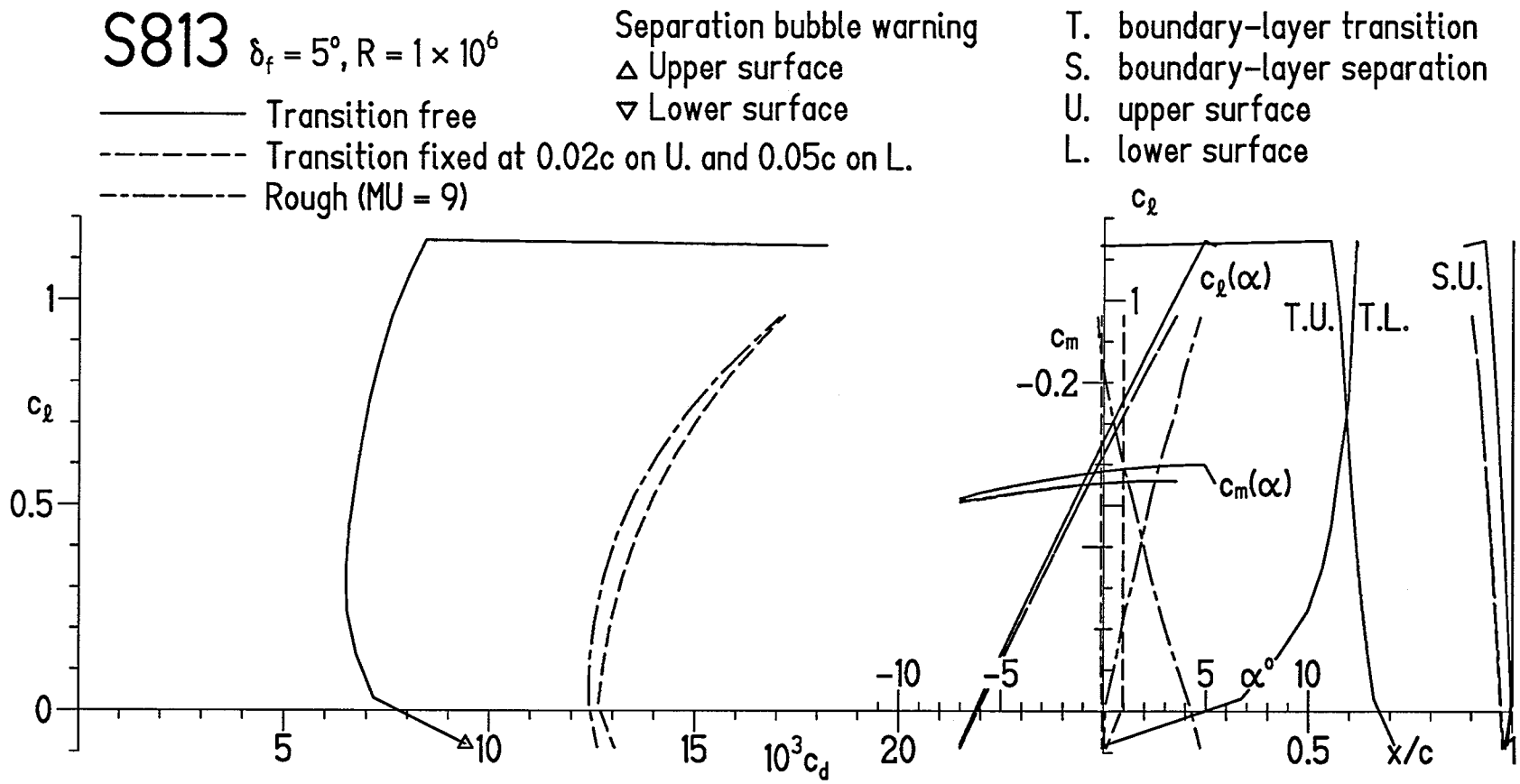

(a) $R = 1 \times 10^6$.

Figure 19.- Section characteristics with $\delta_f = 5°$ and transition free, transition fixed, and rough.

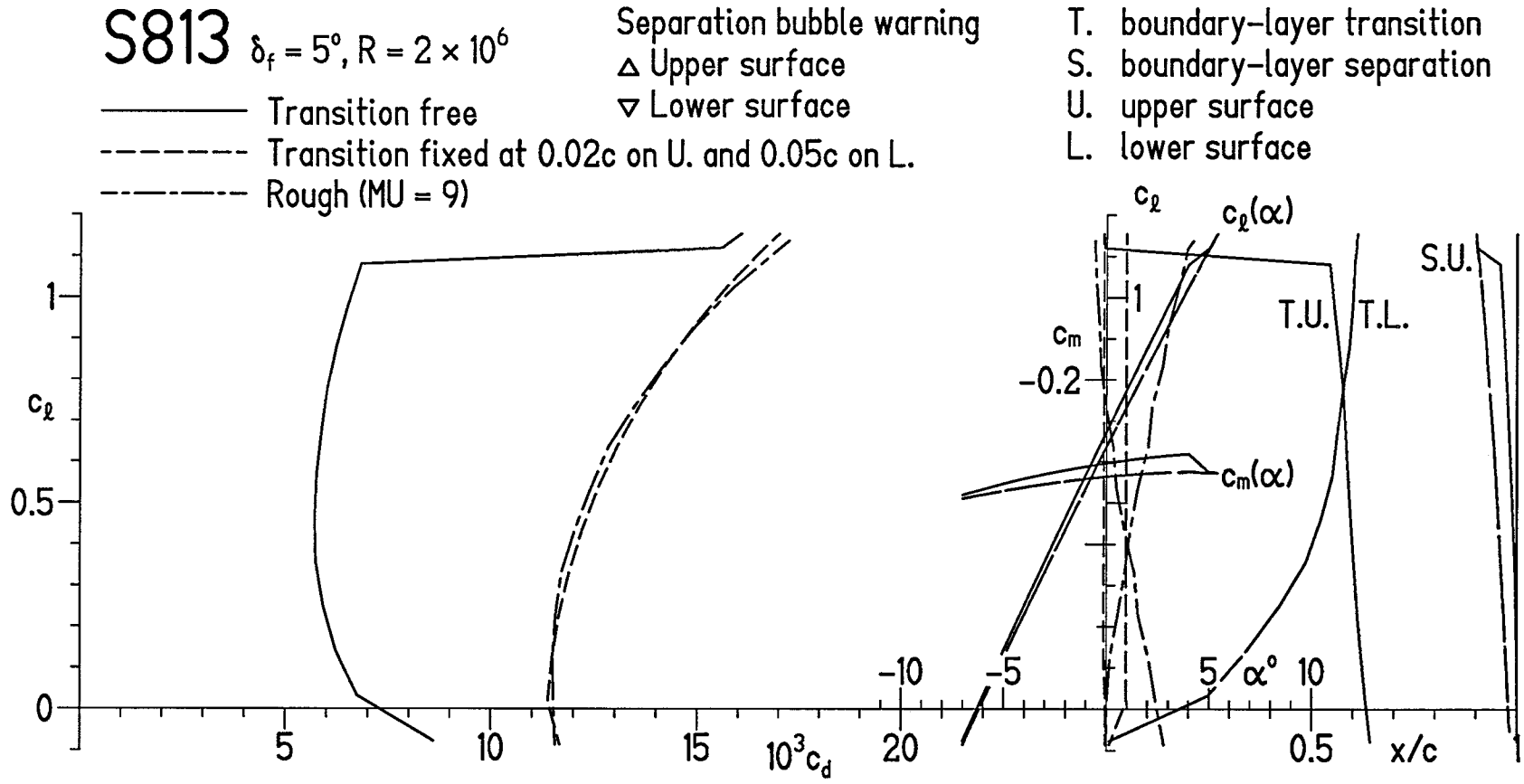

(b) $R = 2 \times 10^6$.

Figure 19.- Continued.

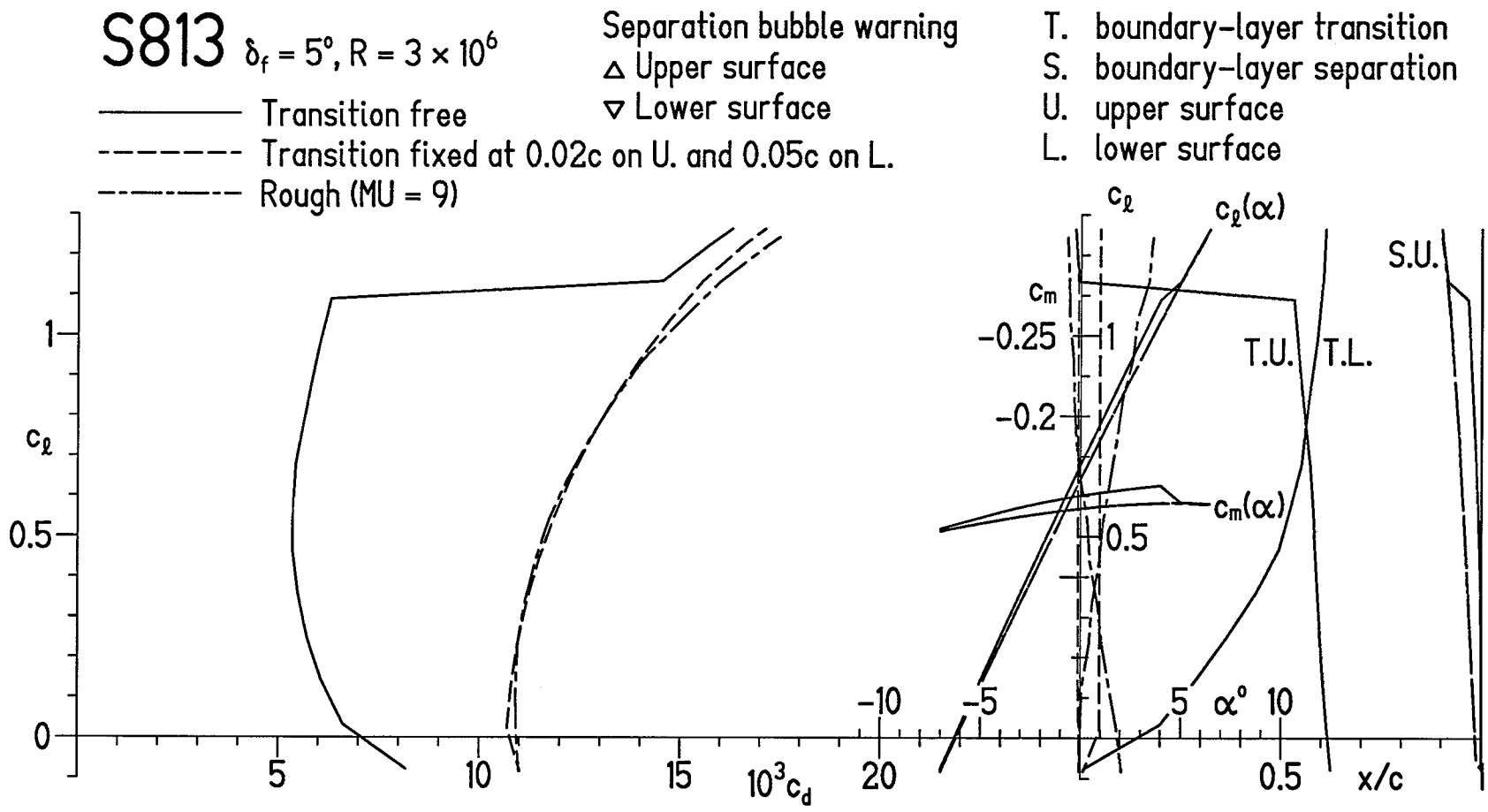

(c) R = 3×10^6.

Figure 19.- Concluded.

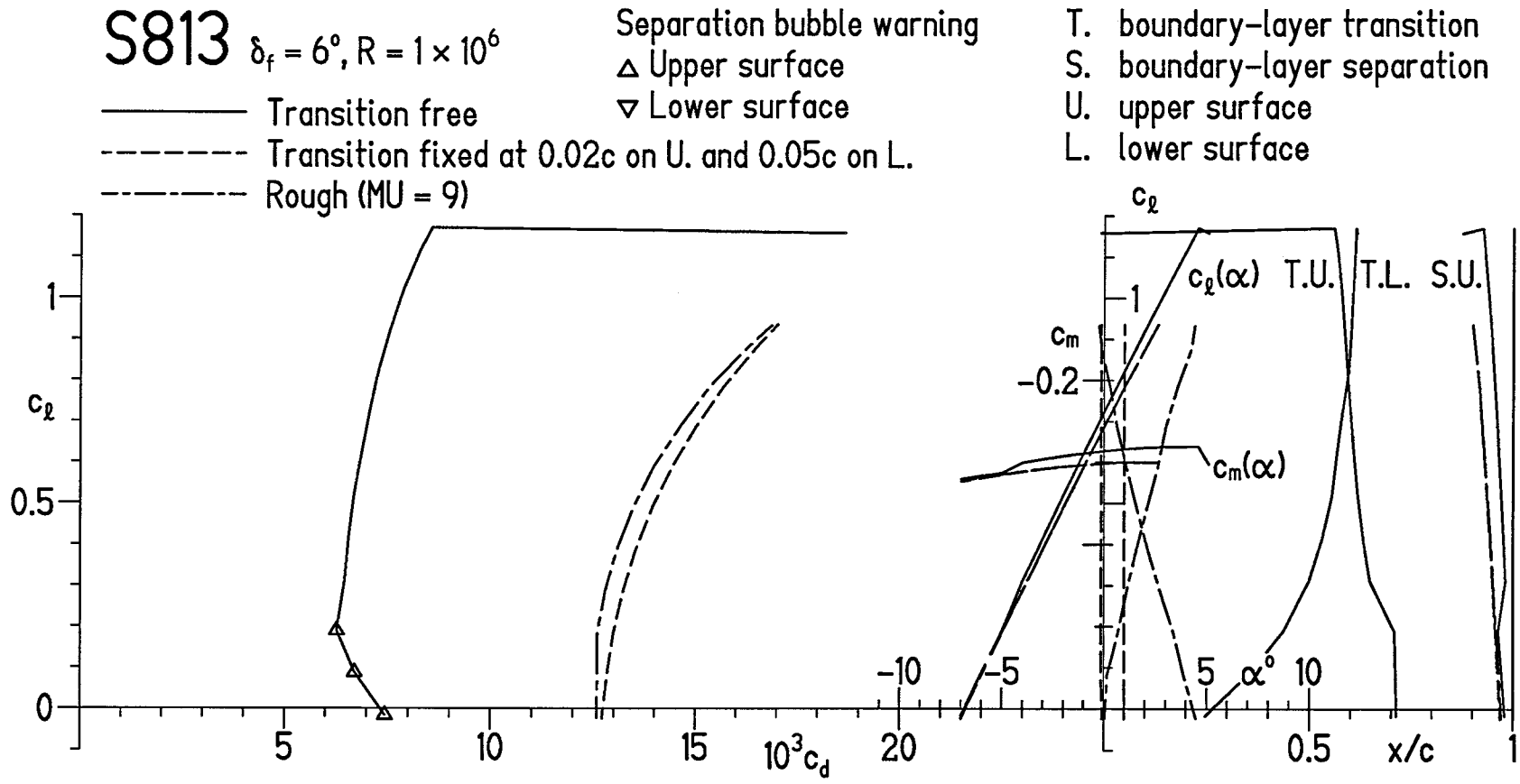

(a) $R = 1 \times 10^6$.

Figure 20.- Section characteristics with $\delta_f = 6°$ and transition free, transition fixed, and rough.

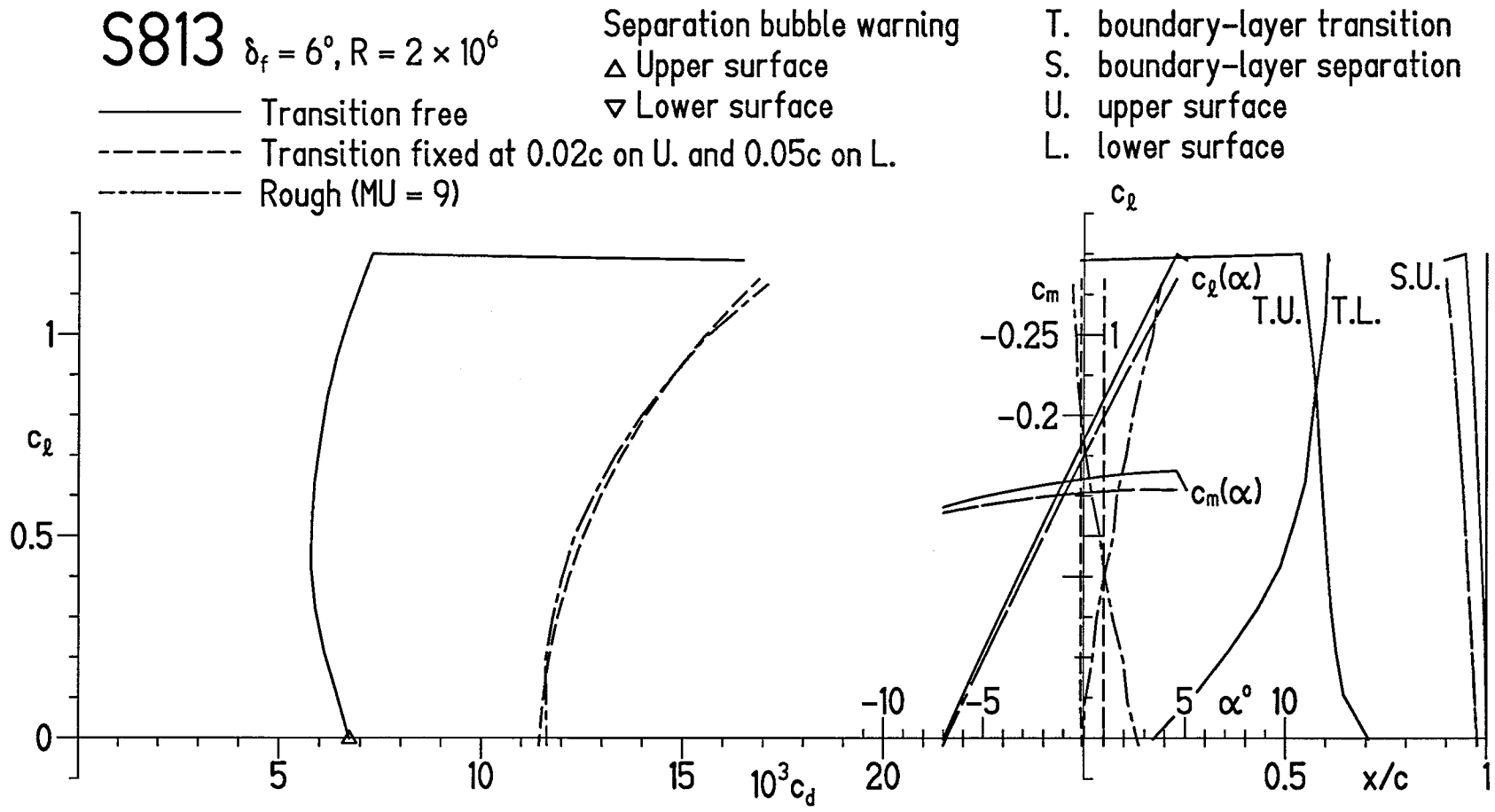

(b) $R = 2 \times 10^6$.

Figure 20.- Continued.

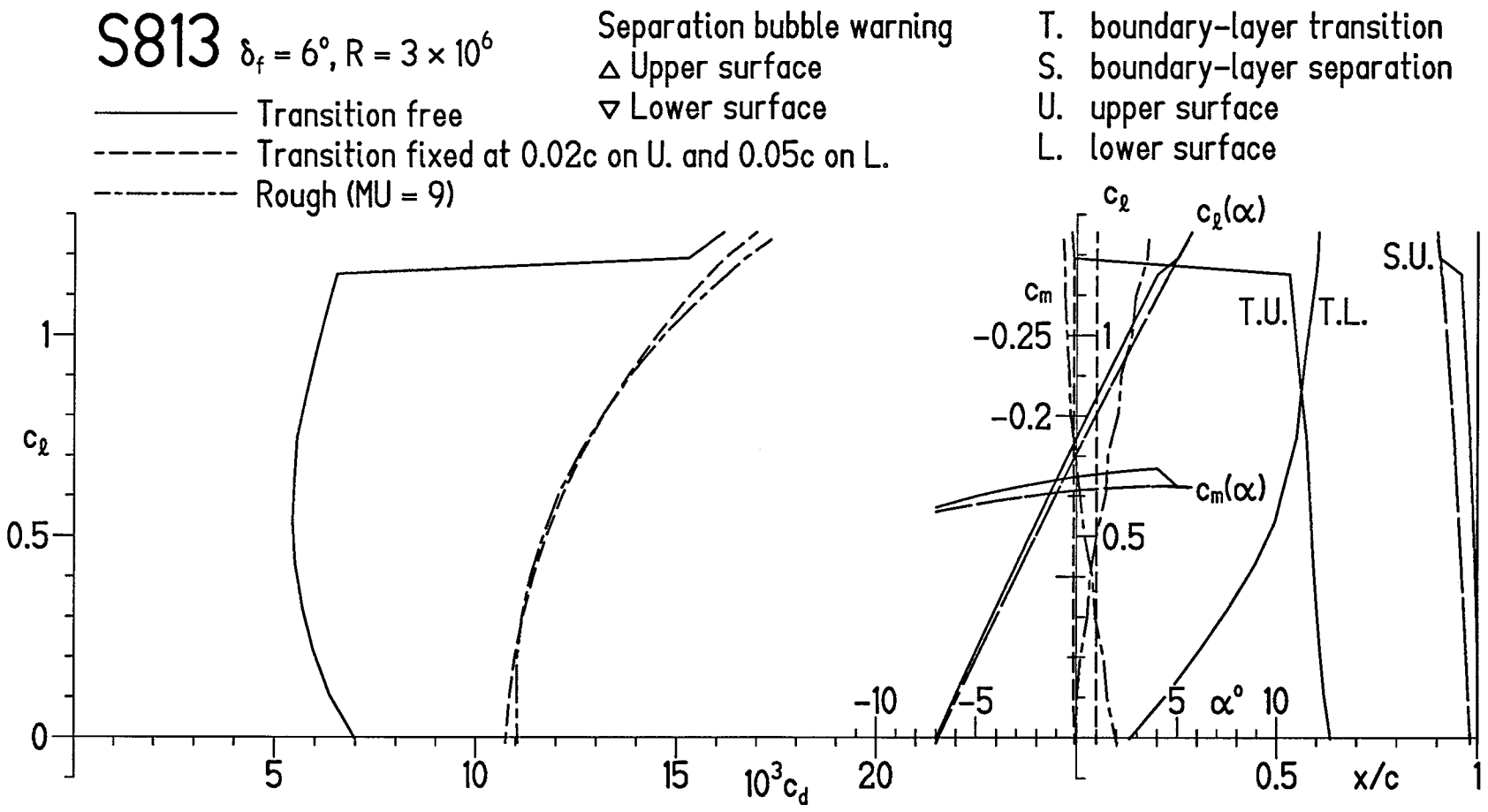

(c) R = 3×10^6.

Figure 20.- Concluded.

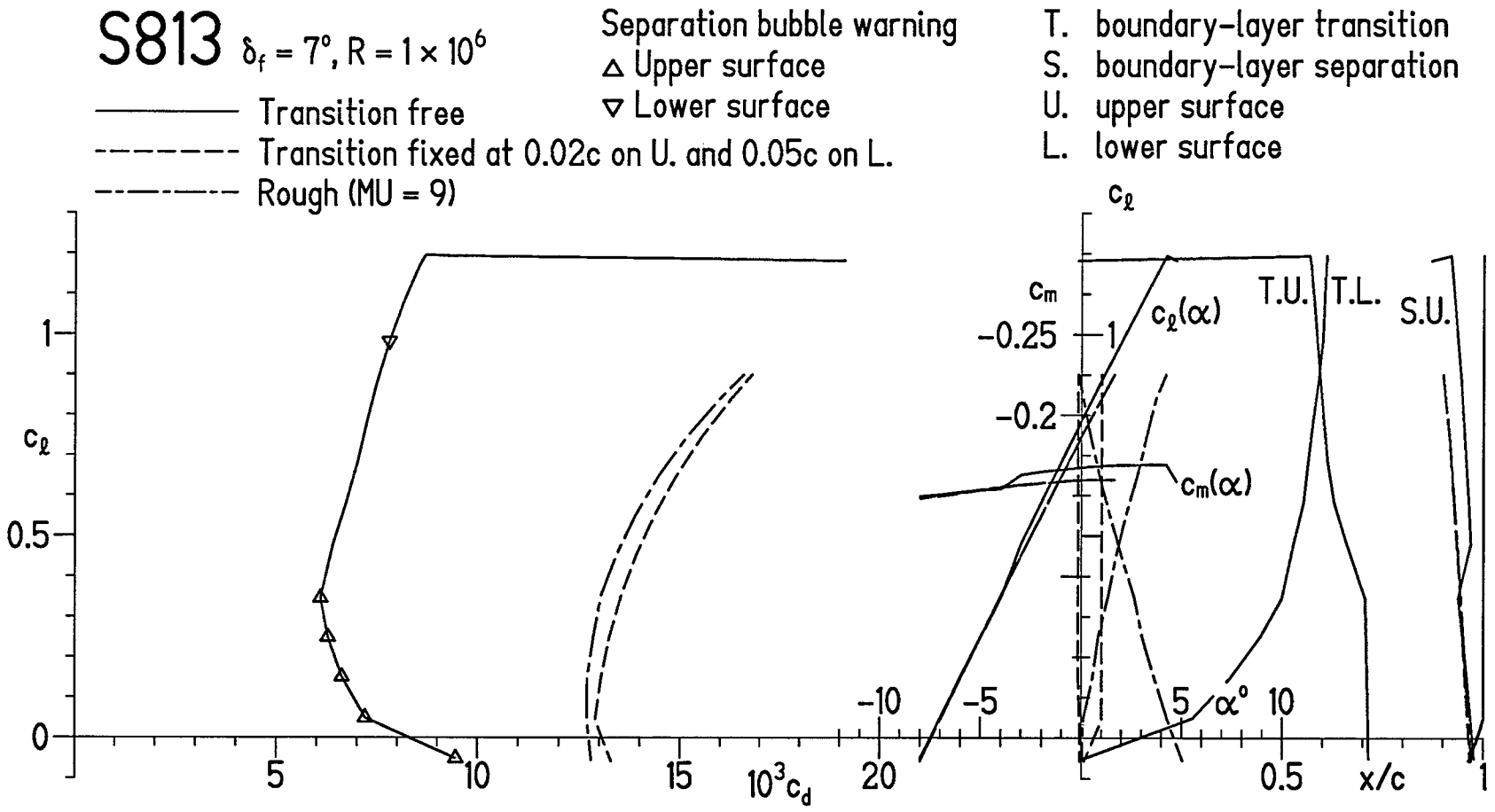

(a) $R = 1 \times 10^6$.

Figure 21.- Section characteristics with $\delta_f = 7°$ and transition free, transition fixed, and rough.

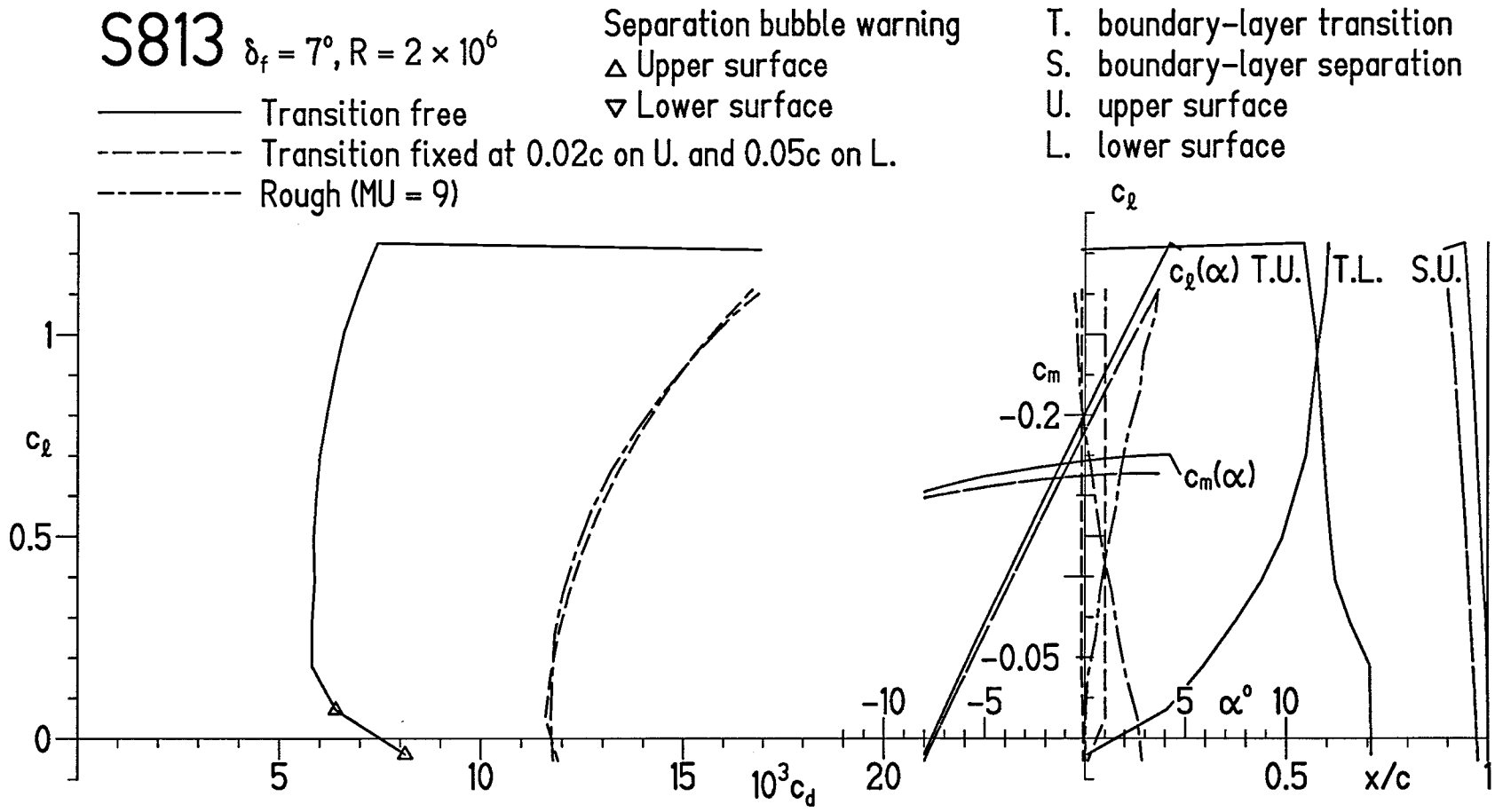

(b) R = 2 × 10^6.

Figure 21.- Continued.

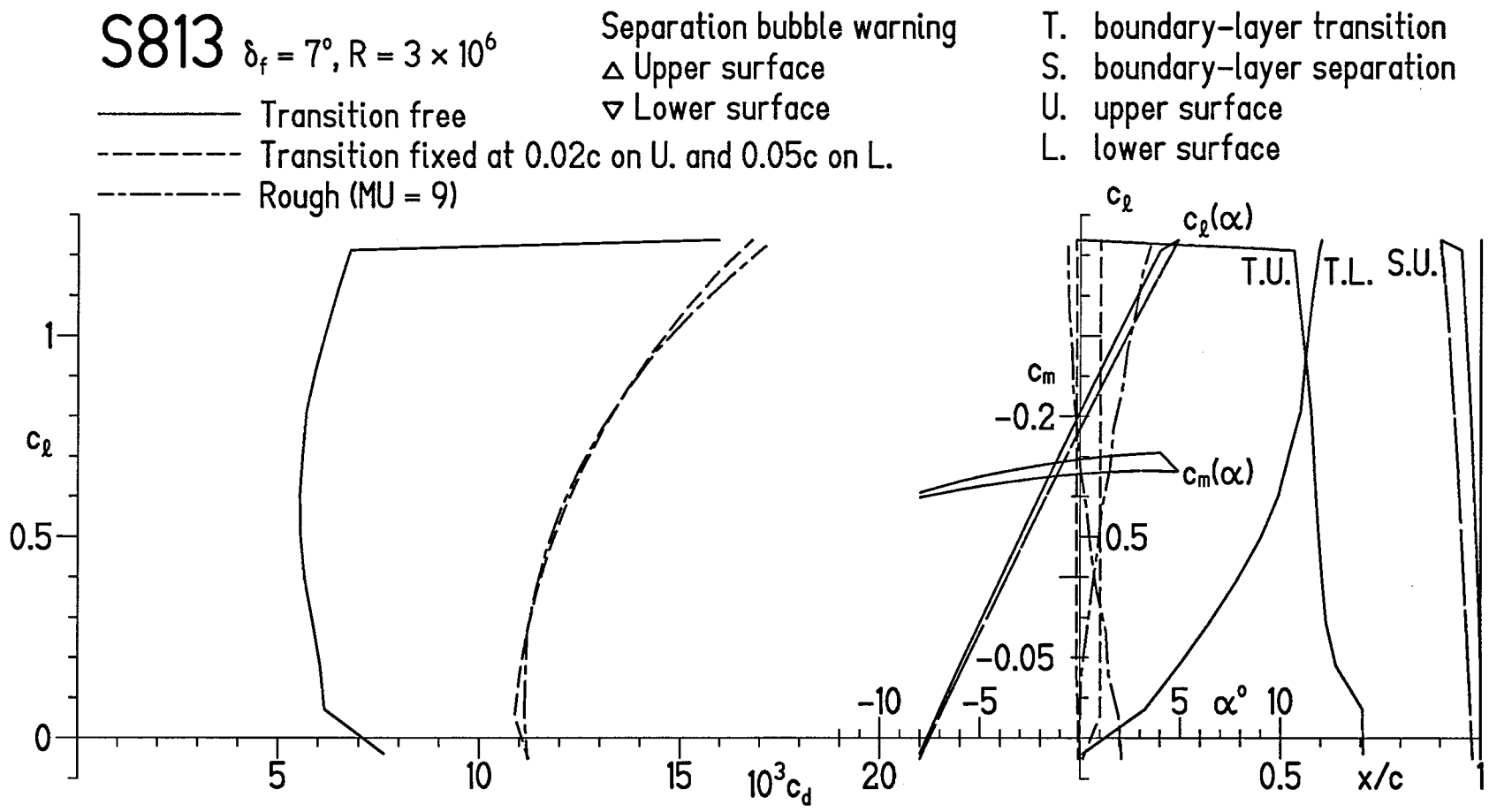

(c) R = 3×10^6.

Figure 21.- Concluded.

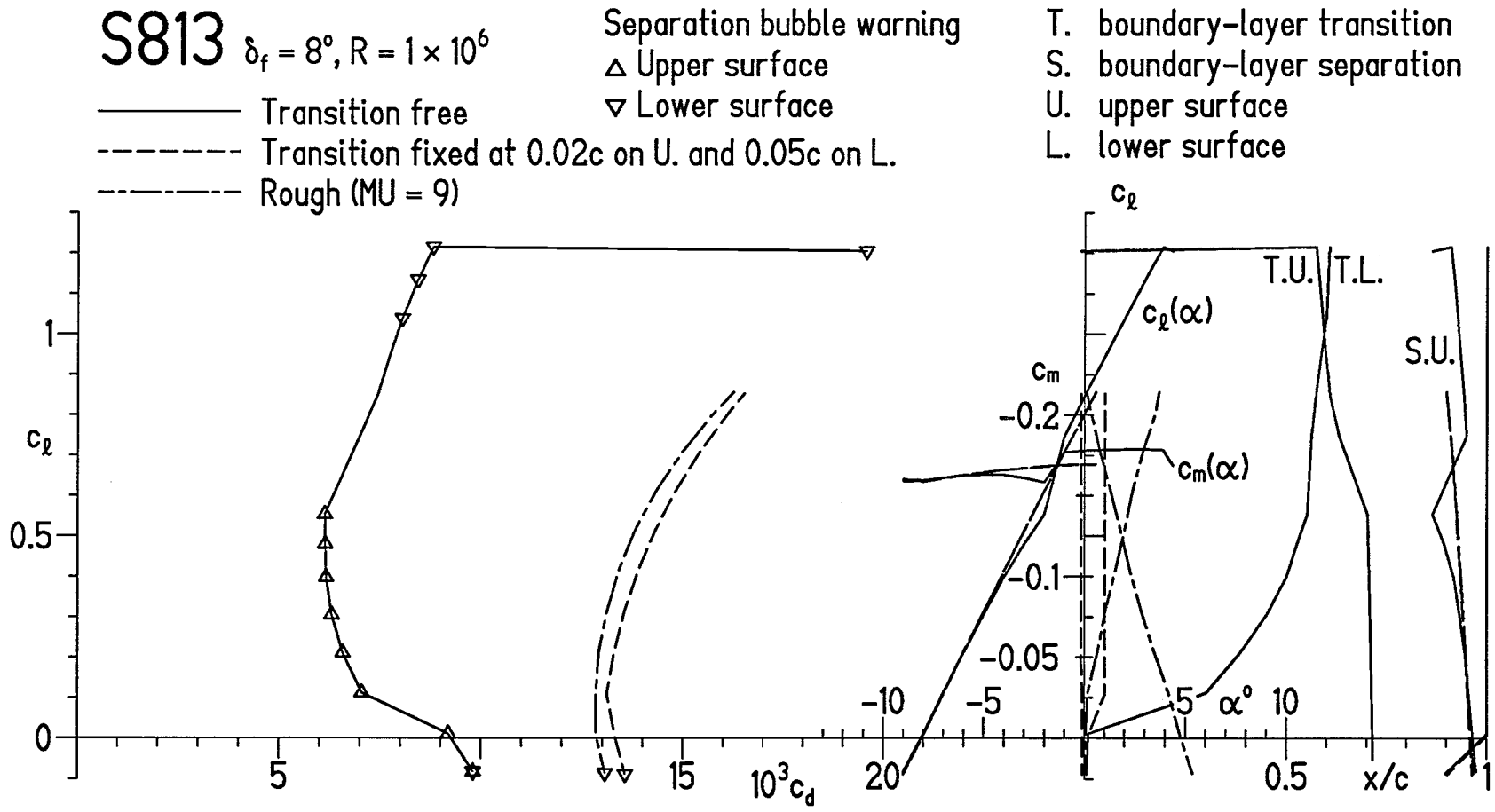

(a) $R = 1 \times 10^6$.

Figure 22.- Section characteristics with $\delta_f = 8°$ and transition free, transition fixed, and rough.

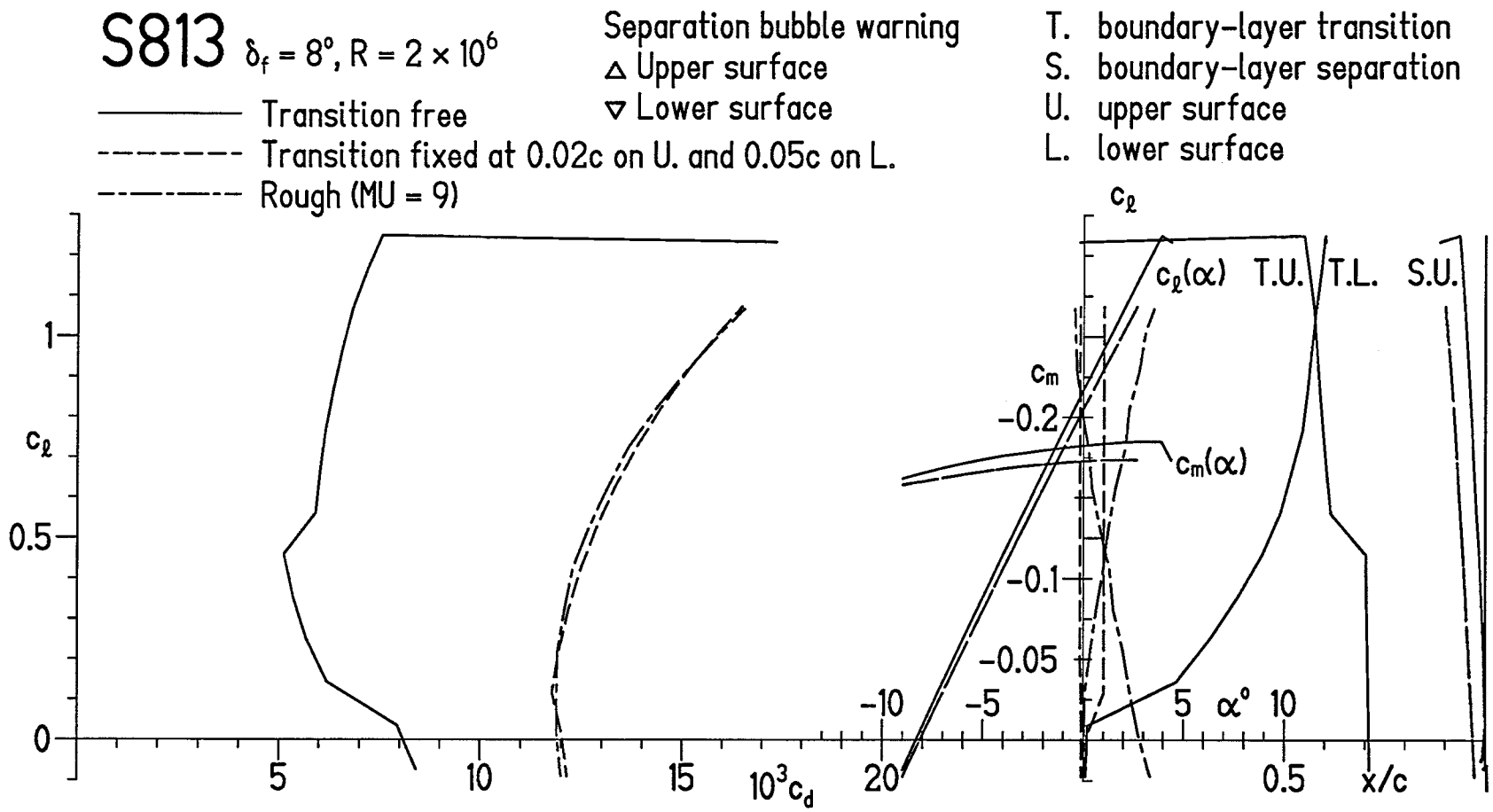

(b) R = 2 × 10^6.

Figure 22.- Continued.

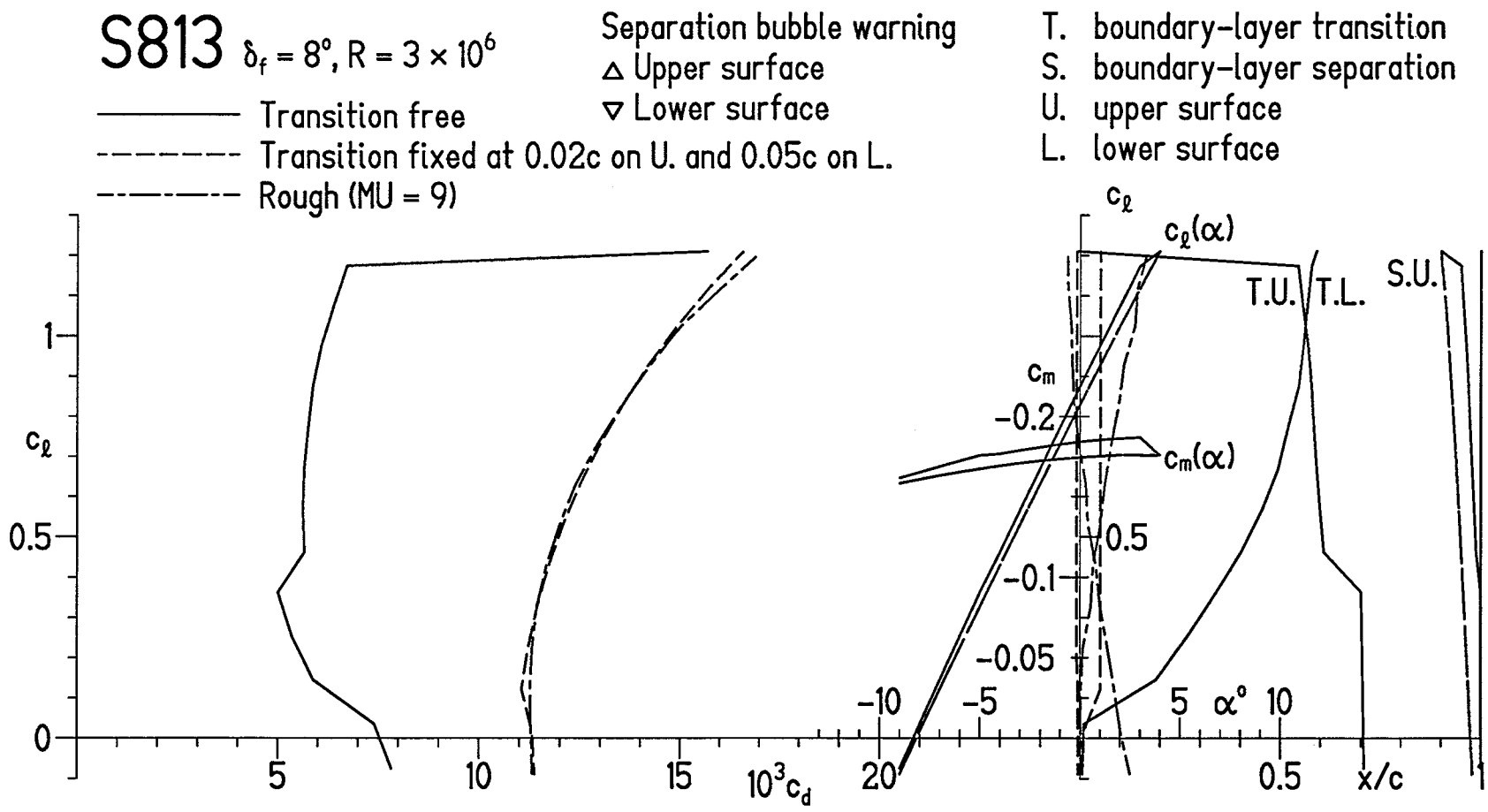

(c) R = 3×10^6.

Figure 22.- Concluded.

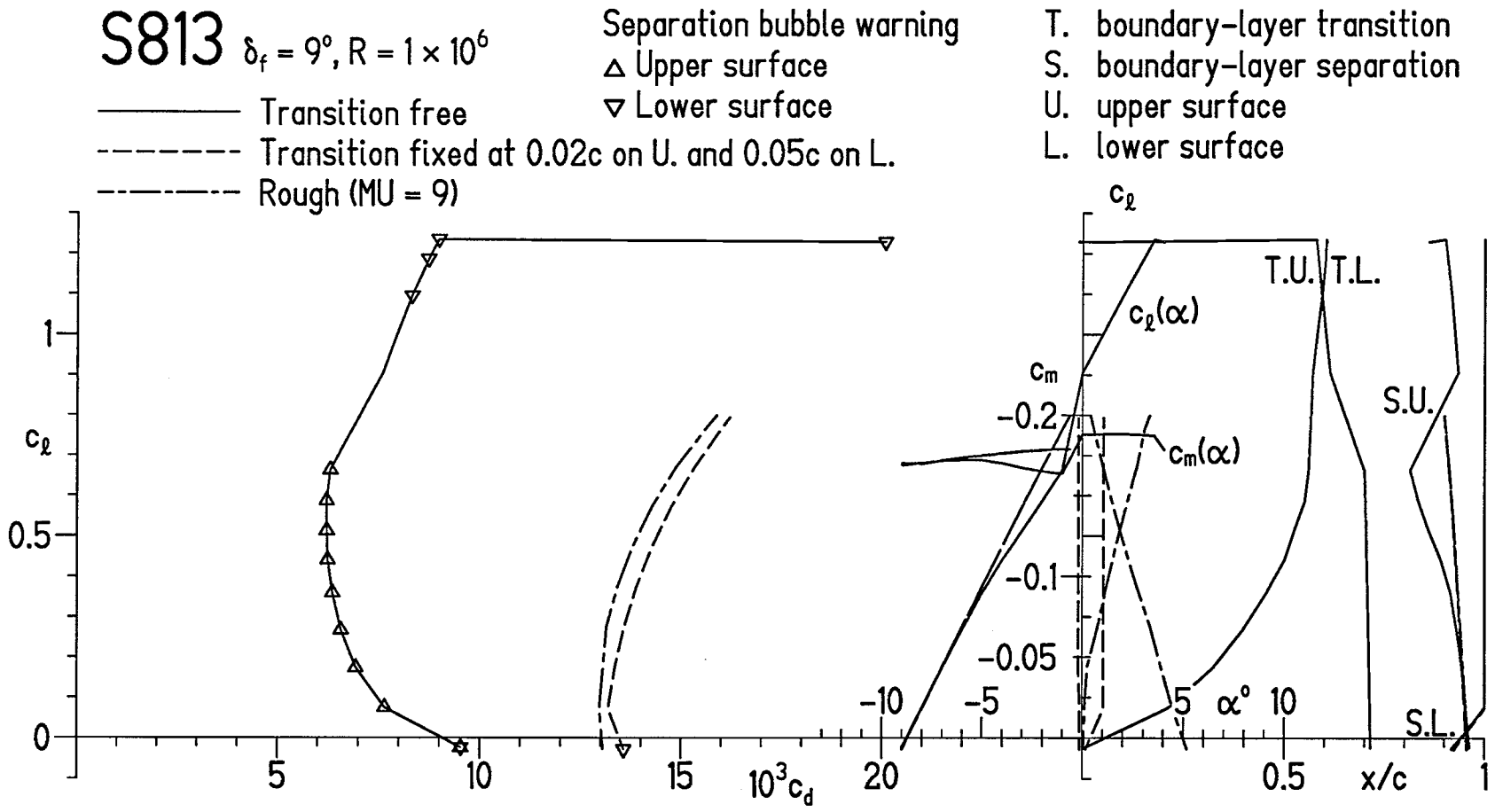

(a) R = 1 × 10^6.

Figure 23.- Section characteristics with $\delta_f = 9°$ and transition free, transition fixed, and rough.

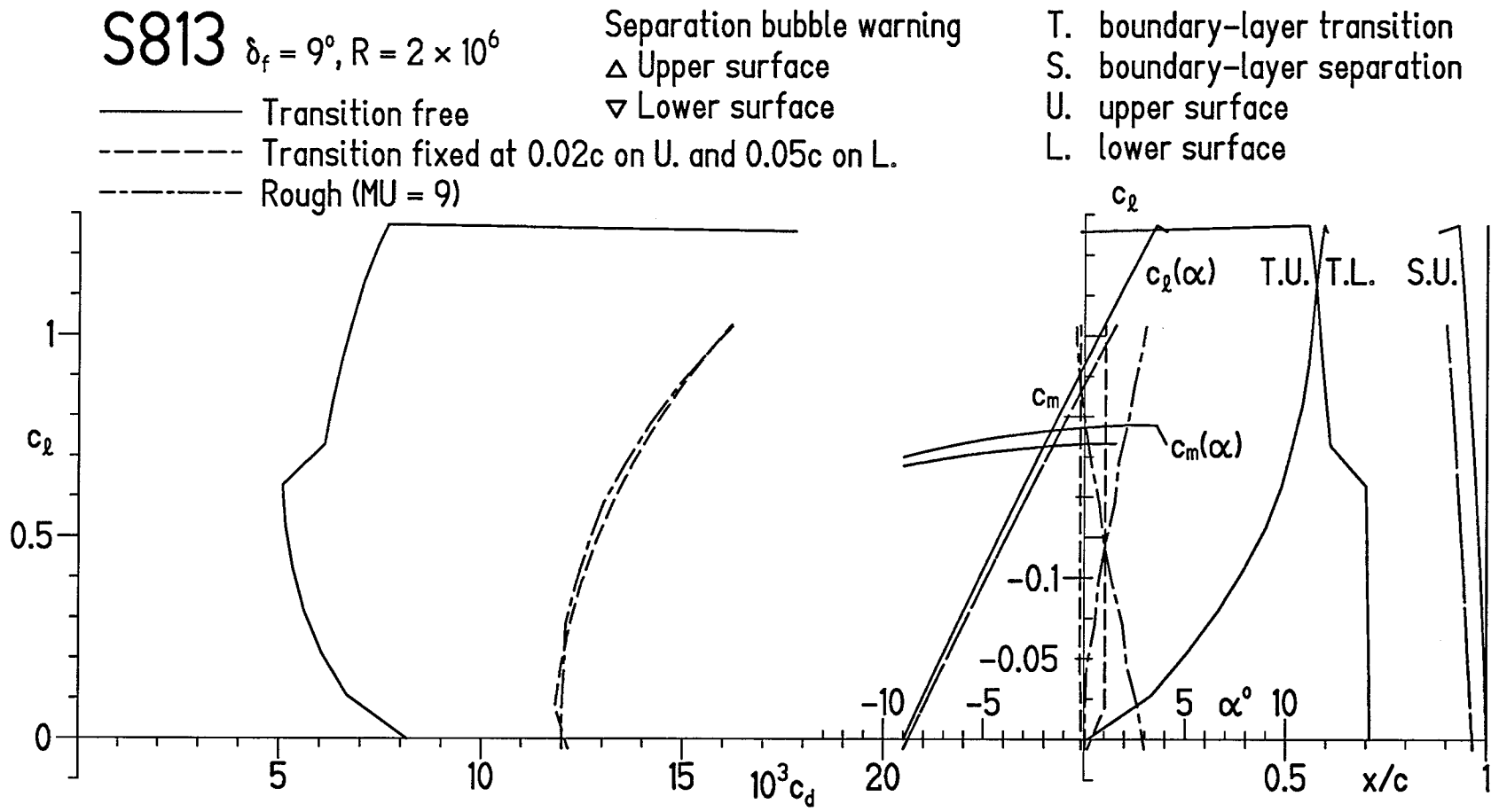

(b) R = 2 × 10^6.

Figure 23.- Continued.

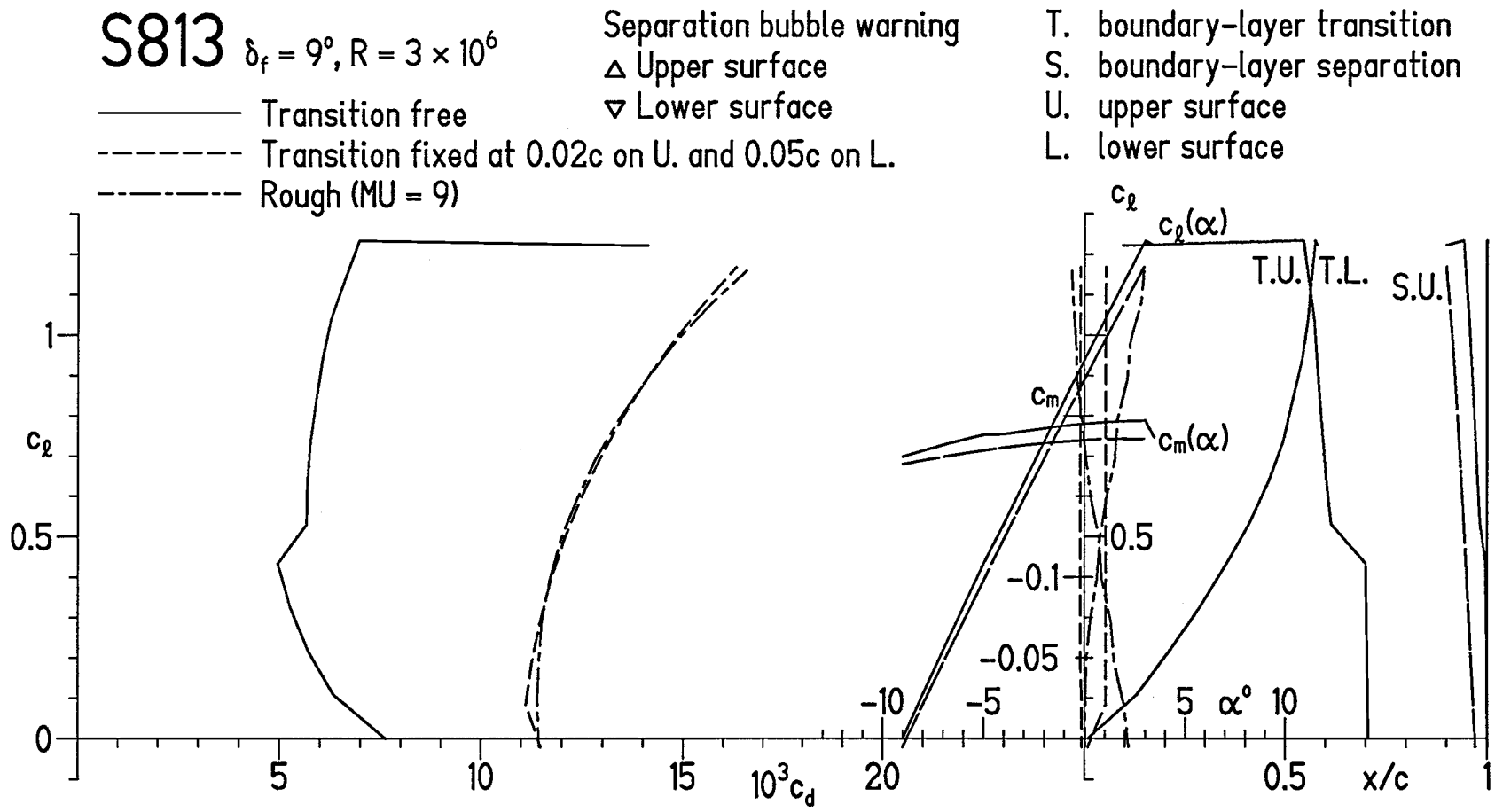

(c) R = 3×10^6.

Figure 23.- Concluded.

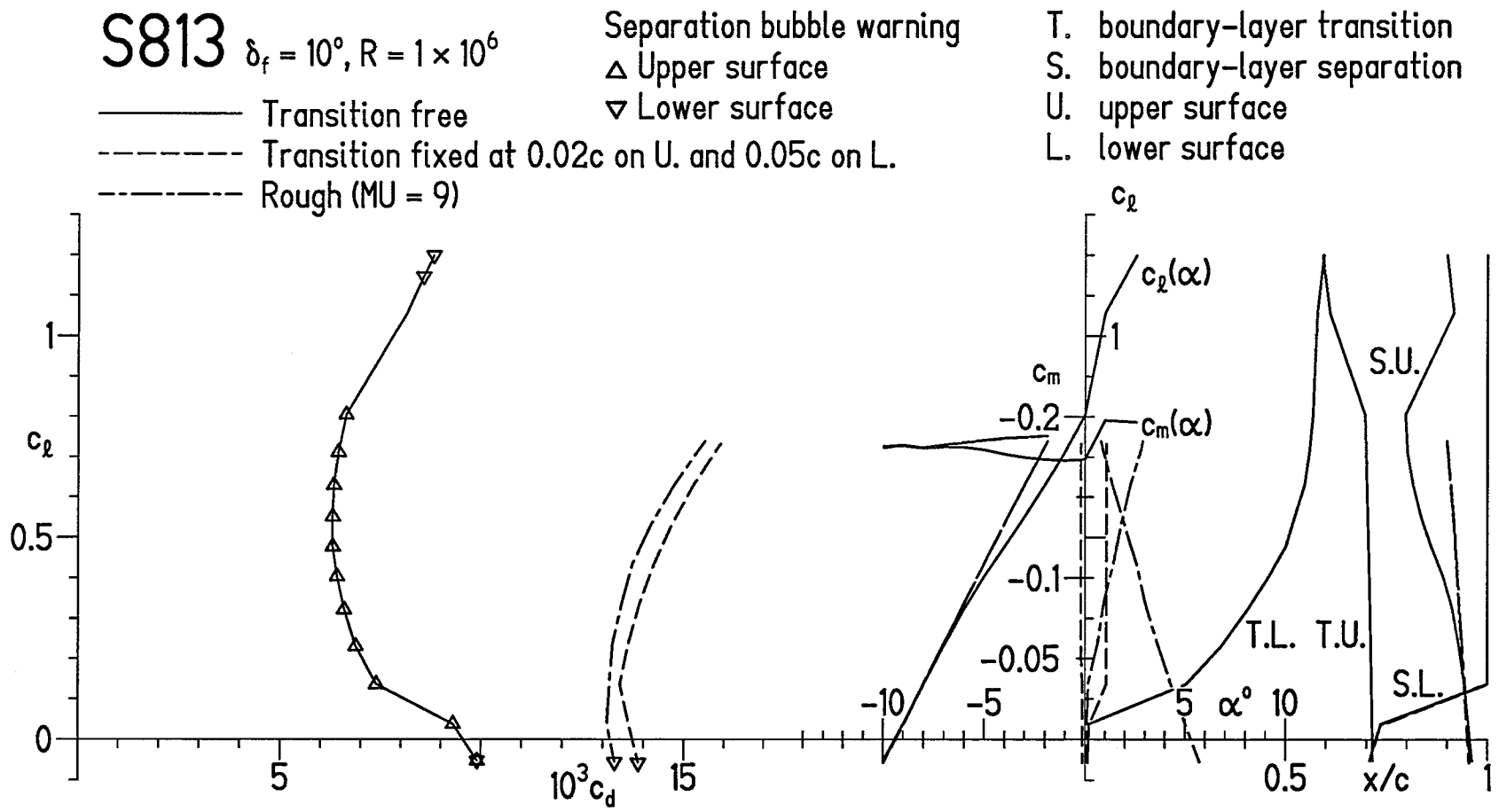

(a) $R = 1 \times 10^6$.

Figure 24.- Section characteristics with $\delta_f = 10°$ and transition free, transition fixed, and rough.

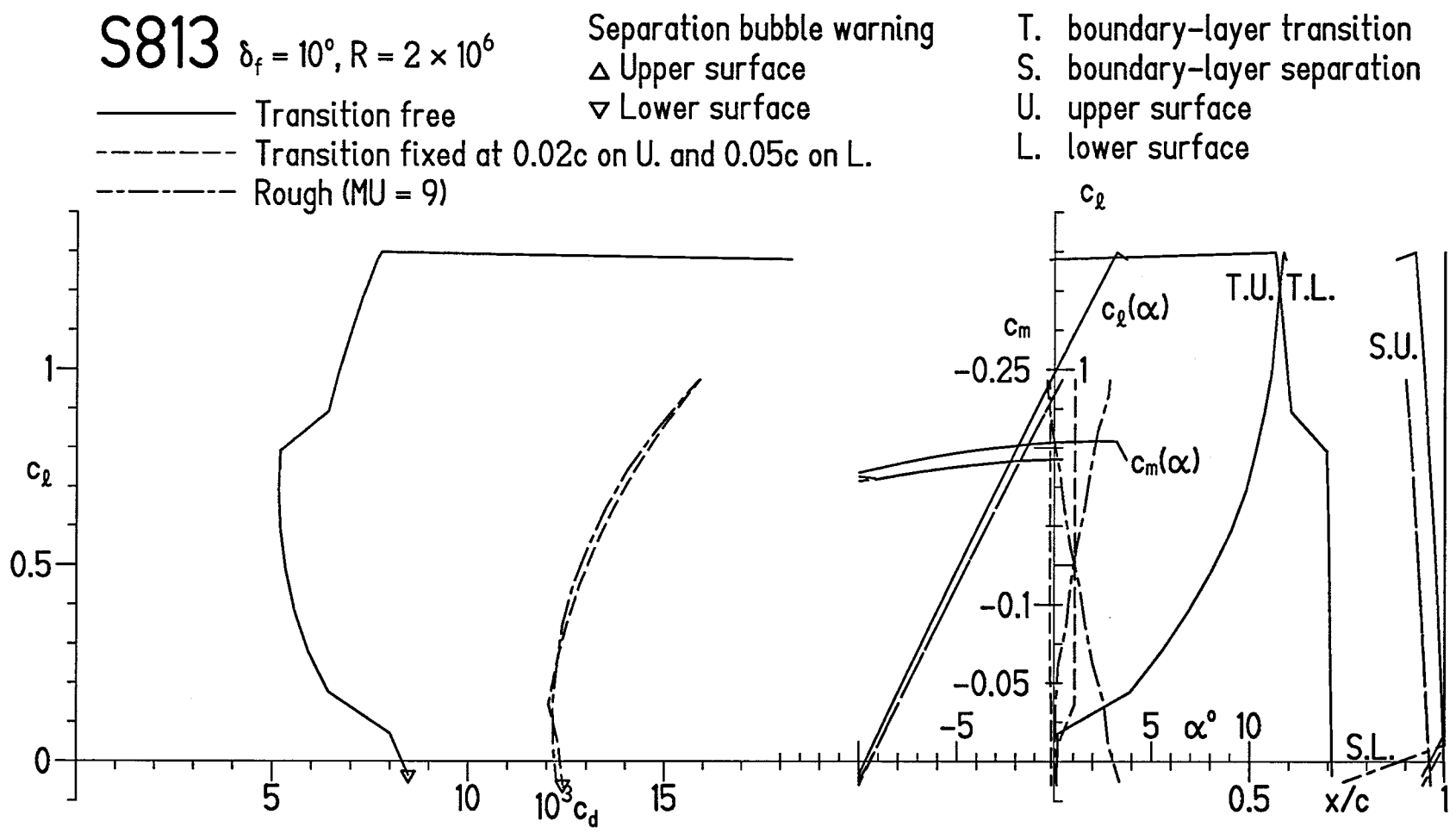

(b) R = 2×10^6.

Figure 24.- Continued.

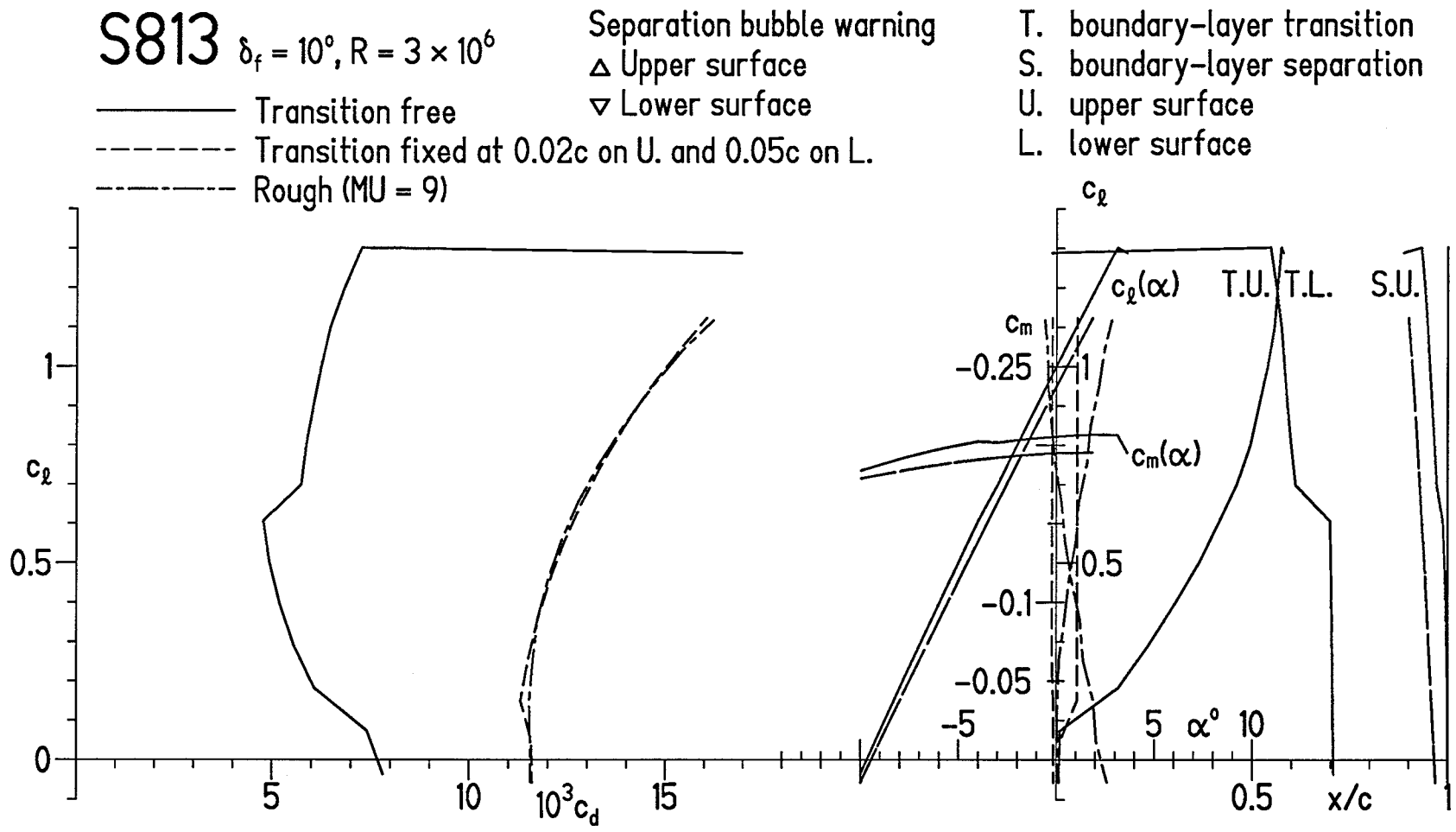

(c) R = 3×10^6.

Figure 24.- Concluded.

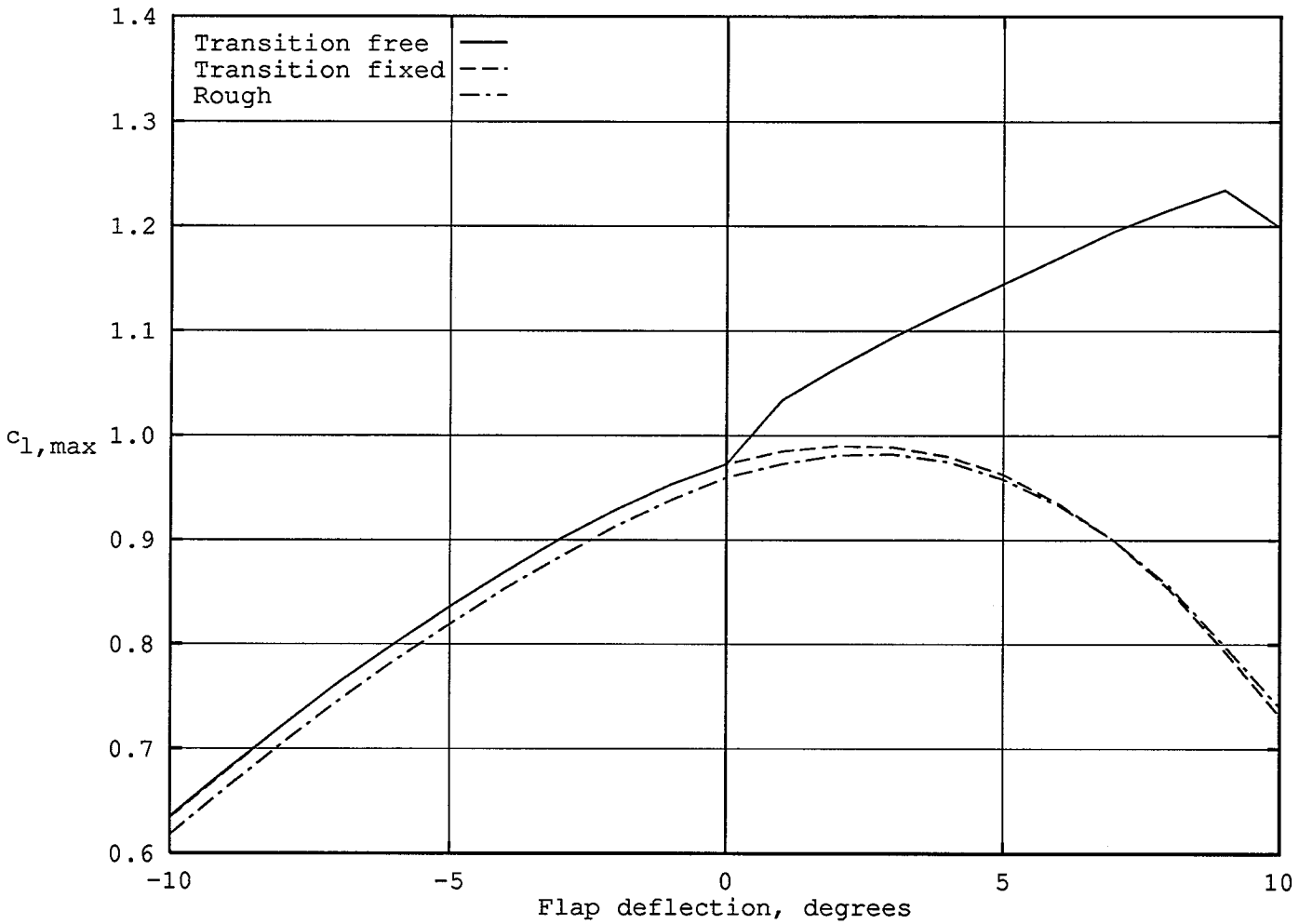

(a) $R = 1 \times 10^6$.

Figure 25.- Effect of flap deflection on maximum lift coefficient with transition free, transition fixed, and rough.

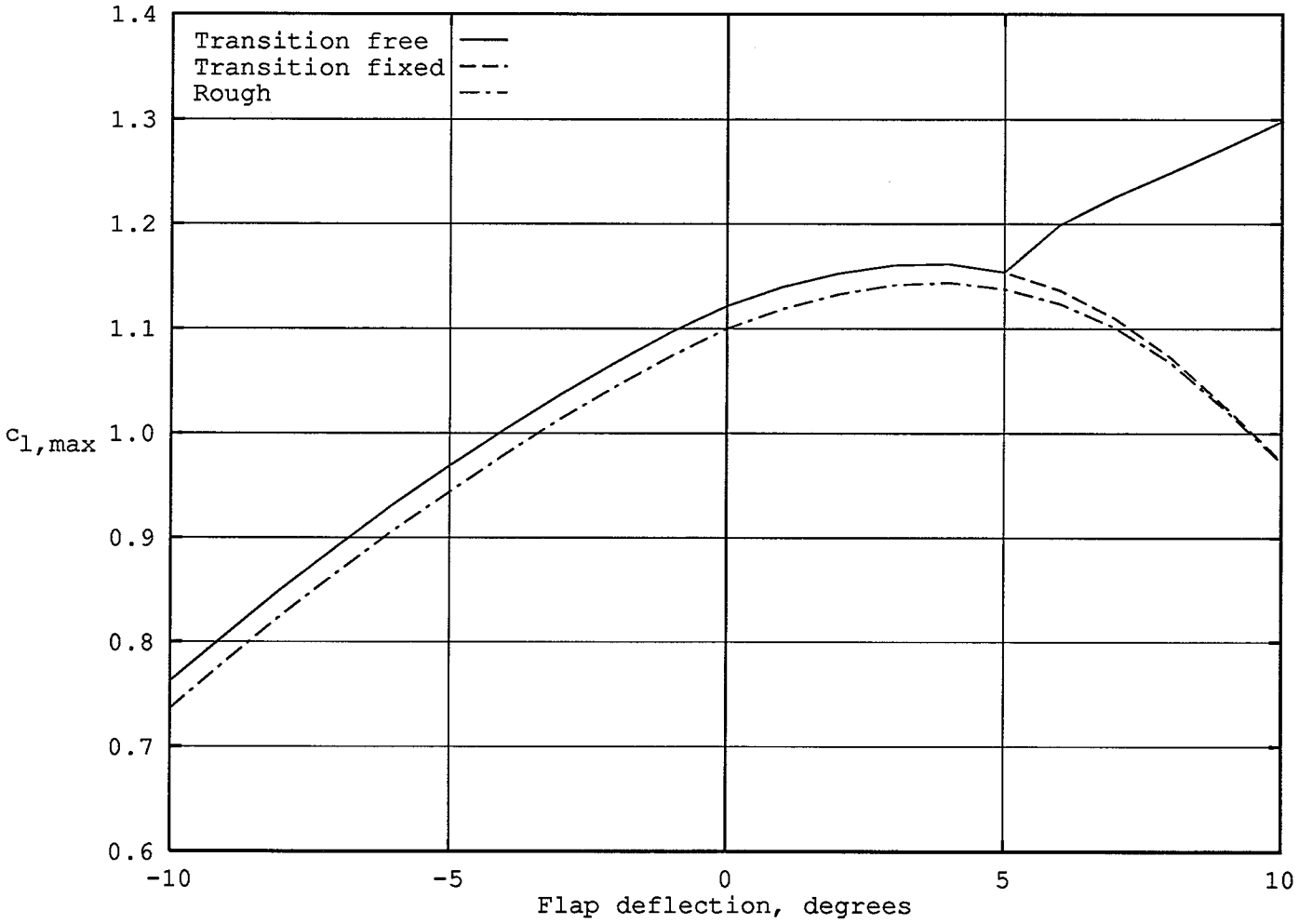

(b) $R = 2 \times 10^6$.

Figure 25.- Continued.

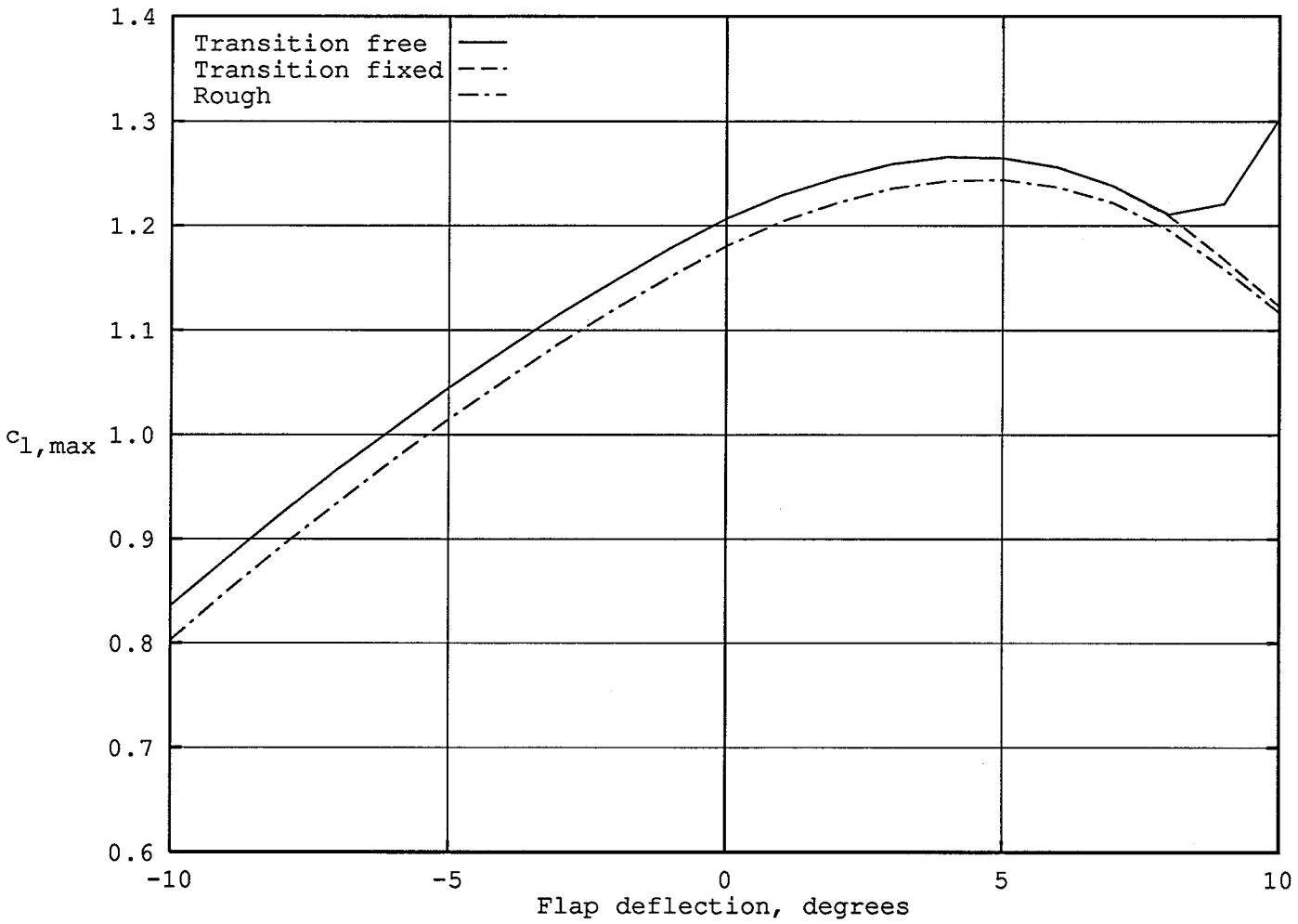

(c) $R = 3 \times 10^6$.

Figure 25.- Concluded.

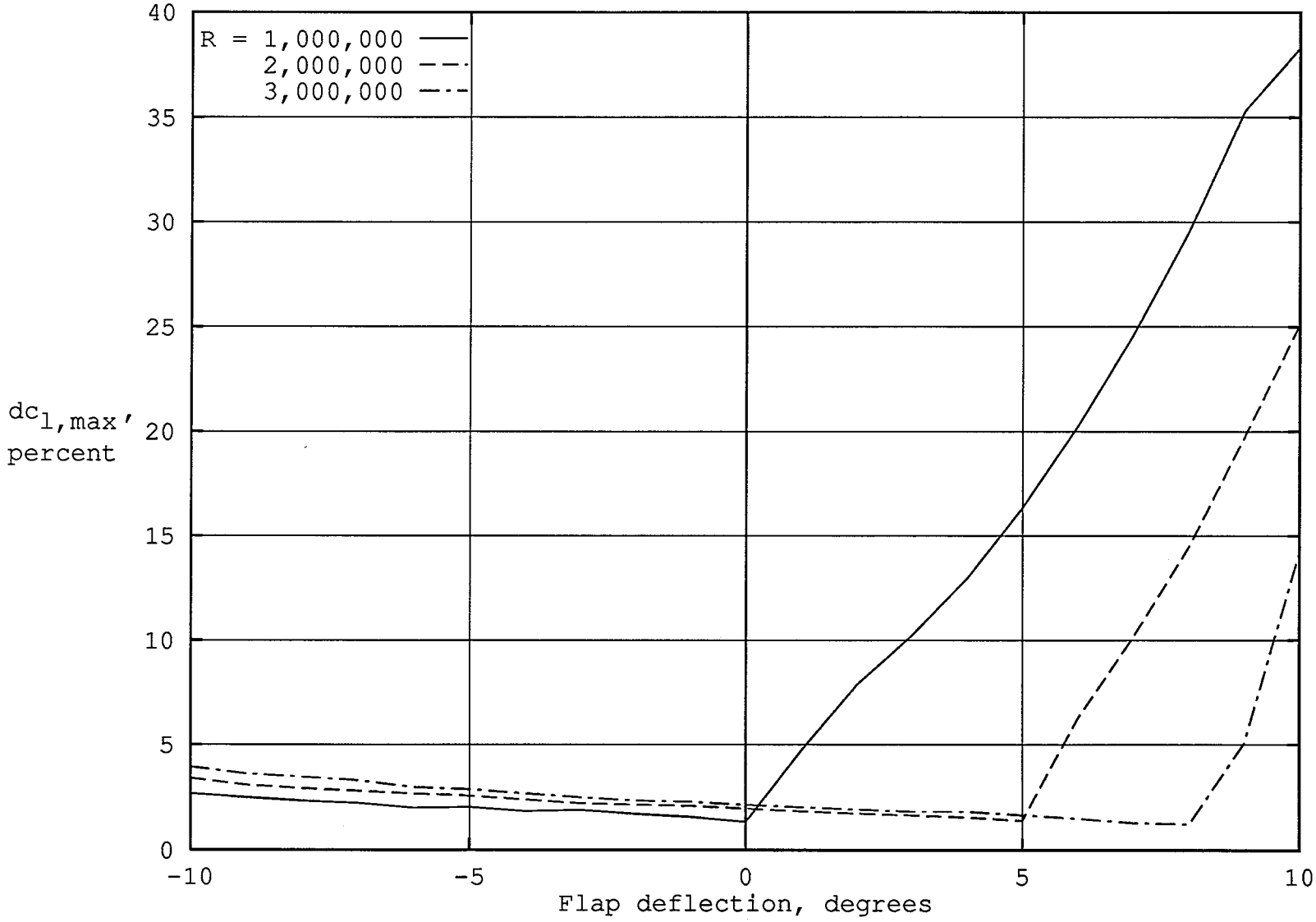

Figure 26.- Effect of flap deflection on change in maximum lift coefficient due to leading-edge roughness.

REPORT DOCUMENTATION PAGE

Form Approved
OMB No. 0704-0188

PLEASE DO NOT RETURN YOUR FORM TO THE ABOVE ORGANIZATION.

1. REPORT DATE *(DD-MM-YYYY)*	2. REPORT TYPE	3. DATES COVERED *(From - To)*
January 2005	Subcontract report	1993 - 1994

4. TITLE AND SUBTITLE
Effect of Flap Deflection on Section Characteristics of S813 Airfoil

5a. CONTRACT NUMBER
DE-AC36-99-GO10337

5b. GRANT NUMBER

5c. PROGRAM ELEMENT NUMBER

6. AUTHOR(S)
D.M. Somers

5d. PROJECT NUMBER
NREL/SR-500-36335

5e. TASK NUMBER
WER4.3110

5f. WORK UNIT NUMBER

7. PERFORMING ORGANIZATION NAME(S) AND ADDRESS(ES)
Airfoils, Inc.
601 Cricklewood Drive
State College, PA 16083

8. PERFORMING ORGANIZATION REPORT NUMBER

9. SPONSORING/MONITORING AGENCY NAME(S) AND ADDRESS(ES)
National Renewable Energy Laboratory
1617 Cole Blvd.
Golden, CO 80401-3393

10. SPONSOR/MONITOR'S ACRONYM(S)
NREL

11. SPONSORING/MONITORING AGENCY REPORT NUMBER
NREL/SR-500-36335

12. DISTRIBUTION AVAILABILITY STATEMENT
National Technical Information Service
U.S. Department of Commerce
5285 Port Royal Road
Springfield, VA 22161

13. SUPPLEMENTARY NOTES
NREL Technical Monitor: J. Tangler

14. ABSTRACT *(Maximum 200 Words)*
The effect of small deflections of a 30% chord, simple flap on the section characteristics of a tip airfoil, the S813, designed for 20- to 30-meter, stall-regulated, horizontal-axis wind turbines has been evaluated theoretically. The decrease in maximum lift coefficient due to leading-edge roughness increases in magnitude with increasing, positive flap deflection and with decreasing Reynolds number.

15. SUBJECT TERMS
airfoils; horizontal-axis wind turbine; airfoil design; Pennsylvania State University; wind energy

16. SECURITY CLASSIFICATION OF:			17. LIMITATION OF ABSTRACT	18. NUMBER OF PAGES	19a. NAME OF RESPONSIBLE PERSON
a. REPORT	b. ABSTRACT	c. THIS PAGE			
Unclassified	Unclassified	Unclassified	UL		19b. TELEPONE NUMBER (*Include area code)*

Standard Form 298 (Rev. 8/98)
Prescribed by ANSI Std. Z39.18